

# The initial mass function of stars

Pavel Kroupa<sup>a,b</sup>, Eda Gjergo<sup>c,d</sup>, Tereza Jerabkova<sup>e</sup> and Zhiqiang Yan<sup>c,d</sup>

<sup>a</sup>University of Bonn, Helmholtz-Institut fuer Strahlen und Kernphysik, Nussallee 14-16, 53115 Bonn, Germany

<sup>b</sup>Charles University, Astronomical Institute, V Holesovickach 2, 18000 Prague, Czech Republic

<sup>c</sup>Nanjing University, School of Astronomy and Space Science, Nanjing 210093, People's Republic of China

<sup>d</sup>Nanjing University, Key Laboratory of Modern Astronomy and Astrophysics, Ministry of Education, Nanjing 210093, People's Republic of China

<sup>e</sup>European Southern Observatory, Karl-Schwarzschild-Strasse 2, 85748 Garching, Germany

© 20xx Elsevier Ltd. All rights reserved.

## Glossary

**Bottom/top-heavy/light IMF** With an IMF normalised to unity at  $m = 1 M_{\odot}$  and relative to the canonical IMF:

*Bottom-heavy*: An IMF with a larger number of low-mass ( $< 1 M_{\odot}$ ) stars.

*Bottom-light IMF*: An IMF with a smaller number of low-mass ( $< 1 M_{\odot}$ ) stars.

*Top-heavy*: An IMF with a larger number of high-mass ( $> 1 M_{\odot}$ ) stars.

*Top-light IMF*: An IMF with a smaller number of high-mass ( $> 1 M_{\odot}$ ) stars.

**Brown dwarf (BD)** A substellar object with insufficient mass to ignite the hydrogen fusion that powers stars, but massive enough to trigger deuterium burning.

**Chemical enrichment** The progressive enrichment of gas in a galaxy by elements heavier than H and He, driven primarily by stellar nucleosynthesis.

**Dark star formation** A dwarf galaxy with a very small true SFR ( $\psi < 10^{-3} M_{\odot}/\text{yr}$ ) can appear as an H $\alpha$ -dark galaxy because its gwIMF is significantly top-light.

**Early/late-type star** *Early-type stars* are hot and massive white-to-blue stars (O-, B- and A-type stars) with high luminosities and short lifespans. Their mass exceeds  $m = 1.4 M_{\odot}$ .

*Late-type stars* are less hot and less massive red-to-yellow stars (F-, G-, K-, and M-type stars) with low luminosities and long lifespans.

Their mass does not exceed  $m = 1.4 M_{\odot}$ .

**Embedded cluster** A spatially (about  $< 1$  pc) and temporally (about  $< 1$  Myr) correlated dense region in a molecular cloud that undergoes gravitational collapse and forms stars. Embedded clusters are the fundamental building blocks of galaxies and contain a simple stellar population.

**Galaxy** A gravitationally bound stellar population with a half-mass two-body relaxation time (i.e. energy equipartition time scale) longer than a Hubble time. A galaxy can contain multiple stellar populations and gas from which new stars can be forming.

*Late-type galaxy*: A rotationally-supported, thin-disk star-forming galaxy characterized by a mix of old and young stellar populations. Its morphological types include spiral and irregular (dwarf) galaxies. More than 90 per cent of all galaxies are of this type.

*Elliptical (E) galaxy*: Unlike spiral galaxies, which are supported against gravitational collapse by angular momentum, elliptical galaxies are primarily supported by the random motion of stars, making them pressure-supported systems. E galaxies experience negligible star formation, they are passively-evolving and their stellar populations are generally very old. Less than a few per cent of all galaxies are of this type.

*Early-type galaxies (ETGs)* include elliptical (E) and lenticular (S0) galaxies. All ETGs are bulge-dominated and contain mostly old stars with little to no gas. S0 have a prominent smooth and featureless (no arms) thickened disk, while E galaxies have none. E galaxies are dominated by random motions, while S0 galaxies show rotation in their disk component.

*Ultra-compact dwarf galaxy (UCD)*: Very rare extremely massive stellar systems ten to a hundred times more massive than GCs and GC-like radii that increase with their mass similar to those of elliptical galaxies. Despite appearing linked to star clusters, UCDs are referred to as galaxies by them having half-mass two-body relaxation times longer than a Hubble time.

*Ultra-faint dwarf galaxy (UFD)*: Small and faint dwarf galaxies whose stellar luminosity is typically below  $10^4 L_{\odot}$ , where  $L_{\odot}$  is the solar luminosity. While their stellar mass is comparable to that of a massive open star cluster, its size is  $\lesssim$  ten times larger.

**H $\alpha$  emission in the context of the IMF** Emission originating from the recombination of hydrogen in ionised gas. The gas ionisation is driven by nearby young, massive stars. H $\alpha$  emission is used as a SFR tracer for a galaxy, but the conversion is strongly sensitive to the shape of the gwIMF.

**IGIMF Theory** The integrated-galaxy initial-mass-function theory for calculating the gwIMF by adding the stellar IMFs in all freshly formed embedded clusters.

**Initial mass function (IMF)** A function that represents the number distribution of the initial stellar masses in a complete population of stars. All IMFs have units of number of stars per solar mass [ $\#/M_{\odot}$ ].

The *stellar IMF* constitutes the IMF of stars born in a single embedded cluster in one molecular cloud clump. It is the distribution of all initial stellar masses in a simple stellar population.

The *composite IMF* is the initial mass distribution of a population of stars born in a larger region encompassing more than one embedded cluster, for example, that of a molecular cloud or of multiple molecular clouds. i.e., it is the sum of more than one stellar IMF. It can be calculated using the LIGIMF theory.

## 2 The initial mass function of stars

The *canonical IMF* is the composite IMF derived from star counts in the local Solar neighborhood and is therewith a bench mark distribution function by being an average constituting the mixture of embedded clusters that gave rise to the Solar neighbourhood stellar ensemble. This distribution aligns with star formation processes in most environments within spiral galaxies.

The *canonical stellar IMF* is the stellar IMF with a shape equal to that of the canonical IMF.

*Galaxy-wide IMF (gwIMF)*: The *galaxy-wide IMF* is the sum of all stellar IMFs in a galaxy. It is the composite IMF of a whole galaxy. This quantity can vary over time.

*Present-day stellar mass function (PDMF)*: The distribution of stellar masses in a population of stars that are currently alive.

**Interstellar medium (ISM)** The matter dispersed in between stars in a galaxy. It is mainly composed of gas and dust. It can form stars after cooling sufficiently (to below 100° K) under sufficiently high density to form molecular clouds.

**Isotopologues** Molecules that differ only in their isotopic composition with at least one atom having a different number of neutrons.

**LIGIMF theory** The local IGIMF, also known as the composite IMF, is obtained by adding the stellar IMFs in all embedded clusters found within a given region in a galaxy (e.g. in one molecular cloud).

**Luminosity function of stars (LF)** The number distribution of stellar luminosities among main sequence stars.

**Main sequence stars** Stars in a stable phase of their evolution (being "alive"), during which they undergo hydrogen burning in their cores.

**Mass of an embedded cluster ( $M_{\text{ecl}}$ )** The total stellar mass of all stars formed within an embedded cluster. Just like the IMF, this quantity emerges over a time interval of about a million years. It is therefore not directly observable.

**Molecular cloud clump** A dense region in a molecular cloud that is gravitationally unstable and eventually collapses to form an embedded cluster. Typically, it has a scale of less than 1 pc.

**Optimal sampling** Deterministic sampling of a distribution function without Poisson scatter upon arbitrary binning of the sampled quantity.

**Pre-stellar molecular cloud core** A collapsing gas core, progenitor to a proto-star. It has a size of  $< 0.01 - 0.1$  pc.

**Proto-star** An accreting pre-stellar core that will end up as a star.

**Simple-stellar population** A stellar population of an embedded star cluster formed within a few free-fall times of the molecular cloud clump. Simple stellar populations are composed of stars with the same ages and chemical abundances.

**Star cluster** A gravitationally bound simple stellar population with a half-mass two-body relaxation time (i.e. energy equipartition time scale) shorter than a Hubble time.

*Open star cluster*: Open star clusters typically have half-mass radii of a few pc and are typically found on near-circular orbits in the disks of galaxies. They are thought to be remnants of embedded star clusters after these have blown out their residual gas from which they formed.

*Globular star cluster (GC)*: A densely-packed, mostly spherical simple but partially chemically self-enriched stellar population typically of great age. A present-day GC may contain a few hundred thousand to a few million of ancient, late-type stars and have a half-mass radius of a few pc. GCs are massive versions of open star clusters with life times surpassing a Hubble time by virtue of their large masses. GCs form in galaxies with very large SFRs ( $\psi > \text{hundreds } M_{\odot}/\text{yr}$ ) and are typically the fossils of the violent onset of star formation in the early Universe.

**Star-formation history (SFH)** The temporal evolution of the star formation rate (SFR,  $\psi$ , in units of  $M_{\odot}/\text{yr}$ ), i.e., the SFH is  $\psi(t)$ . It is a record of a galaxy or a system's star-formation rate over its lifetime.

### Nomenclature

BD	Brown dwarf
GC	Globular star cluster
ETG	Early-type galaxy
gwIMF	Galaxy-wide IMF
IGIMF	Integrated-galaxy initial-mass-function theory for calculating the gwIMF
IMF	Initial mass function of stars
ISM	Inter-stellar medium
LIGIMF	Local IGIMF encompassing a region in a galaxy
LF	Luminosity function of main sequence stars
$M_{\text{ecl}}$	Cumulative mass of all stars formed within an embedded cluster, i.e. a molecular cloud clump
ONC	Orion Nebula Cluster
PDMF	Present-day stellar mass function of a population of stars
SFE	Star formation efficiency, $\epsilon$ , of a molecular cloud clump (i.e., embedded star cluster)
SFH	Star-formation history
SFR	Star-formation rate, $\psi$ , of a galaxy
SMBH	Super-massive black hole
stellar IMF	Initial mass function of stars born in one molecular cloud core, i.e. in one embedded cluster and at the same time
UCD	Ultra-compact dwarf galaxy
UFD	Ultra-faint dwarf galaxy
VLMS	Very low mass star (of mass $m < 0.2 M_{\odot}$ )

## Abstract

The initial mass function of stars (IMF) is one of the most important functions in astrophysics because it is key to reconstructing the cosmological matter cycle, understanding the formation of super-massive black holes, and deciphering the light from high-redshift stellar populations. The IMF's dependency on the physical conditions of the star-forming gas and its connection to the galaxy-wide IMF connects the molecular clump scale to the cosmological scale.

Significant advancements have been made in extracting the IMF from observational data. This process requires a thorough understanding of stellar evolution, the time-dependent stellar multiplicity, the stellar-dynamical evolution of dense stellar populations, and the structures, star formation histories, and chemical enrichment histories of galaxies. The IMF in galaxies, referred to as the galaxy-wide IMF (gwIMF), and the IMF in individual star-forming regions (the stellar IMF) need not be the same, although the former must be related to the latter.

Observational surveys inform on whether star-forming regions provide evidence for the stellar IMF being a probability density distribution function. They may also indicate star formation to optimally follow an IMF shaped by the physical conditions of the star-forming gas. Both theoretical and observational evidence suggest a relationship between the initial mass function of brown dwarfs and that of stars. Late-type stars may arise from feedback-regulated fragmentation of molecular cloud filaments, which build up embedded clusters. In contrast, early-type stars form under more violent accretion and feedback-regulated conditions near the centers of these clusters.

The integration over all star-forming molecular cloud clumps and their stellar IMFs in a galaxy via the IGIMF theory yields its gwIMF which sensitively depends on the physical properties of the molecular cloud clumps and the range of their masses that depends on the SFR of the galaxy.

### Key points/Objectives box

- Explain the current knowledge on the shape of the stellar initial mass function (IMF) as an outcome of star formation in molecular cloud clumps. Investigate the dependence of the variation of the IMF on physical conditions.
- Discuss the nature of the stellar IMF as a probability-density distribution function or an optimally sampled distribution function.
- Explore the relation between this stellar IMF and the galaxy-wide IMF (gwIMF) and their implied variations.
- Consider the astrophysical and cosmological implications of the systematically varying stellar IMF and gwIMF.

## 1 Introduction

The advent of quantum mechanics during the first half of the 20th century allowed the understanding of the energy source that enables stars to shine for billions of years, namely hydrogen fusion, which eventually leads to the synthesis of heavier elements. This breakthrough made it possible to explain both stellar luminosities and to derive stellar lifetimes. Heavier stars of about 100 solar masses ( $M_{\odot}$ ) live for a few million years (Myr), while less massive stars of around  $1 M_{\odot}$  may live for billions of years (Gyr). High mass and low mass stars are routinely observed, implying that star formation is ongoing, and that the stellar mass distribution in galaxies changes over time. Furthermore, this process needs theories of gas accretion onto galaxies, gas cooling, and fragmentation to sustain the observed ongoing formation of stars.

With such questions in mind, Salpeter (1955) bridged quantum physics into cosmology by assessing the “*relative probability for the creation of stars of mass  $m$* ” (Kroupa and Jerabkova, 2019). Salpeter used the available distribution of stellar luminosities, which had been obtained by astronomers from star counts in the Solar neighborhood, and applied corrections for stellar death to estimate this relative stellar creation probability, which today is referred to as the initial mass function of stars (IMF). The observed ensemble of stars, after correcting the stellar luminosities for stellar evolution (e.g., main sequence brightening), yields the present-day mass function of stars (PDMF). The calculation of the IMF from the PDMF requires several assumptions, including an understanding of the star-formation rate (SFR), the evolution of the SFR over time (SFH), the age of the Galaxy's disk and its stellar-age-dependent thickness, and how stellar orbits diffuse over time in the galaxy. These assumptions are important for connecting the local counts, which are mostly composed of faint, long-lived stars in a small volume (less than 100 pc) around the Sun, to the kpc-distant counts of rare, bright, short-lived massive stars. Salpeter initially estimated the age of the Galactic disk to be 6 Gyr. This value is about half of the presently-known age of approximately 12 Gyr. Despite this discrepancy, the star counts and structure of the Galactic disk known at the time led to the formulation of the “*Salpeter-power-law IMF*”.

Salpeter assumed the IMF to be an invariant probability density distribution function. He then considered field stars with masses  $0.4 < m/M_{\odot} < 10$  and found the IMF to be a power-law whose index is  $\alpha_S \approx 2.35$ , where the number of stars  $dN$  with masses  $m$  in the range to  $m + dm$  is:

$$dN = \xi(m) dm, \quad (1)$$

where  $\xi(m) \propto m^{-\alpha_S}$  is the Salpeter IMF. A thorough explanation and discussion of the above assumptions and of the biases affecting star counts has been compiled by Scalo (1986); Kroupa et al. (2013); Hopkins (2018).

The following chapter documents the present-day knowledge of the IMF based on Solar-neighbourhood star counts and resolved stellar populations (Sec. 2). Theoretical ideas on the IMF and the sub-stellar problem are touched upon in Sec. 3. Over the past decade, evidence has accumulated that indicates the IMF is dependent on the density and metallicity of the star-forming gas cloud, i.e. on its ability to cool (Sec. 4). The fundamental question whether the IMF is a probability density distribution function or an optimal, self-regulated function of stellar mass is raised in Sec. 5. Sec. 6 discusses the relation between the stellar IMF and the composite IMF such as the galaxy-

## 4 The initial mass function of stars

wide IMF (gwIMF) and thus the redshift-dependent evolution of initial stellar-populations with an outline of the IGIMF theory. The observational evidence is addressed in Sec. 7 of the connection between the IMF and star-forming galaxies, early-type galaxies (ETGs), ultra-compact dwarf galaxies (UCDs) and globular star clusters (GCs), and supermassive black holes (SMBHs). The existence and reality of the distribution functions that define a new stellar population is addressed in Sec. 8. Available computer programs to set-up and simulate stellar populations and galaxies are listed in Sec. 9. Sec. 10 contains the conclusions and an outlook.

Note:

The *stellar IMF*,  $\xi(m)$ , is defined as the number distribution of initial stellar masses for all stars born in one molecular cloud clump, i.e., in one embedded star cluster, representing a simple stellar population. Note that  $m$  is always in units of the Solar mass,  $M_\odot$ , unless stated otherwise and that if  $m$  is the argument in a function (e.g. as in eq. 5, 10 or  $\log_{10}m$ ) then implicitly it is assumed that  $m = m/M_\odot$ . The *composite IMF* is defined as the number distribution of initial stellar masses of multiple simple stellar populations, i.e., it is the sum of several stellar IMFs forming at the same time. The composite IMF can be a galaxy-wide IMF, gwIMF. It is equal in shape to the stellar IMF if the physical properties of the star-forming gas are sufficiently similar for all simple stellar populations included in the composite IMF, or if the stellar IMF is an invariant probability density distribution function.

Different notations have been adopted in the literature concerning the IMF: The function  $\xi(m)$  can be rewritten in terms of the logarithmic mass scale as  $\xi_L(m) = (m \ln 10) \xi(m)$  such that

$$dN = \xi(m) dm = \xi_L(m) d\log_{10}m, \quad (2)$$

where  $\log_{10}m = \ln m / (\ln 10)$ . Given  $\xi(m) \propto m^{-\alpha}$  and  $\xi_L(m) \propto m^\Gamma \propto m^{-x}$ , we have  $\Gamma = -x = 1 - \alpha$ .

## 2 The canonical stellar IMF and its functional form

Currently, it is possible in the solar neighbourhood to obtain volume-complete star counts of the faintest M dwarf stars to a distance of not much more than 5 pc, and of G dwarfs out to distances of about 20 pc. These distances are known through trigonometric parallax measurements, and enable to derive their stellar luminosity function (LF). Independent and larger ensembles of late-type stars, based on photometric-parallax measurements, reach to larger distances. Late-type stars do not evolve much over a Hubble time, but it is necessary to account for two parts: the main-sequence brightening at their massive-end ( $m > 0.8 M_\odot$ ), and the pre-main-sequence long contraction times below a few tenths of a Solar-mass. It is necessary to apply statistical corrections for incompleteness as introduced by Kroupa et al. (1991), because approximately half of all late-type stars in the Solar-neighbourhood are binary systems (e.g. Fig. 5 below). Some systems are even higher-order multiples, this being particularly relevant for the deep photometric-parallax ensembles. In a survey of 100 late-type Galactic field “stars”, typically about 40 would be binaries and 5 triples with perhaps a quadruple being there too. The observer would thus miss 53 faint stars if none of the multiples were to be resolved. While most IMF constraints have been based on the trigonometric-parallax-based sample (e.g. Kirkpatrick et al. 2023 using Gaia data), the combination with photometric-parallax-based star counts provides a more robust assessment of the shape of the stellar IMF. That is, as long as all biases are taken into account. For example, parallax measurements are affected by the Lutz-Kelker bias, while photometric-parallax surveys are affected by the Malmquist bias (Kroupa et al. 1993 and references therein).

Of central importance when constructing a stellar IMF from a star-count survey after a suitably-complete ensemble of main-sequence stellar masses has been obtained is the following: Either individual stellar masses need to be calculated from their luminosities, or the stellar luminosity function,  $\Psi_X(M_X)$ , needs to be transformed into  $\xi(m)$ , with

$$dN = \Psi_X dM_X \quad (3)$$

being the number of stars in the absolute magnitude interval  $M_X$  to  $M_X + dM_X$  and  $X$  being a photometric pass band (e.g.  $X=V$  for the V-band). The stellar IMF,  $\xi$ , and luminosity function,  $\Psi$ , are related by

$$\xi(m) = -(dm/dM_X)^{-1} \Psi_X(M_X). \quad (4)$$

In this step of constructing  $\xi(m)$ , a point of fundamental importance is the use of the correct stellar-luminosity–mass,  $l(m)$ , relation because the short-lived  $H^-$  ion becomes an important opacity source in stars with  $m < 0.9 M_\odot$ , the formation of the  $H_2$  molecule affects the opacity and mean molecular weight for stars  $m < 0.4 M_\odot$ , stars with  $m < 0.3 M_\odot$  are fully convective, while more massive stars have a radiative core (e.g. Mansfield and Kroupa 2023), and the core of a star with  $m < 0.1 M_\odot$  is supported significantly by degenerate electron pressure. This leads to inflections, noted by Kroupa et al. (1990), in the  $l(m)$  relation that causes the “Wielen dip” near  $m \approx 0.7 M_\odot$  and a very pronounced sharp metallicity-dependent and age-dependent maximum in the stellar luminosity function at  $M_V \approx 11.5$ ,  $M_I \approx 8.5$  ( $m \approx 0.3 M_\odot$ ) seen in all simple and composite stellar populations (Fig. 1).

Errors can be introduced into  $\xi(m)$  when an incorrect mass-luminosity relation is applied. This is demonstrated in Fig. 2, which displays the relation between the stellar mass  $m$  and the respective magnitude  $M_V$ <sup>1</sup>. Purely theoretical mass-luminosity relations are likely to result in

<sup>1</sup>The red lines in Fig. 2 are the  $m(M_V)$  relation gauged from Galactic-field data by Kroupa et al. (1993) subject to strong constraints given by the stellar-mass and luminosity

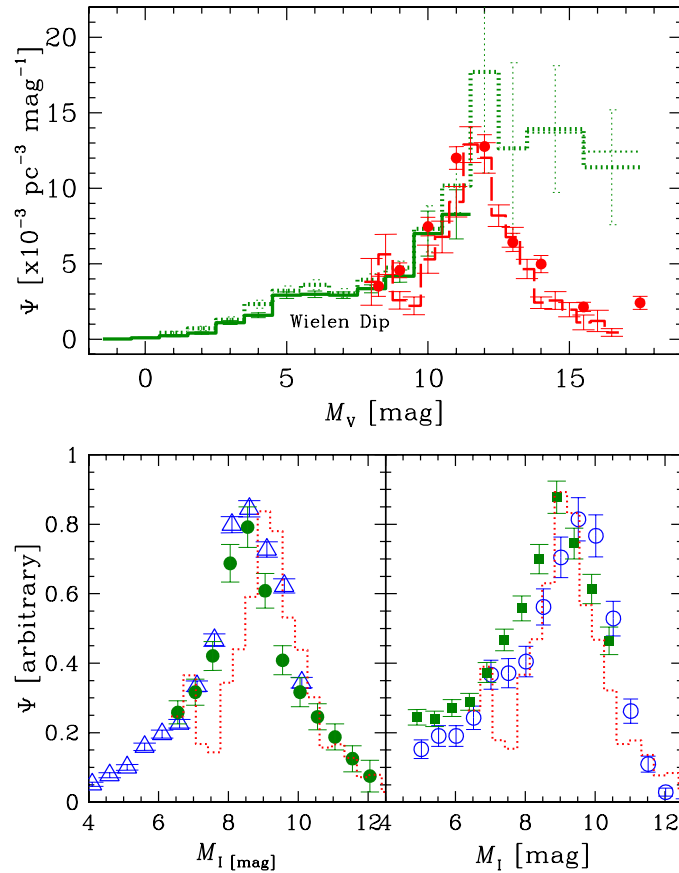


**Fig. 1** Stellar luminosity function of late-type stars,  $\Psi(M_X)$ , as a function of their photometric magnitudes in V- (*top panel*) and I-bands (*bottom panels*). Note that all the stellar luminosities have sharp maxima at  $\approx 11.5$  for  $M_V$ , and at  $\approx 8.5$  for  $M_I$ . These peaks match in location, amplitude, and width the red curves in the lower panels of Fig. 2. (*Top panel*): In green are the histograms for the ensemble of stars in the solar neighborhood, employing a trigonometric-parallax based method. The *solid green line* includes the complete sample up to about 20 pc, while the *dotted green lines* include the complete sample up to about 5 pc from the Sun. The *red histogram data with a dashed line and solid circles* show the star samples based on photometric parallax distance estimates in pencil beam sky surveys out to distances of 100 pc to 300 pc. Marked on the graph is the “Wielan Dip,” which originates from structure in the mass-luminosity relation. The H-ion provides an increasing opacity source in the outer stellar envelope with decreasing stellar masses. For higher V-band magnitudes ( $M_V > 11$ ), faint stellar companions are not counted in the deep surveys. This causes a difference in star counts obtained via trigonometric vs. photometric parallax, which manifests as different stellar volume densities,  $\Psi$ . (*Left bottom panel*): The LFs of simple stellar populations. Here we see the stellar luminosity,  $\Psi$ , as a function of the I-band magnitude,  $M_I$ , for two globular clusters: M15 (*blue triangles*) and NGC 6397 (*green solid circles*). (*Right bottom panel*): Similarly to the left bottom panel, but for the young Pleiades star cluster (*blue open circles*) and the globular cluster 47 Tuc (*green solid squares*). In both of the bottom panels, the red histogram matches the red histogram from the upper panel, scaled to a peak value matching that of the LFs in the clusters. Note that although the upper panels show the LFs of the composite Solar-neighbourhood population, correcting the star counts for Lutz-Kelker and Malmquist bias makes the LFs equivalent to those of an average simple stellar population. This simple stellar population represents a population with an average age of about 5 Gyr with near-Solar metallicity. For more details, see figures 9 and 10 in Kroupa et al. (2013).

incorrect estimates of the stellar IMF. The mass-luminosity relation is also affected by stellar rotation. The theoretical relations generally do not reproduce the mass-luminosity relation sufficiently well (Kroupa and Tout, 1997). It is therefore essential to gauge carefully the mass-

data from the orbital solutions of binary stars and the amplitude and width of the bias-corrected stellar luminosity function,  $\Psi_V(M_V)$ . The black lines are stellar isochrones generated by CMD 3.7 (<http://stev.oapd.inaf.it/cgi-bin/cmd.3.7>), based on PARSEC release v1.2S, for Solar metallicity stars ( $Z = 0.01471$ ) with an age of 1 Gyr or 5 Gyr (main-sequence stars) for the UBVRIJK photometric system (Maíz Apellániz, 2006) using the YBC version of bolometric corrections (Chen et al., 2019) and assuming a dust composition of 60% Silicate and 40% AlOx for M stars, 85% AMC and 15% SiC for C stars (Groenewegen, 2006), and no interstellar extinction.

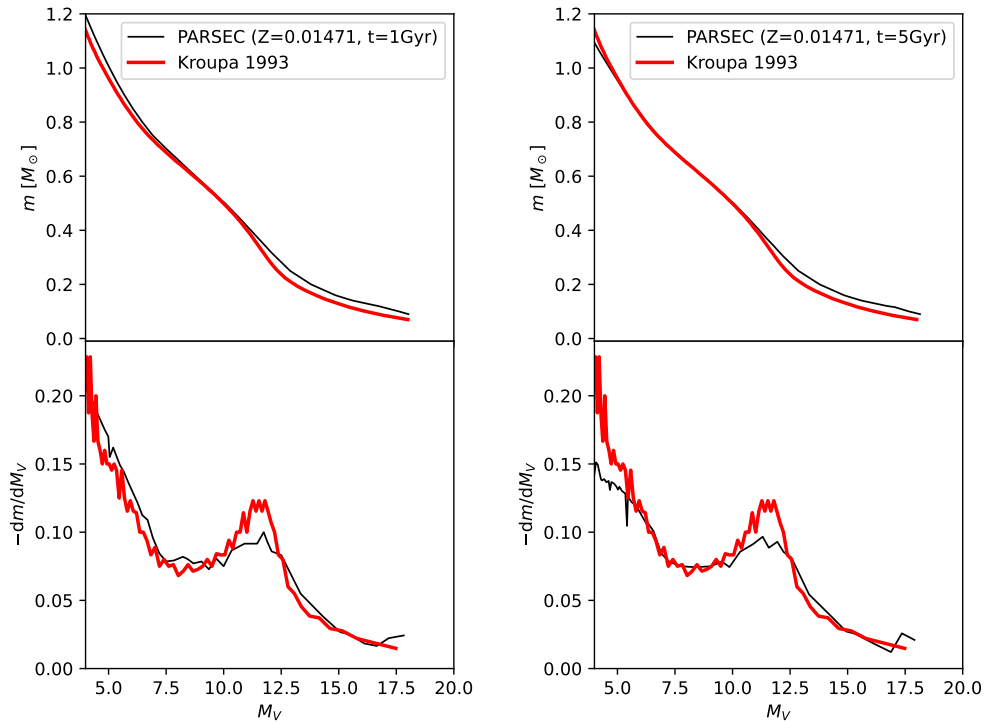


**Fig. 2** Visualisation of the problems encountered when transforming stellar luminosities to stellar masses. The stellar mass–luminosity relation ( $m(M_V)$ , upper panels) and the derivative ( $-dm/dM_V$ ), lower panels) in the V-photometric pass band for a theoretical (black curves, for details see footnote 1) population of stars of age 1 Gyr (left panels) and 5 Gyr (right panels) are shown. The red lines are for an empirically gauged  $m(M_V)$  relation valid for a population of Solar-neighbourhood stars of an average age of about 5 Gyr and of solar metallicity. In the upper panels, main-sequence brightening of the theoretical (black curves) stars with  $m > 0.75 M_\odot$  is evident in the 5 Gyr panel. If an observer chooses the theoretical (black) model then the observed amplitude of the stellar luminosity function at  $M_V \approx 11.5$  needs to be compensated by values of the power-law indices of the stellar IMF of  $\alpha_1$  and  $\alpha_2$  that are approximately twice larger than when using the red  $m(M_V)$  relation, given that the theoretical (black)  $m(M_V)$  relation has an approximately two times smaller amplitude in  $-dm/dM_V$  than the red relation. The stellar IMF derived from star counts will thus be more bottom-heavy in the approximate stellar mass range  $0.3 < m/M_\odot < 0.7$  for the theoretical  $m(M_V)$  relation than the empirically gauged one.

luminosity relation in order to calculate correctly the shape of the stellar IMF. Fig. 1 demonstrates that the radiative/convection boundary in late type stars near  $M_V = 11.5$  (Fig. 2) is evident in a very pronounced and sharp maximum in the stellar LFs of different simple stellar populations. This maximum needs to be mapped correctly to the IMF,  $\xi(m)$ . Failing to do so affects the value of the deduced IMF power-law index  $\alpha_{1,2}$ , as explained in Fig. 2. This issue is of great importance when the power-law index of the IMF is estimated from star counts of stars with masses in the range  $0.3 - 0.7 M_\odot$ , as is the case for distant GCs and ultra-faint dwarf galaxies (UFDs), for example.

#### The derivative of the stellar-luminosity–mass relation

If purely theoretical stellar models are used, the amplitude of the derivative,  $dm/dM_X$ , of the stellar-luminosity–mass relation will map into an incorrect value of the power-law index of the stellar IMF.

After correcting the star counts statistically for unresolved binary systems (Kroupa et al., 1991), i.e. counting all individual stars, the combined solution to the nearby trigonometric-parallax-based and photometric-parallax-based star counts (Kroupa et al., 1993) provides a benchmark stellar population, referred to as the canonical IMF (Kroupa et al., 2013). It is representative of the late-type stellar population in the Solar vicinity accumulated from many star-formation events over a wide range of metallicities (with  $m_H \approx 0.08 M_\odot$  being the slightly-metallicity-dependent hydrogen-burning mass limit below which the objects are referred to as brown dwarfs, BDs, Burrows et al. 2011). Adapting the field star-count analysis by Scalo (1986) for early-type stars one obtains the *canonical field-star IMF*. Combining instead star-count data of early-type stars in young star clusters and associations in the Galaxy, the Large and Small Magellanic Clouds with stellar-evolution models by Massey (2003) and stellar-dynamical models of initially binary-rich star clusters (Kroupa, 2001) one obtains the *canonical stellar IMF*. The most-massive star in a population,  $m_{\max}$ , is discussed in Sec. 3. We thus have:

**The canonical field-star and stellar IMF**

With continuity ( $k_i$ ) and normalisation ( $k_\xi$ ) constants, the canonical field-star and the canonical stellar IMF can be written as

$$\xi(m) = k_\xi k_i m^{-\alpha_i}, \quad (5)$$

where

$$\alpha_{1,\text{can}} = 1.3 \pm 0.3 \quad (m_{s0} \lesssim m/M_\odot \leq m_{s1}) \quad (6)$$

$$\alpha_{2,\text{can}} = 2.3 \pm 0.3 \quad (m_{s1} < m/M_\odot \leq m_{s2}), \quad (7)$$

with  $m_{s0} = m_H = 0.08 M_\odot$ ,  $m_{s1} = 0.5 M_\odot$  and  $m_{s2} = 1.0 M_\odot$ .

For the *canonical stellar IMF*:

$$\alpha_{3,\text{can}} = 2.3 \pm 0.36 \quad (m_{s2} < m/M_\odot \leq m_{\text{max}}). \quad (8)$$

and for the *canonical field-star IMF*

$$\alpha_{3,\text{field}} = 2.7 \pm 0.4 \quad (m_{s2} < m/M_\odot), \quad (9)$$

The more recent trigonometric-parallax-based star-count analysis by Kirkpatrick et al. (2023) confirms these values but suggests that  $\alpha_{1,\text{Kirk}} = 0.25$  for  $m < 0.25 M_\odot$  which is similar to  $\alpha_0 = 0.3 \pm 0.4$  for  $0.01 \lesssim m/M_\odot \lesssim 0.15$  in Kroupa et al. (2013), where for very low-mass stars and brown dwarfs,  $\xi_{\text{BD}}(m) = k_\xi k_{\text{BD}} (m/0.07)^{-\alpha_0}$  with  $k_{\text{BD}} \approx 1/3$  (for a discussion of the sub-stellar/brown dwarf regime see Sec. 3.5).

With  $\alpha_{3,\text{field}} > \alpha_{3,\text{can}}$ , the canonical field-star IMF contains a smaller number of massive stars per late-type star than the canonical stellar IMF, the former thus being *top-light* relative to the latter which represents stellar populations born in one embedded cluster, i.e. in one molecular cloud clump. This difference appears to be real and it is confirmed by Rybizki and Just (2015); Mor et al. (2017, 2018). This difference can be understood in terms of the IGIMF theory (Sec. 6.3).

A log-normal form for the canonical IMF has been suggested by Miller and Scalo (1979) and other researchers (e.g. Chabrier 2003) instead of a multi-power-law form. To be consistent with the star-counts, the log-normal form needs a power-law extension for  $m \gtrsim 1 M_\odot$  which is as above ( $\alpha_{3,\text{can}}$ ) such that this IMF is very similar to the above two-part-power-law form of the canonical stellar IMF (fig. 24 in Kroupa et al. 2013). The *log-normal canonical IMF* can be written

$$\xi_{\text{star}}(m) = k_\xi \begin{cases} \frac{1}{m} \exp\left[-\frac{(\log_{10} m - \log_{10} m_c)^2}{2\sigma_{lm}^2}\right] & , \quad 0.1 \lesssim m/M_\odot \leq 1.0, \\ A m^{-2.3 \pm 0.36} & , \quad 1.0 < m/M_\odot \leq 150 \end{cases} \quad (10)$$

In eq. 10 continuity (but not differentiability) is assured at  $1 M_\odot$  and  $\xi_{\text{BD}}(m)$  is as above.

A least-squares fit to the two-part power-law form (eq. 5–8), whereby  $\int_{0.07}^{150} m \xi(m) dm = 1 M_\odot$  for both, yields (Kroupa et al., 2013)  $m_c = 0.055 M_\odot$  and  $\sigma_{lm} = 0.75$  with  $A = 0.2440$  for continuity at  $1 M_\odot$  and  $k_{\text{BD}} = 4.46$  as being the best log-normal plus power-law representation of the canonical IMF. Alternatively, a reduced analysis based only on the trigonometric-parallax-based star counts has (table 1 in Chabrier 2003)  $m_c = 0.079_{+0.021}^{-0.016} M_\odot$  and  $\sigma_{lm} = 0.69_{+0.05}^{-0.01}$  with  $A = 0.2791$  and  $k_{\text{BD}} = 4.53$  (Kroupa et al., 2013).

As explained in Sec. 3, the theoretical motivation for the log-normal form however fails below  $m \lesssim 0.1 M_\odot$ , and the analysis of Gaia data by Kirkpatrick et al. (2023) shows the log-normal form to be unviable below about  $0.3 M_\odot$ , confirming the results by Thies et al. (2015). Given that quantities over a mass range  $m_a$  to  $m_b$  often need to be computed such as the mass in stars,  $M_{m_a}^{m_b} = \int_{m_a}^{m_b} m \xi(m) dm$ , or the number of stars,  $N_{m_a}^{m_b} = \int_{m_a}^{m_b} \xi(m) dm$ , the advantage of the two-part-power-law form becomes apparent in stellar sampling applications (Sec. 5). Thus, according to the canonical stellar IMF with  $m_{s0} = 0.07 M_\odot$ , the average stellar mass

$$m_{\text{av}} = \frac{\int_{m_{s0}}^{m_b} m \xi(m) dm}{\int_{m_{s0}}^{m_b} \xi(m) dm}, \quad (11)$$

is  $m_{\text{av}} = 0.5(0.3) M_\odot$  for  $m_b = 150.0(1.0) M_\odot$ . BDs contribute negligible mass (about 4 per cent) to a simple stellar population. The above formulations count every single star in the stellar population. In the Solar neighbourhood about every second "star" is a binary system leading to the Solar neighbourhood IMF appearing flatter (Kroupa et al. 2013 and references therein). This IMF of stellar systems, the "system IMF", has, however, no physical meaning. Because most if not all stars are born as multiple systems (see Sec. 3.4) a system-stellar IMF is meaningful if it is constructed from this initial or birth population (Kroupa et al., 2013). The analysis of star-forming regions and young stellar populations in the Galaxy and the Large and Small Magellanic Clouds has been showing the IMF to be similar to the canonical stellar IMF which has therewith been deemed to be universal and invariant (fig. 1 in De Marchi et al. 2010).

Fig. 3 shows the canonical stellar IMF in comparison to a compilation of power-law mass function indices of different stellar populations,  $\alpha(\bar{m})$ , in dependence of the stellar mass range with average value  $\bar{m}$  over which they are constrained. The data are consistent with the canonical stellar IMF. At a given  $\bar{m}$  the  $\alpha$  values show a small and symmetric dispersion about the canonical index despite different observing teams providing the data and the measurement uncertainties. Together with the existence of the  $m_{\text{max}}(M_{\text{eci}})$  relation (Fig. 4), this is an indication (Kroupa et al., 2013) for the stellar IMF being an optimally sampled distribution function (no dispersion of  $\alpha$  values)

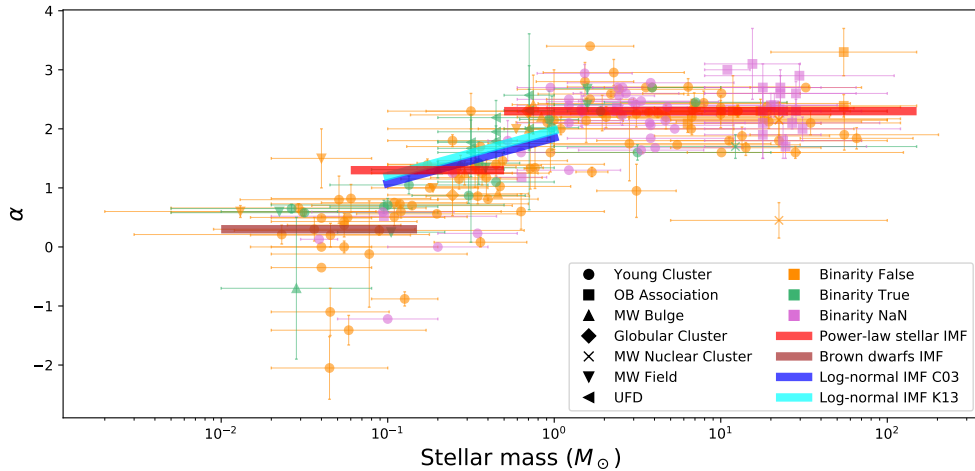


**Fig. 3** The alpha plot: The data points are the  $\alpha$  indices for various young populations in dependence of the stellar mass range over which they are observationally constrained with the  $\alpha$  index plotted at the mid-range value  $\bar{m}$  (from Kroupa 2001, 2002 and Hennebelle and Grudić 2024). The canonical stellar IMF is shown by the thick red lines while the brown dwarf regime ( $\alpha_0$ ) is indicated by the thick brown line. Both overlap for reasons given in Sec. 3.5. The canonical power-law form of the stellar IMF comes from a detailed star-count analysis using trigonometric *and* photometric surveys as described in the text. The systematic offset in the mass range  $0.1 - 1 M_\odot$  of the data compared to the canonical stellar IMF is due to unresolved multiple stars that hide faint companions in the orange data such that the observationally-deduced  $\alpha$  values are smaller than the real ones defining the canonical stellar IMF. The green data points have been corrected for unresolved multiple systems. There is no universal correction for unresolved multiple systems because the details of a binary population depend on their past dynamical history. The light-blue line is the log-normal fit to the canonical stellar IMF (eq. 10, from Kroupa et al. 2013, K13) while the dark blue line results from a reduced analysis of only the trigonometric parallax data (Chabrier 2003, C03). Adapted from fig. 26 in Kroupa et al. (2013), and fig. 1 in Hennebelle and Grudić (2024) which contains a representation of the log-normal IMF based on the 8 pc sample of nearby stars and ignores the constraints on stellar number densities from the deep photometric-parallax-surveys thus leading to a flatter IMF (i.e. smaller  $\alpha$  values).

rather than a probability distribution function that would lead to a larger dispersion of  $\alpha$  indices than evident in the data (see Sec. 5).

### 3 The origin of the IMF, the binary-star population and the sub-stellar regime

The properties of the stellar IMF and its relation to a freshly born stellar population in an embedded cluster depend on the dynamical structures in which stars form and on the feedback-self-regulated star-formation process. Understanding these provides the context to the galaxy-wide population of newly formed stars (Sec. 6).

#### 3.1 The dynamical structures in which stars form

Star formation occurs in spatially and temporarily correlated structures, i.e. in *molecular cloud clumps*, that developed to become gravitationally unstable and collapse. A minimum mass,  $M_J$ , for a gravitationally unstable region in a molecular cloud can be estimated using the Jeans instability criterion for characteristic densities in nearby molecular clouds. For a gas temperature of  $T = 10$  K, the sound speed in molecular hydrogen gas is

$$c_g = \left( k_B T / (\mu m_p) \right)^{1/2}, \quad (12)$$

where  $k_B$  is the Boltzmann constant,  $\mu$  the mean molecular weight and  $m_p$  the mass of a Hydrogen atom. For Solar abundance  $\mu \approx 2.4$  and  $c_{g0} \approx 0.063 T^{1/2} \approx 0.2$  km/s. According to the Jeans instability criterion, a region of a hydrogen molecular cloud with a density of  $\rho_{g0} \approx 10^3/\text{cm}^3$  becomes gravitationally unstable when its mass surpasses

$$M_J/M_\odot \approx 2 \left( c_g/c_{g0} \right)^3 \left( \rho_g/\rho_{g0} \right)^{-1/2} \quad (13)$$

within a spherical radius  $r_J/\text{pc} \approx 0.4 \left( c_g/c_{g0} \right) \left( \rho_g/\rho_{g0} \right)^{-1/2}$ . Overdense regions, the molecular cloud clumps, collapse on a free-fall time-scale,  $t_{\text{ff}}/\text{Myr} \approx 2 \left( \rho_{g0}/\rho_g \right)^{1/2}$ . Given the empirically determined life-times of molecular clouds of  $\delta t \approx 10$  Myr (Murray, 2011), ten times less-dense regions will not collapse. Less-massive cloud regions would need a higher density for collapse, and thus the smallest observed star-forming events are indeed in clumps of the above scale with a mass of a few  $M_\odot$  and diameters of less than a pc (e.g. the NESTs of



Joncour et al. 2018 in the nearest star-forming cloud Taurus-Auriga).

Because  $M_J \gg m_{\text{av}}$  an embedded cluster of stellar binaries always forms within  $r_J$ . Surveys of nearby molecular clouds show the youngest proto-stars to be highly clustered (e.g. Megeath et al. 2016 for the Orion star-forming clouds). An analysis of open star clusters based on the widest binary star orbits in them suggests that the embedded-star-cluster forming cloud clumps that are the progenitors of the open star clusters have half-mass radii at the stage of highest density of (Marks and Kroupa, 2012),

$$r_{0.5} \approx 0.1_{-0.04}^{+0.07} (M_{\text{ecl}}/M_{\odot})^{0.13 \pm 0.04}, \quad (14)$$

where  $M_{\text{ecl}}$  is the mass of the embedded cluster in stars. It's relation to the residual gas mass,  $M_g$ , within  $r_{0.5}$  is given by the canonical star-formation efficiency (SFE) of about  $\epsilon \approx M_{\text{ecl}} / (M_{\text{ecl}} + M_g) \approx 1/3$  (Lada and Lada 2003, e.g fig. 25 in Megeath et al. 2016). The deduced densities of the embedded clusters,  $\rho_{\text{ecl}} = (3 M_{\text{ecl}}) / (8 \pi \epsilon r_{0.5}^3)$ , are consistent with the observed molecular cloud clump densities. While this canonical value of  $\epsilon$  has been useful in understanding observed open and globular star clusters and their relation to embedded clusters, it is likely to decrease with increasing metallicity and to increase with increasing  $M_{\text{ecl}}$  (e.g. Dib et al. 2011; Megeath et al. 2016). Also,  $r_{0.5}$  is likely to be smaller at low than at high metallicity because the molecular cloud clump will have more time to collapse to a denser state before fragmenting. For a given  $M_{\text{ecl}}$ , it is thus likely that the stellar IMF emerging from the molecular cloud clump and  $r_{0.5}$  are correlated, but empirically this is not yet established. Since only about 10 per cent of the mass of a molecular cloud is in dense clumps (Battisti and Heyer, 2014), the overall star formation efficiency per molecular cloud is about 3 per cent.

In galaxies similar to the Milky Way, individual molecular cloud clumps and their embedded star clusters are unlikely to merge to form more massive clusters (Mahani et al., 2021, and references therein). The molecular clouds follow a mass–radius relation,  $M_{\text{mcl}}/M_{\odot} \approx 36.7 (R_{\text{mcl}}/\text{pc})^{2.2}$ . The free-fall time,  $t_{\text{ff}} = (3 \pi / (32 G \rho_{\text{mcl}}))^{1/2}$  with the density  $\rho_{\text{mcl}} = 3 M_{\text{mcl}} / (4 \pi R_{\text{mcl}}^3)$  such that  $t_{\text{ff}}/\text{Myr} = 1.37 (M_{\text{mcl}}/M_{\odot})^{0.18}$ . Under Milky Way conditions more massive clouds are therefore likely to form more, and more massive, individual embedded clusters. However, these take longer to fall towards each other the more massive the clouds are. Since the molecular cloud clumps turn into largely gas-free expanding very young star clusters within 1-2 Myr these do not have time to fall towards each other to merge. That most open star clusters in the Galaxy form singly and monolithically is also suggested by the analysis of the self-similar cluster structures in massive star-forming molecular clouds by Zhou et al. (2024b). In strongly interacting gas-rich galaxies the radii of molecular clouds are smaller for a given mass because the inter stellar medium is pressurised through the encounter, and this allows the massive embedded clusters to merge. If this occurs, the IMF of a merged cluster complex is the sum of the stellar IMFs in each pre-merger embedded cluster (Mahani et al. 2021, see also Sec. 7.3).

#### Embedded clusters

These space-and time-correlated star formation events within a molecular cloud can practically and stellar-dynamically be described as embedded star clusters (Lada and Lada, 2003) that form in gravitationally collapsing dense molecular cloud clumps ranging in mass from  $M_{\text{ecl},\text{min}} \approx 5 M_{\odot}$  to  $M_{\text{ecl}} > \text{many } 10^6 M_{\odot}$  in extreme star-burst galaxies where convergent gas flows create large localised gas densities.

Across all stellar masses, a proto-star grows to about 90 per cent of its final mass within about  $10^5$  yr (Wuchterl and Tscharnuter, 2003; Duarte-Cabral et al., 2013), with growth tapering out through the competition between the proto-star's feedback energy and outflow versus accretion (Adams and Fatuzzo, 1996; Dib et al., 2011). Within a time  $< 10^5$  yr the proto-star thus decouples from the hydrodynamical motions in its filament and becomes a ballistic pre-main-sequence star subject to strong gravitational forces in close encounters with other such pre-main sequence stars. Because the embedded cluster assembles over  $t_{\text{ff}} \approx \text{few Myr}$ , its dynamical state at the time when star formation ceases due to gas blow out can be approximated to be virialised. These early processes on a time scale of a Myr have important implications on observationally deducing an IMF as stellar-dynamical ejections, stellar mergers and binary-star disruptions affect the young stellar population rendering the stellar IMF as not being observable (Sec. 8). Stellar-feedback driven outflow of the residual gas leads to stellar-dynamical expansion of the embedded clusters forming, once the molecular cloud has dissolved, T-Tauri or OB associations with remnants of the expanded embedded clusters surviving as open star clusters (Kroupa, 2008). That young stellar populations are expanding has been confirmed by Guilherme-Garcia et al. 2023; Wright et al. 2024; Jadhav et al. 2024.

Given that the stellar IMF is directly linked to the birth of stars in molecular cloud clumps, it is natural to seek for its origin in the hydrodynamics of the molecular cloud clump. The inter-stellar medium (ISM) is a turbulent fluid, so the shape of the stellar IMF is likely to be influenced by the cascade of kinetic energy at different scales in the ISM. Incidentally, the power spectrum,  $P(k_p) \propto k_p^{-\gamma_p}$ , of this cascade is described by a power law with an exponent of  $\gamma_p = -5/3$  for subsonic turbulence, and by a log-normal form ( $\gamma_p = -2$ ) for supersonic turbulence. Similarly then, under this premise the stellar IMF may be described by a combination of these two functions, a power law and a log-normal form. This is the rationale for the gravo-turbulent theory for the stellar IMF, and a detailed study incorporating the structure of molecular clouds is provided by Elmegreen (2011). Under the gravo-turbulent theory, density peaks form in the shockwave fronts. These peaks, when dense enough, collapse to proto-stars. The stellar IMF can be deduced from the theoretical distribution of such peaks. But detailed simulations have shown that the low-mass density peaks are destroyed by the next shock before they can collapse to a proto-star. Therefore, it is implausible that the shape of the stellar IMF is driven by turbulence (Bertelli Motta et al., 2016). Furthermore, the gravo-turbulent theory of the stellar IMF is severely challenged by the observational result (e.g., André et al., 2014, see also Sec. 3.2) that stars form in thin molecular cloud filaments with near-regularly spaced proto-stars. Such structures are not compatible with the stochastic appearance of density peaks in a turbulent medium.

### 3.2 Emergence of the stellar IMF of late-type stars

Important progress in understanding the theoretical origin of the stellar IMF came with the observation that late-type stars mostly form in certain regions of molecular clouds, specifically, 0.1 pc-thick and up to 1 pc long, cold, kinematically coherent filaments (Larson, 1992; Myers, 2009; André et al., 2010). The detailed filamentary fine structure of the molecular cloud clump and its embedded proto-stars has been documented in one of the nearest star-forming embedded clusters by Hacar et al. (2017). Assuming that pre-stellar cores form in thermally virialised filaments and that the fragmentation of a filament depends only on the line mass-density (mass per unit length) of the parent filament the mass function of molecular cloud cores within which proto-stars form can be studied. A filament of total mass  $M_{\text{tot,fil}}$  and length  $L$  has a line-mass  $M_{\text{line}} = M_{\text{tot,fil}}/L$ . It evolves (or breaks up) into a set of overdensities, i.e. pre-stellar cores if the line mass is larger than the critical mass,  $M_{\text{line}} > M_{\text{line,crit}} = 2c_s^2/G$ , ignoring non-thermal motions and magnetic fields. Gas falls along the filament into these cores feeding the proto-stellar multiple systems forming there which self-regulates this accretion through feedback. The mass function of pre-stellar cores emanating from a system of molecular cloud filaments forming an embedded cluster is thus given by integration over the filaments (André et al., 2019),

$$\xi_{\text{psc}}(m_{\text{psc}}) = \int f_{M_{\text{line}}}(m_{\text{psc}}) w(M_{\text{line}}) g(M_{\text{line}}) d\log_{10} M_{\text{line}}, \quad (15)$$

where  $f_{M_{\text{line}}}(m_{\text{psc}})$  is the differential mass function of pre-stellar cores in a filament of line-mass  $M_{\text{line}}$ ,  $w(M_{\text{line}})$  is the relative  $M_{\text{line}}$ -dependent weight calculated from the pre-stellar formation efficiency and the line length, and  $g(M_{\text{line}})$  is the mass function of filaments, i.e. the differential number of filaments per unit length per unit log line mass. This allows André et al. (2019) to explore different toy models of filamentary structures and their relation to  $\xi_{\text{psc}}$ , with further details being available in Zhang et al. (2024). The relation of the core-mass function,  $\xi_{\text{psc}}(m_{\text{psc}})$ , to the stellar IMF,  $\xi(m)$ , depends on the role the feedback from the forming proto-stars plays in throttling the mass growth of a proto-star (e.g. Adams and Fatuzzo 1996; Dib et al. 2011, but the shape of the stellar IMF for late-type stars ( $m < 0.5 - 1.0 M_{\odot}$ ) appears to be largely set through the primary fragmentation of the filaments. A sufficiently long filament of uniform line-density will form similarly-spaced cores of similar mass. This theoretically suggests that the stellar IMF flattens at the low-mass end and may be a reason for  $\alpha_1 \approx \alpha_2 - 1$ . In very low-mass embedded clusters as observed in the Taurus-Auriga molecular cloud, the flattening may be even more extreme ( $\alpha_1 \approx \alpha_2 \approx 0$ , Luhman 2004. This star-forming region is spawning embedded clusters of very small mass (Joncour et al., 2018) in which the binary fraction remains high such (Kroupa, 1995a) the observationally-deduced IMF is still consistent with the canonical stellar mass (fig.7 in Thies and Kroupa 2007).

### 3.3 Emergence of the stellar IMF of early-type stars

At the intersection of filaments reside embedded clusters. Accretion rates along the filaments increase toward these intersections, reaching a peak in embedded clusters (e.g. Kirk et al. 2013. Indeed, the most massive stars form in concentrated regions in the centers of these embedded clusters (Kirk and Myers, 2011; Pavlík et al., 2019; Zhou et al., 2022). More massive stars thus appear to be formed through more violent accretion and dynamical processes in the densest regions of the embedded clusters and may not be related directly to the hydrodynamical evolution of individual filaments.

In an embedded cluster with a mass  $M_{\text{ecl}}$ , stars form with masses ranging from the metallicity dependent hydrogen burning mass limit  $m_{\text{H}}$  to a maximum stellar mass  $m_{\text{max}}(M_{\text{ecl}}) \leq m_{\text{max}^*}$  the empirically-determined upper limit of which is  $m_{\text{max}^*} \approx 150 M_{\odot}$  (Kroupa et al. 2013 and references therein). While the value of  $m_{\text{max}^*}$  is not fully understood, it is likely related to the feedback-self-regulation of accretion in connection with stellar stability. A metallicity dependence is expected but has not yet been confirmed. While stars with  $m > m_{\text{max}^*}$  have been observed, these are likely to result from stellar mergers that are common in initially binary-rich populations in the massive and dense embedded clusters (Banerjee et al., 2012).

Surveys of nearby molecular clouds and in the Large Magellanic Cloud uncover that the most massive star's mass,  $m_{\text{max}}$ , in an embedded cluster depends on the cluster's stellar mass,  $M_{\text{ecl}}$ . This  $m_{\text{max}} = m_{\text{max}}(M_{\text{ecl}})$  relation is shown in Fig. 4 and is probably the result of feedback-modulation of the fragmentation and accretion-growth of proto-stars, given the available mass in the molecular cloud clump (Yan et al. 2023 and references therein). The bolometric luminosities of molecular cloud clumps in a volume-complete survey of Galactic molecular clouds are well represented by a model in which the clumps are spawning embedded clusters with accreting stars optimally sampled (Sec. 5) from the canonical stellar IMF such that they obey this  $m_{\text{max}} = m_{\text{max}}(M_{\text{ecl}})$  relation (Zhou et al., 2024a). Thus, low-mass embedded clusters ( $M_{\text{ecl}} < \text{few } M_{\odot}$ ) cannot form stars more massive than a few  $M_{\odot}$  – as particularly evident in the Orion star-forming region (Hsu et al., 2012). A good approximation to the empirically gauged  $m_{\text{max}} = m_{\text{max}}(M_{\text{ecl}})$  relation (Fig. 4) can be obtained by solving the two equations,

$$1 = \int_{m_{\text{max}}}^{m_{\text{max}^*}} \xi(m) dm, \quad (16)$$

$$M_{\text{ecl}} = \int_{m_{\text{H}}}^{m_{\text{max}}} m \xi(m) dm, \quad (17)$$

that link the one most massive star in an embedded cluster to the mass in stars of the embedded cluster, respectively, for the normalisation constant and  $m_{\text{max}}$ . The initial stellar population in an embedded cluster thus depends on its mass through the  $m_{\text{max}} = m_{\text{max}}(M_{\text{ecl}})$  relation therewith constituting a variation of the stellar IMF without it changing its shape.

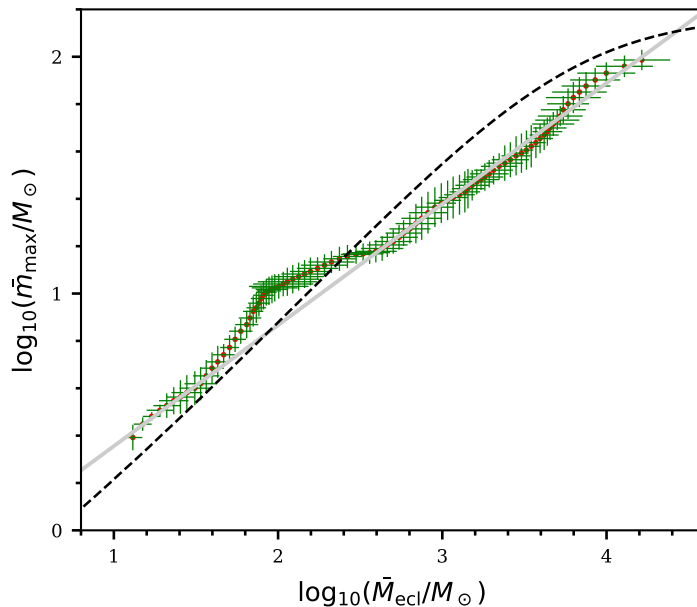


**Fig. 4** The observed correlation between the most-massive star,  $m_{\max}$ , and the stellar mass of the embedded cluster,  $M_{\text{ecl}}$ , for nearby very young populations. The red data points constitute a running-mean of the observational data with associated uncertainties in green. The grey line is a linear relation to emphasise the flattening near  $\bar{m}_{\max} \approx 10 M_{\odot}$  which may be related to feedback processes affecting the formation of ionising stars. The solution (dashed black line) to eqs. 16 and 17 for the canonical stellar IMF (eqs 5–8) is an adequate approximation to the data. The observational data have a dispersion of  $m_{\max}$  values at a given  $M_{\text{ecl}}$  which is consistent with the observational uncertainties leaving no evidence for an intrinsic dispersion (Weidner et al., 2013; Yan et al., 2023) indicating a deterministic self-regulated star-formation process within a molecular cloud clump (i.e. an embedded star cluster) suggesting optimal sampling to be physically relevant (Sec. 5). Adapted from fig. 6 in Yan et al. (2023).

#### Star formation is feedback regulated

The correlation  $m_{\max} = m_{\max}(M_{\text{ecl}})$  (Fig. 4) indicates that the star-formation process within an embedded cluster may be highly self-regulated, as is also implied by the small value of  $\epsilon$  (see also Sec. 4).

That feedback-self-regulation in an embedded cluster may be a dominant process rather than the Jeans mass in setting the stellar IMF has been considered theoretically by Adams and Fatuzzo (1996); Dib et al. (2011). Recent magneto-hydrodynamical simulations that take into account stellar feedback (e.g. Bate 2019; González-Samaniego and Vazquez-Semadeni 2020; Li et al. 2021; Grudić et al. 2022; Lewis et al. 2023) are approaching a high degree of realism but do not yet reach reliable predictions concerning the shape of the stellar IMF and its variation with physical conditions. Such numerical work needs to demonstrate realism by reproducing the observed star-formation activity in the nearby Taurus-Auriga molecular cloud in the form of the many small embedded clusters, or “NESTs” (Joncour et al., 2018). Also, simulations have not yet been able to reproduce the Orion Nebula Cluster (ONC). The ONC is the nearest star-forming site which formed and ejected ionizing stars (e.g. Kroupa et al. 2018; Jerabkova et al. 2019).

### 3.4 The binary-star population

Collapsing molecular cloud cores spin up and the contracting system’s angular momentum is shared between at least two proto-stars. Star-counts in about Myr old low-density populations show these to be dominated by binary stars such that the stellar-dynamical decay of initial triple or quadruple systems on their crossing-time scale of  $10^4 - 10^5$  yr requires the vast majority of stars to form as binary or hierarchical multiple systems (Goodwin et al., 2007; Moe and Di Stefano, 2017). Defining the binary fraction

$$f_{\text{bin}} = N_{\text{bin}} / (N_{\text{sing}} + N_{\text{bin}}), \quad (18)$$

where  $N_{\text{sing}}, N_{\text{bin}}$  are, respectively, the number of single and binary stars in the sample, stars at birth have  $f_{\text{bin}} \approx 1$  (Fig. 5). The birth distribution functions of the semi-major axes or periods,  $f_p(P)$ , mass-ratios,  $f_q(q)$ , and eccentricities,  $f_e(e)$ , of late-type binary systems, and their evolution with time are well understood (Kroupa, 1995b; Belloni et al., 2017). Most initial binaries have wide orbits (eqn. 46 in Kroupa et al. 2013) and companion masses randomly distributed from the canonical stellar IMF. This is qualitatively consistent with most late-type stars being born in fragmenting molecular cloud filaments (Sec. 3.2). Systems with orbital periods shorter than about a 1000 days tend

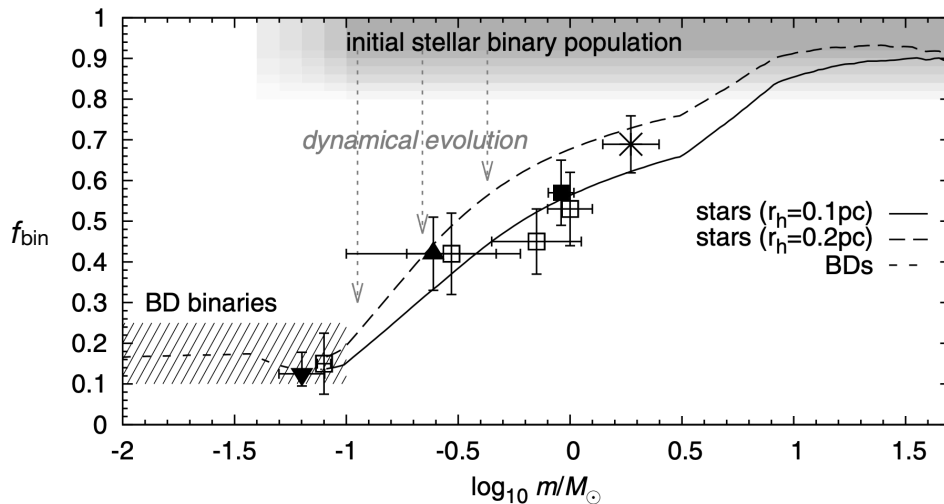


**Fig. 5** The binary fraction,  $f_{\text{bin}}$  (eqn. 18) as a function of the mass of the primary star. The extraction of the stellar IMF for any observed population of stars must carefully account for the different binary fractions in different environments and at different ages. Thus, after the vast majority of stars form as binaries ( $f_{\text{bin}} \approx 1$ ), the binary fraction decreases through stellar-dynamical processing in the embedded clusters they were born in. The value of  $f_{\text{bin}}$  decreases and depends on the time when the stars are observed, on the initial density of the embedded cluster (here indicated by the half-mass radius,  $r_h$ ) and on the mass of the primary because with a less-massive primary the binary system has a smaller binding energy and is more easily disrupted in the embedded cluster. The Galactic field population shown by the data (for details see fig. 6 in Thies et al. 2015) corresponds to the integrated population of about 5 Gyr old stars that stem from embedded clusters, while the early-type primaries ( $m > 1 M_\odot$ ) are young and have high binding energies and thus more directly indicate the high binary fraction at stellar birth. BDs (the shaded region indicates the uncertainty of their binary fraction) and very low mass stars ( $m < 0.2 M_\odot$ , VLMSs) appear to be a continuous extension of the stellar population but are in fact disjoint as explained in Sec. 3.5. From fig. 6 in Thies et al. (2015). Reproduced with permission.

to have similar-mass companions which can be understood in terms of pre-main sequence eigenevolution (fig. 17 in Kroupa 2008). The correction of star counts for unresolved stellar companions in any stellar population sensitively depends on how dynamically processed the observed population is (Fig. 5). For example, a population of late-type stars that came from Taurus-Auriga type NESTs would retain a high late-type binary fraction,  $f_{\text{bin}} \approx 0.8$ , while a population stemming from a dense embedded cluster similar or more massive than the ONC has  $f_{\text{bin}} < 0.5$  (Kroupa, 2008). This leads to a deduced apparent variation of the stellar IMF if not accounted for in surveys of different young stellar populations.

Stars more massive than  $\approx 1 - 5 M_\odot$  follow different pairing rules to late-type stars by having an initial distribution of periods that is significantly shorter and an initial mass ratio distribution with mass ratios  $q = m_2/m_1 > 0.1$  ( $m_1 > m_2$  being the primary and secondary star masses, respectively). Also, while most late-type stars form as star–star binaries, a large fraction of  $m \gtrsim 5 M_\odot$  stars appear to form in triple, quadruple or even higher-order systems (e.g. Moe and Di Stefano 2017, Kroupa and Jerabkova 2021 and references therein). This is probably related to early-type stars forming in the inner parts of more massive embedded clusters (Sec. 3.3). The significantly larger binding-energies of these massive star binaries and their preferred formation in the innermost regions of their embedded clusters leads to them being frequently violently stellar-dynamically ejected (Oh and Kroupa, 2016). The correction for unresolved multiple companions among the massive stellar binary population has a negligible influence on the deduced IMF power-law slope. But near the transition mass of about  $5 M_\odot$  where the initial multiplicity rules change, a dip in the observationally deduced IMF is expected (Kroupa and Jerabkova, 2018) even though the underlying stellar IMF is given by the canonical two-part power law form of Sec. 2.

The massive ( $m > 5 M_\odot$ ) part of the stellar IMF is thus subject to complicated biases: for example, star counts in very young clusters need to be corrected for the massive stars ejected from them. These corrections are substantial and depend on the mass of the young star cluster (Oh and Kroupa, 2016). Also, wind mass loss can affect the shape of the observationally deduced stellar IMF if not accounted for correctly, and because most massive stars reside in binary systems, rapid binary–stellar evolution affects the masses of the companions through mutual mass overflow and accretion (Schneider et al., 2015). The detailed shape of the stellar IMF for massive stars remains thus uncertain, although the canonical value,  $\alpha_{3,\text{can}} = 2.3$ , serves as a benchmark.

The knowledge documented above is essential for uncovering the shape of the stellar IMF, but it is strictly only valid for near-Solar metallicity. The properties of the birth distribution functions of binaries are largely unknown for star formation at low metallicity. This will hopefully change in the future as large space-based telescopes may reach sufficient resolving power to allow an assessment of the stellar populations in star-forming regions in nearby low-metallicity dwarf galaxies (e.g. Watts et al. 2018). Given observational data on a population of stars, the extraction of the birth functions,  $f_P(P)$ ,  $f_q(q)$ ,  $f_e(e)$ , depend on the properties of the embedded clusters they stem

from (Kroupa, 1995a,b). The relationship between these functions and the half-mass radii,  $r_{0.5}$ , of the embedded clusters at low metallicity need to be explored (e.g. Marks et al. 2022). The observational constraints available to-date indicate that the old field population with  $[Z] \approx -2$  has a similar binary fraction as the Solar neighbourhood ( $[Z] \approx 0$ , fig. 2 in Carney et al. 2005). If  $r_{0.5}([Z] \approx -2) < r_{0.5}([Z] \approx 0)$  (see Sec. 3.1) then this would indicate that  $f(P, [Z] \approx -2)$  would be compressed to smaller  $P$  if all stars also form as binaries at  $[Z] \approx -2$  in order to allow a sufficient fraction of the initial binaries to survive the dynamical processing in the denser low-metallicity embedded clusters.

### 3.5 Brown dwarfs

It is often thought that BDs constitute the low-mass end of the stellar population. But the probability that a density enhancement forms in a filament that is sufficiently low-mass and dense to undergo gravitational collapse without accreting gas to grow beyond  $m_H$  is very small so that BDs are unlikely to arise by primary fragmentation of filaments as stars do. The IMF that emerges through primary fragmentation of filaments thus falls off rapidly below about  $0.1 M_\odot$ , and in this context the observational finding that  $\alpha_{1, \text{Kirk}} \approx 0.25 < \alpha_1 \approx 1.3$  (Sec. 2) may be relevant.

The origin of the large number of observed BDs – about 1 BD per 4-5 stars – therefore lies in the same embedded-cluster-forming molecular cloud clumps but following different physical processes than those of stars (Thies et al., 2015). The hydrodynamical simulations of accreting proto-stars by Thies et al. (2010); Bate (2012) suggest BDs to mostly form through “peripheral fragmentation” at distances of many dozens to hundreds of AU from the proto-star. For BD–BD binaries the simulations yield  $f_{\text{bin, BD}} \approx 0.15$  with a narrow distribution of semi-major axes around a few AU and a power-law mass function of BDs with  $\alpha_{\text{BD}} \approx 0.3$  therewith being well consistent with the observed population. The very small fraction amongst stars of observed star–BD systems (the brown dwarf desert) comes about from the wide BD orbits becoming unbound through perturbations in the embedded cluster.

Understanding the properties of the initial binary population of stars and of BDs and the stellar-dynamical evolution of the initial binary population in embedded clusters is of essential importance for deducing the canonical IMF of stars and BDs. The high binary fraction ( $f_{\text{bin}} \approx 1$ ) in primary fragmentation of a filament (Sec. 3.4) leads us to the *BD vs star origins problem*:

#### The BD vs star origins problem I

BDs and very low mass stars (VLMSs) have significantly different binary properties than stars: **(ia)** most stars are born as star-star binaries **(ib)** with periods ranging from days to millions of years, while **(iia)** only a small fraction of BDs are in binary systems with **(iib)** a tight semi-major axis distribution around 5AU, **(iii)** star–BD binaries are rare.

Therefore corrections of star and BD counts for unresolved companions leads to the stellar IMF and BD IMF being distinct (Kroupa et al., 2013; Thies et al., 2015) while overlapping (see Fig. 7 below). Some VLMSs form by peripheral fragmentation as most BDs do, while some massive BDs form as stars from primary fragmentation of molecular cloud filaments. BDs thus form with stars but following their own IMF, qualitatively similar to planets forming along with stars but with their own mass distribution.

#### The BD vs star origins problem II

It is not possible to construct a population of stars and of BDs that fulfills the observed counts and at the same time the observed binary properties, unless stars and some of the massive BDs are treated separately from most BDs and some VLMSs in the initialisation. This is of critical importance for stellar and BD population synthesis.

While the ratio of BDs to stars probably varies with physical conditions (e.g. on metallicity, in the presence or absence of ionising radiation, see also Bate 2023), such a variation has not yet been documented in observed populations.

## 4 The variation of the stellar IMF

### 4.1 Theoretical considerations

The cooling rate of metal-rich gas is significantly more rapid than that of metal-free or metal-poor gas owing to the larger number of electronic transitions in the former (e.g. Ploekinger and Schaye 2020). Also, the sound speed,  $c_g$ , is smaller in metal-rich than in metal-poor gas due to the former’s larger molecular weight,  $\mu$ , implying a smaller  $M_J$ . A metal-rich gas filament in a cloud clump will thus fragment into a larger number of less-massive proto-stars than an otherwise identical but metal-free or metal-poor cloud clump, implying a stellar IMF that contains a preponderance of low-mass stars (i.e. being bottom-heavy) in the metal-rich case relative to the stellar IMF in the metal-poor case. The smaller sound speed in metal-rich than in metal-poor gas limits the accretion rate onto proto-stars, slowing their mass increase. At the same time, metal-rich gas increases the photon-to-matter coupling cross section such that accretion is also more restrained through radiation feedback from the accreting proto-star than in metal poor gas. A metal-poor molecular cloud clump is thus expected to produce an embedded cluster with a top-heavy stellar IMF (containing relatively more massive stars) relative to a metal-rich gas cloud. Additionally, magnetic fields (e.g. Krumholz and Federrath 2019) may play a role inducing an additional metallicity dependence through

the ionisation fraction in the cloud (removing an electron from a neutral H, C, Fe atom requires, respectively, 13.6, 11.3, 7.9 eV), cosmic rays from nearby supernova explosions lead to an increase in  $T$  within the cloud clump (Papadopoulos, 2010), and rotation of the molecular cloud clump affects its fragmentation behaviour. In sufficiently dense molecular cloud clumps, individual proto-stars may coalesce before they form individual stars, thus pushing the emerging stellar IMF to be top-heavy (e.g. Dib et al. 2007 for simulations). With the formation times being about  $10^5$  yr for low- and massive stars (Sec. 3.1), the density threshold of a molecular cloud clump above which the stellar IMF is likely to become top-heavy through this coalescence process can be estimated by equating the clump free fall time to  $10^5$  yr. This yields  $\rho_{\text{th,th}} \approx 4 \times 10^2 \rho_{\text{g0}} \approx 4 \times 10^5 / \text{cm}^3 \approx 10^4 M_{\odot} / \text{pc}^3$  such that molecular cloud clumps with significantly larger density ought to be forming embedded clusters with stellar IMFs that are noticeably top-heavy.

To attain a theoretical understanding of the change in the shape of the IMF with physical conditions remains an active area of research (e.g. Hennebelle and Grudić 2024). For example, Bate (2023) points out that the metallicity dependence through the cooling rate of gas of the stellar IMF may change with cosmic epoch given the evolving cosmological background temperature. The stellar IMF may have been bottom-light and top-heavy in the early Universe due to the higher temperature of the molecular gas being heated by the cosmic microwave background. This has been studied by Jermyn et al. (2018) in view of galaxies observed at a redshift  $z > 4$  appearing too massive in comparison to theoretically predicted ones. These authors suggest the stellar IMF to depend on the opacity, mean molecular weight,  $\mu$ , and ambient temperature,  $T$ , of the star-forming gas with the simplified form being given by

$$m_{s0} = 0.08 \left( \frac{T}{T_0} \right)^2, \quad m_{s1} = 0.5 M_{\odot} \left( \frac{T}{T_0} \right)^2, \quad m_{s2} = 1.0 M_{\odot} \left( \frac{T}{T_0} \right)^2. \quad (19)$$

where  $m_{s0}, m_{s1}, m_{s2}$ , the power-law indices  $\alpha_{1,2,3} = \alpha_{1,2,3,\text{can}}$  are as in eqns 5–8 and  $T_0 = 20$  K is the typical temperature of star-forming gas in the Galaxy. This parametrisation (in comparison to eqn. 28 below) thus allows the masses  $m_{s0}, m_{s1}, m_{s2}$  to change with  $T$  but keeps the power-law indices invariant. It is thus possible to calculate the stellar IMF as a function of redshift,  $z$ :  $\xi(m) = \xi(m : T(z))$ . This ansatz is used by Steinhardt et al. (2022) to calculate  $T(z)$  by fitting stellar population models generated with the above stellar IMF to observed galaxies to infer the evolution of  $T(z)$  which can be compared to the background temperature of the cosmic microwave background. These authors thereby implicitly assume the galaxy-wide IMF to be identical to the stellar IMF which need not be the case (Sec. 6). This ansatz needs to be explored further by allowing for the time-evolving distribution of molecular cloud clumps within a galaxy and their fragmentation into stellar IMFs in dependence of their cooling rate as well as  $T$ . Molecular clumps are expected to have different  $T$  (e.g. a clump heated by cosmic rays from a nearby star-burst embedded cluster vs an isolated one in the outer galaxy) such that the gwIMF will in general not equal the stellar IMF.

The empirical approach to testing if the stellar IMF varies with physical conditions does not readily provide access to  $T$  because when the stellar IMF of a given simple stellar population is constructed through star counts this information as been lost. Instead, the density of the molecular gas clump that formed the population can be estimated from the mass,  $M_{\text{ecl}}$ , of this population and from its estimated half-mass radius at birth,  $r_{0.5}$ . These quantities can also be directly compared to observed clumps in molecular clouds to test for consistency (Sec. 3.1). Another quantity related to the ability of the molecular gas to fragment is the metallicity of the stars that formed from the gas, and this metallicity,  $Z$ , is also a measurable quantity. Observational data can thus provide information on  $\xi(m) = \xi(m : M_{\text{ecl}}, Z)$ . Given such information, a composite or gwIMF can be calculated by integrating over  $M_{\text{ecl}}$  and  $Z$ . An additional dependency on  $T$  (via the embedded-cluster-forming molecular cloud clump's pressure) may emerge by comparing, for example, galaxies observed at a high-redshift with models of the same galaxies obtained by the integration over all molecular cloud clumps in a galaxy since its formation. Discrepancies that arise between the model based on the stellar IMF as formulated by eqn 34 below may inform on this dependency. In the next Sec. 4.2 evidence for a possible variation of the stellar IMF (i.e. on the cloud clump scale) is documented. The galaxy-wide problem is approached in Sec. 6.

Thus, in general, the stellar IMF can be written in terms of a dependency on a set of  $\{P_i\}^{N_p}$  physical parameters (e.g.,  $P_1 = M_{\text{ecl}}, P_2 = Z, P_3 = T, P_4 = \omega$  with  $\omega$  being the specific angular momentum of the molecular cloud clump), as

$$\xi(m : \{P_i\}^{N_p}) = k_{\xi} k_i m^{-\alpha_i(m : \{P_i\}^{N_p})}, \quad (20)$$

where  $k_i$  assure continuity and  $k_{\xi}$  is the scaling constant ensuring solution of eqs 16 and 17, and the power-law indices,  $\alpha_i(m : \{P_i\}^{N_p})$  are defined over some initial stellar mass ranges.

## 4.2 Empirical evidence

Do star-count data show evidence for a variation of the stellar IMF with cloud clump density, temperature and metallicity as implied by the above? For quantification purposes a few definitions are useful:

### The relative shapes of IMFs

Relative to the canonical stellar IMF, a *top-heavy stellar IMF* is defined to have

$$\alpha_3 < 2.3 = \alpha_{3,\text{can}}, \quad (21)$$

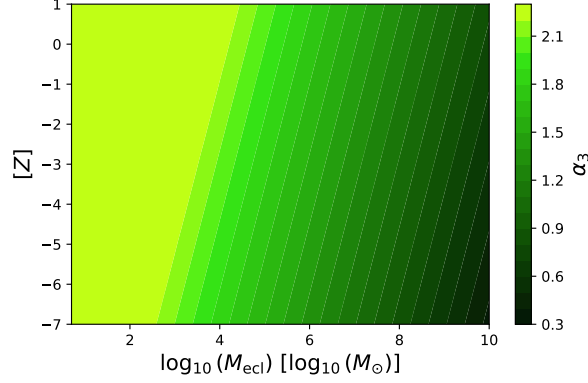


**Fig. 6** The colour coding shows  $\alpha_3$  values in dependence of  $[Z]$  and  $M_{\text{ecl}}$  (eqn. 25). The canonical value,  $\alpha_3 = 2.3$ , is obtained in the lightest green area on the left. The stellar IMF is increasingly top-heavy for smaller metallicity,  $[Z]$ , and larger stellar mass of the embedded cluster,  $M_{\text{ecl}}$ , whereby this figure demonstrates that  $\alpha_3$  mostly depends on the density of the molecular cloud clump, i.e. on  $M_{\text{ecl}}$ . Reproducible with the pyIGIMF software (Sec. 9).

while a *top-light stellar IMF* is defined to have

$$\alpha_3 > 2.3 = \alpha_{3,\text{can}}. \quad (22)$$

A *bottom-heavy stellar IMF* is defined to have

$$\alpha_1 > 1.3 = \alpha_{1,\text{can}}, \quad \alpha_2 > 2.3 = \alpha_{2,\text{can}}, \quad (23)$$

while a *bottom-light stellar IMF* has

$$\alpha_1 < 1.3 = \alpha_{1,\text{can}}, \quad \alpha_2 < 2.3 = \alpha_{2,\text{can}}. \quad (24)$$

A related definition is available through eqs 40–42 below.

The stellar population forming in the observable part of the Galaxy is limited to approximately Solar metallicity and embedded clusters with  $M_{\text{ecl}} < \text{few} \times 10^3 M_{\odot}$  in stars such that any variation of the stellar IMF will be limited and observational surveys have been confirming this.

The 1–4 Myr old and  $\text{few} \times 10^3 M_{\odot}$  heavy Orion Nebula Cluster is, with a distance of about 0.4 kpc, the closest post-gas-expulsion embedded cluster that formed stars more massive than  $10 M_{\odot}$ . It may have formed perfectly mass segregated implying that the stellar IMF would be radially dependent within the embedded cluster (Pavlík et al., 2019). This case however also demonstrates the complexity of the problem, because stellar-dynamical activity has already shot out a substantial number of massive stars such that the stellar IMF may have been top-heavy in the centermost regions where the mass density surpassed  $10^5 M_{\odot}/\text{pc}^3$  (Kroupa et al., 2018). A top-heavy stellar IMF is implied for the metal-poor star-burst R136 cluster ( $M_{\text{ecl}} \approx 10^5 M_{\odot}$ ) once the star-counts are corrected for the ejected massive stars (Banerjee and Kroupa, 2012), being supported by direct star counts in the 30 Dor star-forming region that harbours R136 (Schneider et al., 2018). Evidence for a systematic variation of the stellar IMF has been uncovered from the detailed analysis, taking into account the early gas-expulsion process, of globular star clusters and ultra-compact dwarf galaxies (UCDs), objects that formed more than a million stars (Marks et al. 2012, see also Dib 2023). The power-law index for the high-mass stellar IMF ( $1.00 \leq m/M_{\odot} < m_{\text{max}}$ ) is thus gauged by empirical data to depend on the density and metallicity of the star forming molecular gas cloud clump (Haslbauer et al. 2024 and references therein),

$$\alpha_3 = \alpha_3(M_{\text{ecl}}, Z) = \begin{cases} 2.3 & \text{for } x < -0.87, \\ -0.41x + 1.94 & \text{for } x \geq -0.87, \end{cases} \quad (25)$$

with

$$x = -0.14[Z] + 0.6 \log_{10} \left( \frac{M_{\text{ecl}}}{10^6 M_{\odot}} \right) + 2.82, \quad (26)$$

where  $M_{\text{ecl}}$  is the initial stellar mass of the embedded star cluster with half-mass radius  $r_{0.5}$  given by eqn. 14,  $[Z] \equiv \log_{10}(Z/Z_{\odot})$ ,  $Z$  is its metallicity mass fraction (of elements beyond H and He) and  $Z_{\odot} = 0.0142$ . This empirically-gauged stellar IMF becomes top-heavy in metal-poor and massive embedded clusters. Fig. 6 shows the dependency of  $\alpha_3$  on  $[Z]$  and  $M_{\text{ecl}}$ . Uncertainties remain in the exact formulation of the stellar IMF and it is possible that  $\alpha_3 > 2.3$  for  $x < -0.87$ . Given the range of data available, the above formulation captures the variation of the stellar IMF with density and metallicity for about  $-4 < [Z] < 0.2$  and  $5 < M_{\text{ecl}}/M_{\odot} < 10^9$  beyond which the uncertainties

are very major. This can be seen that formally  $\alpha_3 \rightarrow -\infty$  for  $Z \rightarrow 0$  (metal-free gas) which is unphysical. Indeed, the stellar IMF of the first stars (commonly referred to as the population III IMF) remains largely unknown (e.g. Klessen and Glover 2023). That  $M_{\text{ecl}}$  and  $Z$  may not be the only parameters that determine the shape of the stellar IMF is suggested by the metal-rich, high-density and strongly-magnetized star-forming region within about 0.1 pc of the Galactic center where Bartko et al. (2010) report a significantly top-heavy stellar IMF. Only massive pre-stellar cores can collapse if their collapse time is shorter than the time the differential rotation around the Galactic centre shears the clouds apart (Nayakshin and Sunyaev, 2005; Hopkins et al., 2024).

A tendency of the stellar IMF of late-type stars towards a bottom-light form for decreasing  $Z$  was noted by Kroupa (2002) from metal-poorer populations of stars in the Milky Way and its star clusters (see Yan et al. 2024 and references therein). A metallicity-dependency of the stellar IMF of late-type stars is supported by the spectroscopic analysis of 93000 Solar neighbourhood stars (Li et al., 2023). In combination with data from recent work on early-type galaxies, the stellar IMF for late-type stars ( $m < 1 M_{\odot}$ ) is gauged to depend on  $Z$  (Yan et al., 2024),

$$\alpha_{1,2} = \alpha_{1,2,\text{can}} + 79.4 (Z - Z_{\text{MW}}), \quad (27)$$

where  $\log_{10}(Z_{\text{MW}}/Z_{\odot}) = -0.10 \pm 0.05$  is the average metallicity of the Solar neighbourhood stellar ensemble. Metal-rich embedded star clusters ( $Z > Z_{\odot}$ ) thus produce a bottom-heavy stellar IMF in agreement with the constraints available from elliptical galaxies (Yan et al., 2024). A major uncertainty remains in this formulation for  $Z \rightarrow 0$ , with  $\alpha_1 \rightarrow 0.40$ ,  $\alpha_2 \rightarrow 1.40$ . The smallest mass that can form from direct collapse, the opacity limit ( $\approx \text{few} \times 10^{-3} M_{\odot}$ ), is given by the ability of the gas to radiate thermal photons as it collapses and is larger at low metallicity, but details remain unclear (e.g. Hennebelle and Grudić 2024). It is thus unknown how the IMF of BDs depends on  $Z$ , but additional effects such as a strong ionisation field from a top-heavy IMF and proto-stellar encounters are likely to play an important role (e.g., Kroupa and Bouvier 2003). Searches for BDs in globular star clusters will shed light on the variation of the shape of the sub-stellar IMF (e.g. Marino et al. 2024; Gerasimov et al. 2024).

#### The density and metallicity dependent stellar IMF

Given the available observational knowledge ( $N_p = 2$ ), the stellar IMF (eqn. 20) can be written in terms of a dependency on  $M_{\text{ecl}}$  (i.e. with  $r_{0.5}$  and  $\epsilon$  on the molecular cloud clump density) and  $Z$  as

$$\xi(m : M_{\text{ecl}}, Z) = k_{\xi} k_1 m^{-\alpha_1(m; M_{\text{ecl}}, Z)}, \quad (28)$$

where  $k_1$  assure continuity,  $k_{\xi}$  being the scaling constant ensuring solution of eqs 16 and 17 and the  $\alpha_1$  being given by eqns 25 and 27.

Note in comparison with eqn. 19 that this parametrisation allows the power-law indices to change with  $M_{\text{ecl}}$  and  $Z$  but keeps the masses  $m_{s0}, m_{s1}, m_{s2}$  invariant. The variation of the stellar IMF, the mass-ranges over which dominant physical processes in shaping it probably play a role and its relation to the sub-stellar population is visualised in Fig. 7. The dependency of the average stellar mass and of the most-massive star's mass on the mass in stars of the embedded cluster and on metallicity are displayed in Fig. 8. In reality more massive stars can appear through mergers of binary components in the young binary-rich clusters (Banerjee et al., 2012). The calculations show:

#### Massive star clusters as ionisation sources in the early Universe and as dark star clusters at super-Solar metallicity

At low metallicity, massive ( $M_{\text{ecl}} \gtrsim 10^7 M_{\odot}$ ) clusters have a stellar population with an average stellar mass  $m_{\text{av}} \gtrsim 10 M_{\odot}$  and would be significant ionising sources in the early Universe reaching quasar luminosities while appearing as UCDs today (Jeřábková et al., 2017). At high metallicity ( $[Z] > 0$ ), even massive clusters ( $10^4 \lesssim M_{\text{ecl}}/M_{\odot} \lesssim 10^8$ ) lack massive stars ( $m_{\text{max}} \lesssim 10 M_{\odot}$ ) suggesting that very massive "dark clusters" can form in star-bursts at high metallicity. Such objects might be mistaken as being diffuse and only of low mass if an invariant canonical stellar IMF is assumed in the analysis of the observations.

To help to assess how the stellar IMF dictates which embedded clusters are likely to remain bound after loss of mass through stellar evolution, the mass fraction in stars more massive than  $10 M_{\odot}$ ,

$$\eta = \frac{\int_{10 M_{\odot}}^{m_{\text{max}}} \xi(m : M_{\text{ecl}}, Z) m dm}{\int_{m_{\text{H}}}^{m_{\text{max}}} \xi(m : M_{\text{ecl}}, Z) m dm}, \quad (29)$$

is defined. When  $\eta > 0.5$  the cluster is likely to have dissolved when the last supernova has exploded (Fig. 9).

### 4.3 Discussion/caveats

The temperature dependence discussed in Sec. 4.1 is at least partially implicitly contained in eqs. 25 and 27 through the explicit density and metallicity dependence. Essentially, this formulation assumes that star formation always occurs at a similar low temperature near a dozen or two dozen K. It is not likely to be a complete description though because the pressure in the molecular cloud clump does not appear explicitly – a star-forming molecular cloud core of a given density and thus  $M_{\text{ecl}}$ -value can have different pressures depending on the temperature. For the time being no observational information exists on the dependency of this third parameter. It may be uncovered by comparing the gwIMFs calculated via the IGIMF theory (Sec. 6) with the stellar populations of observed galaxies for which  $T$  can be independently measured.



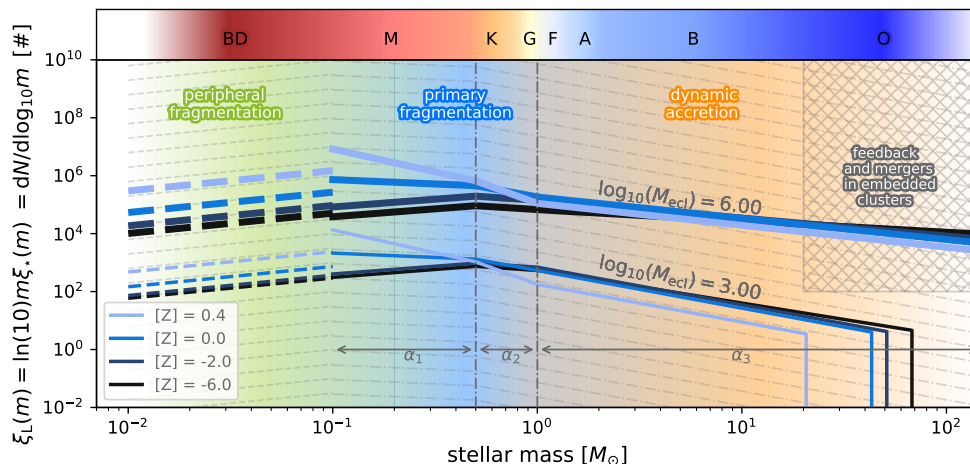


**Fig. 7** The possible physical origin of the shape of the stellar IMF and its variation as encapsulated by eqn. 28. BDs and some VLMSs form through peripheral fragmentation in the outer regions of proto-stellar accretion discs and late-type stars through primary fragmentation of molecular cloud filaments in the molecular cloud clump. Early-type stars increasingly (with larger  $m$ ) self-regulate their accretion in the molecular cloud clump and are also increasingly (with larger  $m$ ) subject to coalescence in the densest regions of the molecular cloud clump. The resulting stellar IMF becomes increasingly top-heavy for larger stellar mass of the embedded cluster,  $M_{\text{ecl}}$ , and for smaller metallicity,  $[Z]$ , and increasingly bottom-heavy for increasingly larger  $[Z]$ . The stellar IMFs are normalised such that the area under the stellar IMF corresponds to the number of stars and have no stars for  $m > m_{\text{max}}(M_{\text{ecl}})$ . The dependency of  $m_{\text{max}}$  on  $M_{\text{ecl}}, Z$  comes from the conditions given by eqs. 16 and 17. The sub-stellar IMFs are shown as the dashed lines which overlap with the stellar IMFs and are normalised such that they contain 1/4.5 the number of stars in their associated stellar population. For the late-type stars a dependency on the density of the gas cloud clump (via  $M_{\text{ecl}}$ ) is unknown, while for the BD IMF information on its possible dependency on  $M_{\text{ecl}}$  and  $Z$  is unknown. The thinner stellar and sub-stellar IMFs are computed for an embedded cluster with a stellar mass of  $M_{\text{ecl}} = 10^3 M_{\odot}$ , whereas the thicker lines represent computations for  $10^6 M_{\odot}$ . The color gradient of the IMFs from darker to lighter goes from lower to higher metallicity.

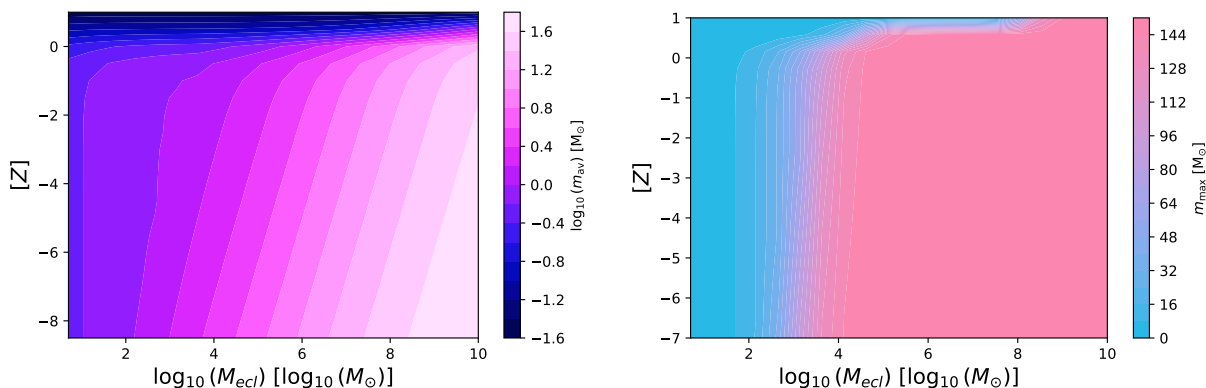


**Fig. 8** The dependency of the average stellar mass,  $m_{\text{av}}$  (eqn 11, left panel), and of the maximum stellar mass,  $m_{\text{max}}$  (eqs. 16 and 17, right panel), on  $M_{\text{ecl}}$  and  $[Z]$ . Reproducible with the pyIGIMF software (Sec. 9).

The dependency of the stellar IMF on the density and metallicity of the star-forming gas is thus still debated and not generally accepted. For example, Baumgardt et al. (2023) find 120 globular clusters (GCs) to have bottom-light IMFs but argue that a metallicity variation cannot be confirmed. As these are of low metallicity, this result does appear to be qualitatively consistent with eqn. 27. Baumgardt et al. (2023) also suggest GCs to have had more massive stars than provided by the canonical stellar IMF, again in qualitative agreement with eqn. 25. Dickson et al. (2023) perform pure stellar-dynamical modelling of 37 Galactic GCs arguing that the data and modelling finds no evidence for a variation of the stellar IMF with density or metallicity in contradiction to eqn. 25. The analysis of Galactic GCs is difficult because they have different Galactic orbits that determine the loss of low-mass stars and may depend on the metallicity as they reflect the formation process of the very young Galaxy. The very early embedded phase and the violent emergence from it also play a role in shaping a present-day GCs.

The stellar IMF dependency on density and metallicity as formulated by eqn. 25 rests on the analysis by Marks et al. (2012) who

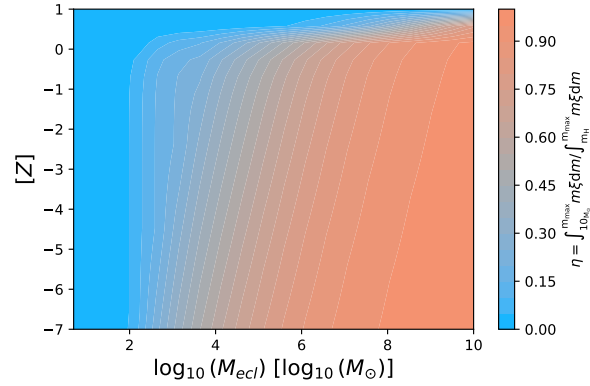


**Fig. 9** The mass fraction,  $\eta$  (eqn. 29), in stars more massive than  $10 M_{\odot}$  in an initial stellar population born in an embedded cluster as a function of its embedded cluster stellar mass,  $M_{\text{ecl}}$ , and its metallicity,  $[Z]$ . When  $\eta > 0.5$  the embedded cluster is likely to have become unbound after mass loss through stellar evolution. Values of  $\eta = 0$  arise through the  $m_{\text{max}} = m_{\text{max}}(M_{\text{ecl}})$  relation (Fig. 4) which has an implicit metallicity dependence through eqs. 16 and 17). Reproducible with the pyIGIMF software (Sec. 9).

used data for ultra-compact dwarf galaxies (UCDs), and the correlation between the concentration of 20 GCs and the power-law index of the stellar mass function at the half-mass radius of the GC where it represents the global stellar mass function of the GC (De Marchi et al. 2007 and references therein). The deficit of low-mass stars in GCs with lower concentration cannot be understood through stellar-dynamical evolution of GCs and is assumed instead to be due to a more top-heavy stellar IMF needed to violently expand the very young mass-segregated GC through feedback self-regulation in the formation process. This approach leads to a strong correlation between  $\alpha_3$ , the GC-forming molecular cloud clump density and  $[Z]$  (eqn. 25). Data on the dynamical mass-to-light ratios and on the numbers of low-mass X-ray emitting sources in UCDs are consistent with this variation, as are the star-count data in the sub-solar metallicity starburst region of 30 Doradus in the Large Magellanic Cloud (Schneider et al., 2018). The observed correlation of the dynamical mass-to-light ratios with metallicity of 163 GCs in the Andromeda galaxy is explained by the above density and metallicity dependency of the stellar IMF (Haghi et al., 2017).

Thus, while more data analysis in conjunction with very detailed stellar-dynamical and astrophysical understanding of the studied systems is required, overall the available information suggests that the stellar IMF may have a density and metallicity dependent form. Direct observational information on the stellar IMF's dependency on other parameters such as the rotation of the embedded cluster, magnetic field strengths and the temperature of the star-forming gas has not emerged yet.

#### Consistency Test on IMF variation

Any proposed formulation of the variation of the stellar IMF on the molecular cloud clump scale (i.e. in an embedded star cluster), such as formulated by eqn. 28, needs to pass two conditions:

- 1) The galaxy-wide IMF calculated from it (Sec. 6) must be consistent with the Solar neighbourhood constraint, i.e. the canonical field-star IMF (eqns 5–7 and 9).
- 2) The galaxy-wide IMFs constructed from it need to come out consistent with the observational constraints on the galaxy-wide IMFs in star-forming dwarf, major disk galaxies and elliptical galaxies (Fig. 14 below). This is addressed in Sec. 7.

The variation of the stellar IMF formulated by eqn. 28 fulfills both conditions.

## 5 Stochastic or optimal? The nature of the IMF

The physical evolution of star clusters and of galaxies critically depends on the nature of the stellar IMF. When an embedded star cluster forms in a molecular cloud clump, is the sequence of stellar masses that appear in it (I) purely random or (II) deterministic? The former case (I) means that forming stars do not influence each other and the stellar IMF must be interpreted as a probability density distribution function. The latter case (II) comes about if the forming stars influence each other such that the sequence of stellar masses is strictly determined by the initial conditions (e.g. mass, temperature, rotation, magnetic field) defining the clump. In this case the stellar IMF can be described as being an optimal distribution function (Kroupa et al., 2013). According to case (I), low mass clumps can contain massive ionising stars, while according to (II) this is never possible. Optimal sampling (case II) thus implies the possibility of dim but significant star formation occurring in a dark system. The mathematical procedures how to sample masses from the stellar IMF are described in detail in Kroupa et al. (2013), Schulz et al. (2015) and Yan et al. (2017). There are thus the two extreme interpretations (cases I and II) of the stellar IMF:

- (Ia) The stellar IMF is a probability density distribution function. This means that a model stellar population consists of an ensemble of  $N_s$  stellar masses randomly drawn from the stellar IMF (e.g. Maschberger and Clarke 2008). After choosing  $N_s$ , the stellar ensemble is constructed by randomly/stochastically drawing stellar masses from the stellar IMF until  $N_s$  stars are assembled. Stochastic sampling has no constraints apart from the shape of the parent distribution function, i.e. of the stellar IMF, and the number of stars drawn from the stellar IMF,  $N_s$ , defines the final mass of the population,  $M_{\text{stars}}$ , through the sum of the drawn stellar masses. Two populations of the same mass,  $M_{\text{stars}}$ , will thus contain different numbers and sets of stars. Consider the probability,  $X_{m_1}^{m_2}$ , of encountering a value for the variable  $m$  in the range  $m_1$  to  $m_2$ ,

$$X_{m_1}^{m_2} = \int_{m_1}^{m_2} p(m') dm', \quad (30)$$

with  $X_{m_H}^{m_H} = 0 \leq X_{m_H}^m \leq X_{m_H}^{m_{\text{max}}} = 1$ , and  $p(m) \propto \xi(m)$  being the probability distribution function. Inversion of the equation to the form  $m = m(X_{m_H}^m)$  provides the *mass generating function* which allows efficient random sampling of the stellar IMF with  $X_{m_H}^m$  being a random number distributed uniformly between 0 and 1. This approach is unphysical when applied to embedded clusters that form in molecular cloud clumps because their masses play no role in the sampling. That is, a molecular cloud clump would produce a number of stars that can add up to any arbitrary mass.

- (Ib) Random sampling of stars from the stellar IMF is physically more realistic if the mass of an embedded cluster in stars,  $M_{\text{ecl}}$  (i.e., the star formation efficiency times the mass of the molecular cloud clump), is imposed as a constraint because  $N_s$  is not a physically meaningful quantity but the molecular cloud clump mass is. That is, a molecular cloud clump of a given mass cannot spawn a population of stars that amounts to a larger mass than  $M_{\text{ecl}}$ . If  $M_{\text{ecl}}$  is applied as a mass-condition on the sampled population of stars, then stars are randomly drawn from the stellar IMF until  $\sum_{i=1}^{N_s} m_i = M_{\text{ecl}} \pm \delta M_{\text{ecl}}$ , where  $\delta M_{\text{ecl}} \ll M_{\text{ecl}}$  is the tolerance within which the sampling of the  $N_s$  stars is completed. This yields  $N_s$ . Case Ib thus has the stellar IMF being a conditional probability distribution function.
- (II) The alternative interpretation is that the stellar IMF is as an optimally sampled distribution function. Optimal sampling from a defined distribution function leads to no statistical scatter of the sampled quantity. This means that every embedded cluster of the same initial conditions (e.g.  $M_{\text{ecl}}$ ) spawns exactly the same, i.e. deterministic, content of stars without Poisson uncertainties upon arbitrary binning of the sampled stellar masses. The physical interpretation of this is that two embedded clusters that form from the same initial conditions  $\{P_i\}^{N_p}$  (Eqn. 20) also yield exactly the same sequence of stellar masses and is related to the star-formation process being strongly feedback regulated.

To sample a stellar IMF optimally for a given  $M_{\text{ecl}}$ , first eqns 16 and 17 are solved to obtain the IMF-normalisation constant and  $m_{\text{max}} \equiv m_1$ . The remaining stellar masses,  $m_i$ , in the embedded cluster are then obtained by calculating

$$1 = \int_{m_{i+1}}^{m_i} \xi(m) dm, \quad (31)$$

$$m_{i+1} = \int_{m_{i+1}}^{m_i} m \xi(m) dm. \quad (32)$$

An improved optimal sampling algorithm is provided by Schulz et al. (2015). The sampling stops when  $m_{i+1} < m_H$  yielding  $N_s$  stars.

Random sampling (case Ia) has been the method of choice in most models of star formation and galaxy evolution because, historically, embedded star clusters were not considered to be relevant building blocks of galaxies. Computer modelling of star formation in galaxies, for example, is simplest with this sampling method which applies no constraints. Statistically the same population of stars can be assumed to form anywhere where star formation can occur even if this means that fractions of supernova explosions need to be treated (see e.g. Steyrleithner and Hensler 2023 for a comparison of the implications of different sampling methods on galaxy evolution). Case Ia has been the backbone for interpreting extragalactic star-formation activity (e.g. eqn. 47 below). Evidence that the stellar IMF is a probability density distribution function is for example fielded by Corbelli et al. (2009) who find a randomly sampled IMF to provide the best fit to the young star-cluster sample of the galaxy M33. Dib et al. (2017) also concludes the IMF to be a probability density distribution function on the basis of an analysis of about 3200 star clusters from different surveys. Systematic errors (through large distances, resolution, photometry) and apparent variations caused by stellar ejections, stellar mergers and different binary fractions as a result of different dynamical histories of the individual stellar populations may contribute to this interpretation needing further study of this problem. Unconstrained stochastic sampling (case Ia) leads to the most massive star in an embedded cluster with a stellar mass  $M_{\text{ecl}}$ ,  $m_{\text{max}}$ , being independent of  $N_s$ . But a weak  $m_{\text{max}} = m_{\text{max}}(M_{\text{ecl}})$  relation emerges because  $m_{\text{max}}$  cannot be larger than  $M_{\text{ecl}}$ . The physical interpretation of this is that a molecular cloud clump fragments randomly into stars of arbitrary mass anywhere within it with the clump mass playing no role.

While unconstrained stochastic sampling is still much applied, an argument for embedded clusters being the fundamental building blocks of galaxies is the need to account for the binary fraction of  $f_{\text{bin}} \approx 0.5$  in the Solar neighbourhood in view of  $f_{\text{bin}} \approx 1$  in nearby star-forming regions: this difference is accounted for by the early disruption of initial binaries in their birth embedded clusters (see Fig. 5, Marks and Kroupa 2011). Direct infrared imaging surveys (Lada and Lada, 2003) also increasingly led to the realisation that molecular clouds spawn embedded clusters such that embedded star clusters are the fundamental building block of galaxies (Kroupa, 2005). Extra-galactic surveys of the fraction of stars in young star clusters in disk galaxies also suggest that stars primarily form in embedded clusters (Dinnbier et al., 2022). In constrained stochastic sampling (case Ib) stars are sampled randomly from the stellar IMF until a value for the mass of the embedded cluster is reached. A  $m_{\text{max}} = m_{\text{max}}(M_{\text{ecl}})$  relation exists because of this constraint (e.g. Stanway and Eldridge 2023). The scatter

of  $m_{\max}$  values produced with this sampling at a given  $M_{\text{ecl}}$  is however larger than allowed by the observational data (Fig. 4, Yan et al. 2023; Weidner et al. 2013).

Extragalactic data of young star clusters can be used to test if the stellar IMF is an unconstrained (case Ia) or a constrained (case Ib) probability density distribution function or if it is an optimal distribution function (case II) by comparing the values and the dispersion of the luminosities (e.g. in the  $H\alpha$  band, see Sec. 6.3, eqn. 47) of the models and data. In the past, an error occurred in this test if the random sampling from the stellar IMF imposes  $m \leq m_{\max}(M_{\text{ecl}})$  as a condition: the pitfall of this approach is that randomly sampling stars from the stellar IMF up to the  $m_{\max}$  value for a given  $M_{\text{ecl}}$  leads to a statistical underestimate of the average value of  $m_{\max}$ . This has been interpreted erroneously to mean that the  $m_{\max} = m_{\max}(M_{\text{ecl}})$  relation depicted in Fig. 4) is not generally valid (see Weidner et al. 2014 and references therein).

The (i) existence of a pronounced observed  $m_{\max} = m_{\max}(M_{\text{ecl}})$  relation (Fig. 4), (ii) the negligible intrinsic scatter of the  $m_{\max}$  values for a given  $M_{\text{ecl}}$  (Fig. 4, Yan et al. 2023; Weidner et al. 2013), and (iii) the lack of a significant intrinsic dispersion in the power-law index  $\alpha_3$  of the stellar IMF amongst many different young stellar ensembles (e.g. fig. 27 in Kroupa et al. 2013) suggest that stochastic sampling (cases Ia and Ib) is not a physically relevant method of discretising star formation. All three (i–iii) pieces of evidence are naturally consistent with the star formation process being described by optimal sampling (case II). Optimal sampling requires the existence of a strict  $m_{\max} = m_{\max}(M_{\text{ecl}})$  relation without intrinsic scatter. The observed relation is consistent with this and shows features possibly related to the regulation of the growth of stars through feedback (Fig. 4). Every ensemble of stars drawn from the stellar IMF will also yield exactly the same power-law indices such that any observed dispersion of, e.g.,  $\alpha_3$  values is only due to observational uncertainties, unrecognised multiple systems and stellar ejections and mergers. The small dispersion of observed  $\alpha_3$  values is consistent with this interpretation (fig. 27 in Kroupa et al. 2013).

As discussed in Sec. 3 the stellar IMF of late-type ( $m \lesssim 1.4 M_{\odot}$ ) stars appears to be given by the fragmentation of molecular cloud filaments which may be approximated as a random process (Fig. 7). This is consistent with these stars being born typically in wide binary systems with companion masses that are randomly drawn from the stellar IMF (Kroupa, 1995b). Feedback self-regulation of the star formation process and likely growth through coalescence of proto-stars in the dense central regions of sufficiently massive embedded clusters may make the stellar IMF an optimally sampled distribution function for larger stellar masses. This would suggest that the late-type stars of an embedded cluster may not be as mass segregated as the early-type ( $m \gtrsim 1.4 M_{\odot}$ ) stars are (Pavlík et al., 2019).

It may thus be possible that the nature of the stellar IMF is intermediate between cases (Ib) and (II) for  $m \lesssim 1.4 M_{\odot}$  and more closely related to case (II) for early-type stars. Magnetohydrodynamic simulations are being conducted to shed light on whether star formation is a stochastic or a physical process (e.g. Grudic et al. 2023). In terms of comparing models with observed systems, the case (II) interpretation leads to deterministic predictions that will appear to be stochastic through measurement uncertainties, multiplicity of stars, stellar ejections, mergers, and mass transfer in multiple systems.

## 6 The composite stellar IMF in galaxies across cosmic time – theoretical background

The stellar population in a region in a galaxy (e.g. the Solar neighbourhood) or in a whole galaxy is the sum of the star formation events that contributed to this population. This concept, introduced by Kroupa and Weidner (2003), leads to powerful results concerning observable properties of galaxies when combined with the  $m_{\max} = m_{\max}(M_{\text{ecl}})$  relation (Fig. 4), simply because galaxies or regions thereof that produce molecular cloud clumps of low mass only will have a deficit of massive stars. The consequences of this integration over star-forming regions strengthen if the physical parameters  $P_i$  (e.g. the gas density and temperature) upon which the stellar IMF depend vary with location in the system and with time. How to calculate the composite, regional or galaxy-wide IMF is discussed in the following sections.

In general, the composite IMF (cIMF) of all stars ever formed with masses in the range  $m$  to  $m + dm$  in a region of volume  $V$  can be formulated to be the integral over this volume and over time (cf. Hopkins 2018),

$$\xi_{\text{cIMF}}(m) = \int_V \int_P \int_t \xi_{\text{dens}}(m : \vec{r}, \{P_i\}^{N_p}, t) dV d^{N_p} P_i dt, \quad (33)$$

where  $dN = \xi_{\text{dens}}(m : \vec{r}, \{P_i\}^{N_p}, t) dV d^{N_p} P_i dt$  is the number of stars with masses in the interval  $m$  to  $m + dm$  formed in the volume  $dV$  at position  $\vec{r}$  (relative to some coordinate system defining the system) where the  $N_p$  physical parameters are in the range  $P_i$  to  $P_i + dP_i$  and in the time interval  $t$  to  $t + dt$ .  $P_i$  may be any or all of chemical composition, temperature, pressure, specific angular momentum of the molecular cloud clump, cosmic ray flux etc., and depend on the past history of the whole system, making this a non-linear and non-trivial problem.  $\xi_{\text{dens}}$  can then be interpreted as the stellar-mass-dependent rate per unit volume with which a localised region of volume  $dV$  turns gas into stars, given the physical conditions described by the set  $\{P_i\}^{N_p}$ .

Whether the stellar IMF is a probability density distribution function or an optimally sampled distribution function (Sec. 5) has fundamental implications on the nature and variation of the galaxy-wide IMF of stars (gwIMF) and on galaxy formation and evolution. In all cases, the shape of the stellar IMF which defines the mass-distribution of newly formed stars can depend on the physical properties of the star-forming gas (e.g. Fumagalli et al. 2011; Dib 2022). There are three broad formulations:

### 6.1 Case A

If the stellar IMF is an invariant probability density distribution function (case Ia in Sec. 5) then the gwIMF will also be an invariant probability density distribution function. This means stars form randomly throughout the galaxy at a rate given by the galaxy-wide or local SFR,  $\psi$  (herein always in  $M_{\odot}/\text{yr}$ ). With this assumption, each model galaxy needs to be computed a large number of times to assess the

range of variation of the outcome (e.g. the metallicity enrichment and the photometric properties differ between galaxies that have the same SFHs due to the different stellar populations in each galaxy, da Silva et al. 2014).

## 6.2 Case B

Assuming all stars from in embedded clusters, the stellar IMF is a conditional probability density distribution function with the constraint being given by the mass of the embedded cluster,  $M_{\text{ecl}}$  (case Ib in Sec. 5). The gwIMF needs to be calculated by adding all stellar IMFs in a galaxy of all embedded clusters (Kroupa and Weidner, 2003). This implies the need to describe where stars form in a galaxy because the mass an embedded cluster can reach depends on the local gas density (Pflamm-Altenburg and Kroupa, 2008). Strong evidence for this comes from the highly-significant dependency of the mass function of embedded clusters on the galactocentric distance in the galaxy M33 (Pflamm-Altenburg et al., 2013). The calculation of the gwIMF thus entails constrained probability distribution functions and for each model of a galaxy a large number of renditions need to be computed to assess that range of variability, as in Case A above.

## 6.3 Case C

If the stellar IMF is an optimal distribution function (case II in Sec. 5), then the gwIMF needs to be calculated by adding all stellar IMFs contributed by all embedded clusters in a galaxy (Kroupa and Weidner, 2003; Yan et al., 2017). Each galaxy needs to be calculated only once because there is no statistical dispersion. Thus a large range of parameters can be explored (e.g. the implications of using different stellar evolution models and/or element yield tables can be explored readily).

### 6.3.1 Case C: the galaxy as a point mass object

Treating a galaxy as a point mass object, eqn. 33 simplifies to an integral over all embedded clusters (Kroupa and Weidner, 2003): for all embedded clusters that form within a time span  $t, t + \delta t$ , the gwIMF contributed to the whole galaxy in this time interval is given by the integrated initial mass function of stars (IGIMF),

$$\xi_{\text{IGIMF}}(m; t) = \int_{M_{\text{ecl},\text{min}}}^{M_{\text{ecl},\text{max}}(\psi(t))} \xi(m \leq m_{\text{max}}(M_{\text{ecl}}) : Z) \xi_{\text{ecl}}(M_{\text{ecl}}) dM_{\text{ecl}}, \quad (34)$$

with the normalisation conditions eqs. 16 and 17 which together yield the  $m_{\text{max}} = m_{\text{max}}(M_{\text{ecl}})$  relation;  $\xi(m \leq m_{\text{max}}(M_{\text{ecl}}) : Z) \xi_{\text{ecl}}(M_{\text{ecl}}) dM_{\text{ecl}}$  is the stellar IMF contributed by  $\xi_{\text{ecl}}(M_{\text{ecl}}) dM_{\text{ecl}}$  embedded clusters with stellar masses in the interval  $M_{\text{ecl}}, M_{\text{ecl}} + dM_{\text{ecl}}$ .  $M_{\text{ecl},\text{min}} \approx 5 M_{\odot}$  corresponds to the smallest “embedded star-cluster units” observed (Sec. 3). Following eqn. 33,  $\xi(m)$  can depend on physical parameters such as  $Z$  and  $M_{\text{ecl}}$  (eqn 28). This variation is assumed to be valid in what follows. The embedded cluster mass function (ECMF),  $\xi_{\text{ecl}}(M_{\text{ecl}})$ , is usually taken to be a power-law probability distribution function, and in the Case C it is an optimally sampled function. Galactic and extra-galactic data suggest  $\xi_{\text{ecl}}$  to be reasonably well represented by a power-law function,

$$\xi_{\text{ecl}}(M_{\text{ecl}}) \propto M_{\text{ecl}}^{-\beta}, \quad (35)$$

with  $\beta \approx 2$ . Not much is known about the possible variation of the ECMF power-law index  $\beta$  with the physical properties of the inter-stellar medium of a galaxy, but it may become top-heavy with increasing SFR (e.g. Yan et al. 2017),

$$\beta = -0.106 \log_{10}(\psi / (M_{\odot}/\text{yr})) + 2.0. \quad (36)$$

A metallicity dependence of  $\beta$  would be naturally expected, but data on this are not yet available.  $M_{\text{ecl},\text{max}}$  follows from the maximum young star-cluster-mass vs SFR ( $M_{\text{ecl},\text{max}} = M_{\text{ecl},\text{max}}(\psi)$ ) relation. Weidner et al. (2004); Randriamanakoto et al. (2013) note that the maximum mass of a very young star cluster,  $M_{\text{ecl},\text{max}}$ , found in galaxies with different SFRs correlates strongly with  $\psi$ , the scatter of the data being smaller than expected from randomly sampling embedded cluster masses from the ECMF. A fit to the data yields (Kroupa et al. 2013 and references therein)

$$\frac{M_{\text{ecl},\text{max}}}{M_{\odot}} \approx 8.5 \times 10^4 \left( \frac{\psi}{M_{\odot}/\text{yr}} \right)^{0.75}. \quad (37)$$

A theoretical relation between  $M_{\text{ecl},\text{max}}$  and  $\psi$ , which is a good description of the empirical data, is obtained as follows: If a galaxy has, at a time  $t$ , a SFR of  $\bar{\psi}(t)$  over a time span  $\delta t$  over which an optimally sampled embedded star cluster distribution builds up with total stellar mass  $M_{\text{tot}}(t)$ , then there is one most massive embedded cluster,

$$1 = \int_{M_{\text{ecl},\text{max}}(\bar{\psi}(t))}^{M_{\text{U}}} \xi_{\text{ecl}}(M_{\text{ecl}}) dM_{\text{ecl}}, \quad (38)$$

with  $M_{\text{U}} \approx 10^{10} M_{\odot}$  being the physical maximum star cluster than can form, and

$$\bar{\psi}(t) = \frac{M_{\text{tot}}(t)}{\delta t} = \frac{1}{\delta t} \int_{M_{\text{ecl},\text{min}}}^{M_{\text{ecl},\text{max}}(\bar{\psi}(t))} M_{\text{ecl}} \xi_{\text{ecl}}(M_{\text{ecl}}) dM_{\text{ecl}}. \quad (39)$$

The time span  $\delta t$  is a “star-formation epoch”, within which the ECMF is sampled optimally, given a SFR. This formulation leads naturally to the observed  $M_{\text{ecl},\text{max}}(\bar{\psi})$  correlation if the “epoch” lasts about  $\delta t = 10$  Myr. This time-scale is consistent with the life-time of molecular clouds in normal galactic disks (Sec. 3). The power-law form for the ECMF (eq. 35 is an approximation stemming from a census of nearby

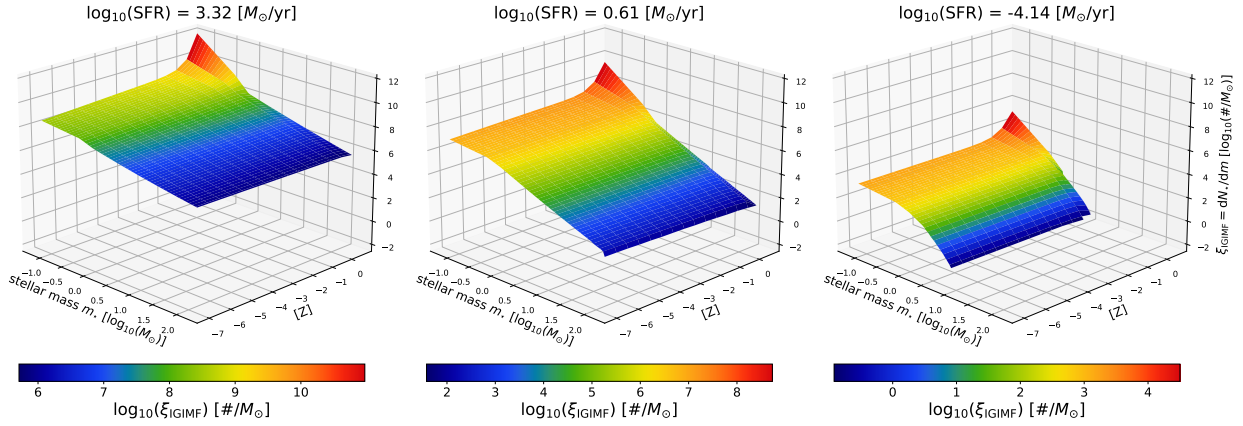


**Fig. 10** The Galaxy wide IMF (z-axis) calculated using the IGIMF theory (eq. 34) as a 3D surface function of stellar mass and metallicity, for three SFRs: an extreme starburst (left panel), a typical Milky-Way-like spiral galaxy (middle panel) and an extremely low SFR, as found in dwarf (irregular) galaxies (right panel). 2D slices of these surfaces are shown in Fig. 11, where they appear, respectively and with similar SFRs, in the bottom right, bottom left and top-left panel. In each panel the rainbow color-bar spans the highest and the lowest  $\log_{10}(\xi_{\text{IGIMF}})$  value in a isoluminant linear gradient. The red peak at high metallicity shows a strongly bottom-heavy gwIMF which is expected to be present in the inner regions of elliptical galaxies (Sec. 7.2). Reproducible with the pyIGIMF software (Sec. 9).

embedded star clusters (Lada and Lada, 2003) and extragalactic data (Weidner et al. 2004). The correct form, not yet implemented in IGIMF calculations, is to use a galaxy-wide ECMF which can be well represented by a Schechter function (Sec. 6.3.2).

The above equations under Case C formulate the “IGIMF theory” which allows the freshly formed stellar populations to be calculated in dependence of the galaxy’s metallicity and SFR. The gwIMF depends on the parametrisation of the dependency of the stellar IMF on the cloud-clump’s density and metallicity which has been improved over time. The galaxy-wide IMF calculated according to the IGIMF theory cannot be represented by a simple mathematical function, and grids of the gwIMF in  $Z - \bar{\psi}$  space are provided by Jeřábková et al. (2018) and Haslbauer et al. (2024).

#### Consistency Test of the IGIMF theory

An important result is that the IGIMF theory leads to the canonical field-star gwIMF (eqns 5-7 and 9) when the Milky Way conditions are reached ( $Z \approx Z_{\odot}$ ,  $\bar{\psi} \approx 1 - 3 M_{\odot}/\text{yr}$ ). This is a non-trivial but necessary outcome (Guszejnov et al., 2019) of the independently gauged stellar IMF (Fig. 11, eqn. 28).

The average stellar mass of all stars and the mass of the most massive star forming in a galaxy can be calculated by applying the IGIMF theory. The dependency of both quantities on the SFR and metallicity are displayed in Fig. 12. More massive stars can appear in galaxies through mergers of binary components in the young binary-rich populations (Banerjee et al., 2012). From this figure follows:

#### Galaxies as early ionising sources and galaxies with dark star formation

At high redshift and at low metallicity, galaxies with large SFRs ( $\bar{\psi} \gtrsim 10^2 M_{\odot}/\text{yr}$ ) have a stellar population with an average stellar mass  $m_{\text{av}} \gtrsim 50 M_{\odot}$  and would be significant ionising sources in the early Universe (Schaerer et al., 2024). At high metallicity ( $[Z] > \gtrsim 0.9$ ), even massively star-bursting galaxies ( $\bar{\psi} \gtrsim 10^2 M_{\odot}/\text{yr}$ ) lack massive stars ( $m_{\text{max}} < \text{few } M_{\odot}$ ) suggesting that at high metallicity galaxies can have profuse dark star formation. Such galaxies might be misinterpreted as having only a minor, if any, SFR if an invariant canonical stellar IMF is assumed in the observational analysis.

The change in the shape of the gwIMF relative to the canonical stellar IMF (eqn. 5–8) for different values of  $Z$  and  $\bar{\psi}(t)$  (Fig. 10 and 11) can be quantified by normalizing the functions to unity at a reference mass which is chosen to be  $m = 1 M_{\odot}$ . This then yields the normalized IGIMF,  $\xi_{\text{nIGIMF}}(m)$ , and the normalised canonical stellar IMF,  $\xi_{\text{ncan}}(m)$ ,

$$\xi_{\text{nw}}(m = 1 M_{\odot}) = 1, \quad (40)$$

where w=IGIMF or w=can (canonical). The shape of a gwIMF can thus be compared to that of the canonical stellar IMF as defined in Sec. 2 by calculating the surplus vs deficit of stars in different mass ranges. For example the ratio  $\zeta_{\text{I}}$  informs whether a gwIMF is bottom-light ( $\zeta_{\text{I}} < 1$ ) or bottom-heavy ( $\zeta_{\text{I}} > 1$ ) relative to the canonical stellar IMF,

$$\zeta_{\text{I}} = \frac{\int_{m_{\text{H}}}^{1 M_{\odot}} \xi_{\text{nIGIMF}}(m) dm}{\int_{m_{\text{H}}}^{1 M_{\odot}} \xi_{\text{ncan}}(m) dm}. \quad (41)$$

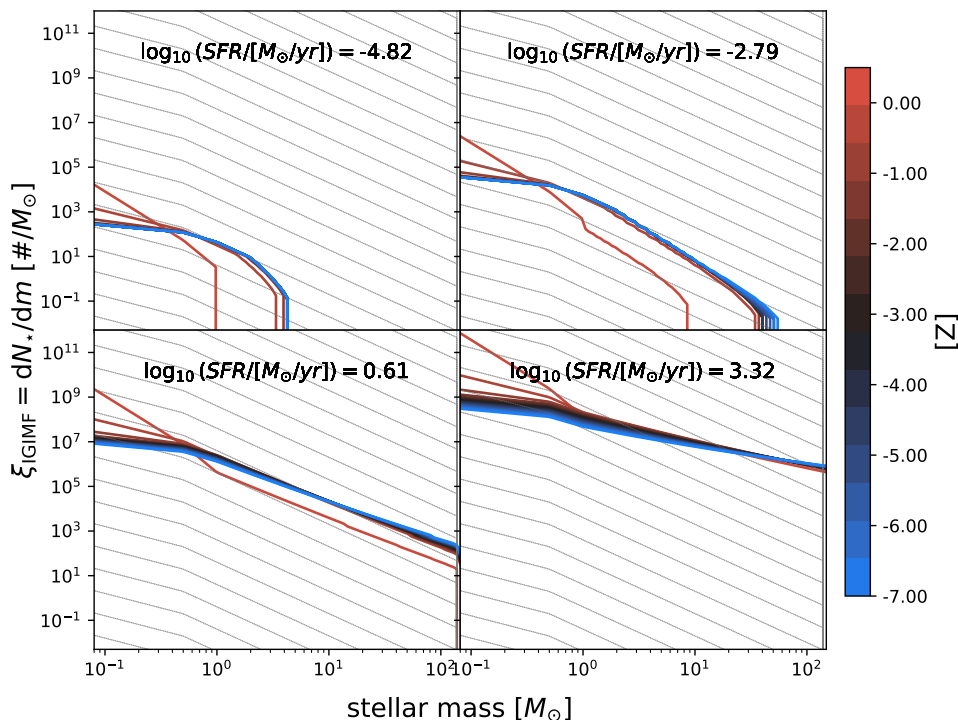


**Fig. 11** The shape of the gwIMF as encapsulated by the IGIMF theory (eqn. 34). The area under each gwIMF curve shows the total number of stars formed in a galaxy with the given SFR and metallicity in the time span of  $\delta t = 10$  Myr. The grey lines represent the canonical stellar IMF (eqs. 5–8). The gwIMFs become increasingly top-heavy for smaller metallicity,  $[Z]$ , and larger SFR, and bottom-heavy for increasingly larger  $[Z]$ . For example, a massive elliptical galaxy begins to form with a low SFR and low metallicity (*top left panel*: with a bottom-light and top light gwIMF), evolves through the *top right* and *lower left panel* with rising SFR and increasing  $[Z]$  and through to the *bottom right panel* where the top-heavy gwIMF leads to rapid chemical enrichment such that the gwIMF also becomes bottom-heavy, ending again at the *top left panel* with a decreasing SFR and a bottom-heavy gwIMF and large  $[Z]$ . Note that the *lower left panel* matches closely the gwIMF of the Galaxy, except for supersolar metallicities. Compare with the full 3D gwIMF surfaces shown in Fig. 10. Reproducible with the pyIGIMF software (Sec. 9).

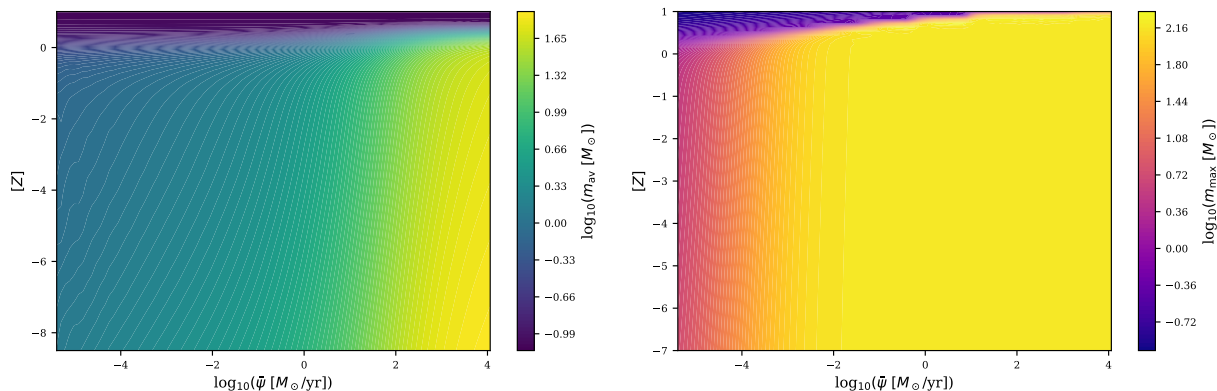


**Fig. 12** The dependency of the average stellar mass,  $m_{\text{av}}$  (left panel), and of the maximum stellar mass,  $m_{\text{max}}$  (right panel), of the forming stellar population in a galaxy on its SFR,  $\psi$ , and  $[Z]$ , assuming the IGIMF theory and calculated using galIMF (Sec. 9).

The following ratio informs if the gwIMF is top-light ( $\zeta_{\text{II}} < 1$ ) or top-heavy ( $\zeta_{\text{II}} > 1$ ) relative to the canonical stellar IMF,

$$\zeta_{\text{II}} = \frac{\int_{1 M_{\odot}}^{150 M_{\odot}} \xi_{\text{IGIMF}}(m) dm}{\int_{1 M_{\odot}}^{150 M_{\odot}} \xi_{\text{ncan}}(m) dm}. \quad (42)$$

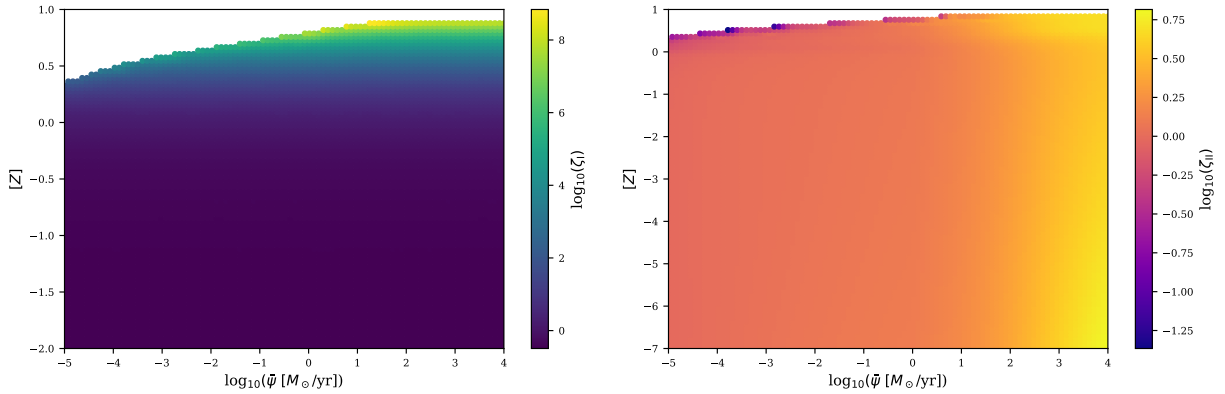


**Fig. 13** The variation of the shape of the gwIMF calculated according to the IGIMF theory (eqn. 34, calculated using galIMF, Sec. 9) in terms of the parameters  $\zeta_I$  (eqn. 41, left panel) and  $\zeta_{II}$  (eqn. 42, right panel). According to the IGIMF theory, the gwIMF is increasingly bottom-heavy (larger  $\zeta_I$ ) for increasing metallicity,  $[Z]$ , and increasingly top-heavy (larger  $\zeta_{II}$ ) for smaller  $[Z]$  and larger SFR,  $\psi$ . The values of  $\zeta_I, \zeta_{II}$ , are cutoff at the top because their gwIMFs do not have stars with  $m > 1 M_\odot$  such that the normalisation is undefined.

Fig. 13 demonstrates how  $\zeta_I$  and  $\zeta_{II}$  vary with metallicity and SFR.

Comparing different galaxies, the IGIMF theory leads to systematic differences in the specific (i.e. per galaxy-wide mass in long-lived late-type stars) rate of the production of various stages of evolved stars, of white dwarfs, core-collapse supernovae, and type Ia explosions (SNIa, Weidner and Kroupa 2005). The number of objects in a particular tracer population per late-type star depends on the SFH of the galaxy, not only through the particular history of  $\psi(t)$  but also through the gas density and metallicity dependent stellar IMF. This comes about because the shape of the gwIMF systematically changes as a galaxy evolves through a changing metallicity and SFR such that the relative fractions of stars being born in different stellar mass ranges change. An important new insight obtained from detailed chemical abundance modelling of elliptical galaxies is the need for the specific rate of SNIa explosions to evolve beyond this rescaling of the specific SNIa rate (Yan et al., 2021). Galaxies with a higher SFR need an “overproduction” of Fe through an overproduction of SNIa explosions compared to galaxies with smaller SFRs. Galaxies that reach large SFR values need an additional source of SNIa progenitors to explain their metal abundances. This is qualitatively consistent with the independent result obtained by Shara and Hurley (2002) based on stellar-dynamical modelling of a massive star cluster: massive star clusters overproduce hard binaries of degenerate remnants as a result of stellar-dynamical encounters. A galaxy can only form massive star clusters ( $M_{\text{ecl}} > 10^6 M_\odot$ ) if its SFR is sufficiently large ( $\psi \gtrsim 260 M_\odot/\text{yr}$ , eq. 37) such that the specific rate of SNIa events is boosted when  $\psi$  is large over galaxies with small SFRs. This problem needs further attention as it is important for understanding the detailed elemental abundances of elliptical galaxies.

### 6.3.2 Case C: the galaxy as an extended object

The above discussion neglects the spatial extent of a galaxy. The IGIMF theory can be formulated to calculate the *composite IMF* of a region in a star-forming galaxy, i.e. the “local IGIMF”. The theoretical development of this has not yet been much explored, but the ansatz available in Pflamm-Altenburg and Kroupa (2008) shows that the radial cutoff in  $H\alpha$  emission in galaxies that have extended-UV disks comes about because the mass of the most-massive embedded cluster decreases with the local gas density in the galactic disk. Outer regions of galactic disks can thus harbour dark ( $H\alpha$ -invisible) star formation. This follows because embedded clusters with smaller  $M_{\text{ecl,max}}$  in the outer galactic regions contain stars with masses  $m \leq m_{\text{max}}(M_{\text{ecl,max}})$ .

Introducing the *local ECMF* at position  $x, y$  in an axisymmetric rotationally-supported disk galaxy with the origin at its center,

$$\xi_{\text{lecl}}(M_{\text{ecl}}, x, y) = \frac{dN_{\text{ecl}}}{dM_{\text{ecl}} dx dy} \propto M_{\text{ecl}}^{-\beta}, \quad (43)$$

with the conjecture that the locally most massive embedded cluster depends on the local gas density,  $\Sigma_{\text{gas}}(x, y)$ , according to

$$M_{\text{lecl,max}}(x, y) = M_{\text{ecl,max}}(\bar{\psi}) \left( \frac{\Sigma_{\text{gas}}(x, y)}{\Sigma_{\text{gas},0}} \right)^\gamma, \quad (44)$$

where  $\Sigma_{\text{gas},0}$  is the gas density at the origin (assuming an axisymmetric galactic disk with an exponentially declining radial gas disk surface density) and  $M_{\text{ecl,max}}$  is the globally most-massive embedded cluster forming (in this particular application) at the center of the galaxy with a SFR,  $\bar{\psi}$  (eqs. 38 and 39). The star-formation rate density,  $\Sigma_{\text{SFR}}(x, y) \propto \Sigma_{\text{gas}}^N(x, y)$  with  $N \approx 1.0$ . The local IGIMF can thus be calculated using the same methodology as in Sec. 6.3.1 in each radial bin. However, eqn. 44 and the required value of  $\gamma = 3/2$  are merely an ansatz and this surface-density IGIMF approach needs deeper elaboration. That Case C is applicable in this approach is supported by the strong falsification of the random formation of star clusters in the disk of the galaxy M33 which shows a statistically highly significant decrease of the most-massive young cluster with radial distance (Pflamm-Altenburg et al., 2013). By assuming that the local ECMF is a power-law function (eq. 43), Lieberz and Kroupa (2017) showed that the integration over the galaxy yields an integrated galaxy-wide ECMF which



can be well approximated by a Schechter function.

According to this approach, interarm regions in spiral galaxies have a top-light local IGIMF relative to spiral arms in which the gas- and star-formation rate density are higher. This comes about because (i) the field is the addition of many embedded clusters each with a stellar IMF that (ii) extends to a most-massive star,  $m_{\max}(M_{\text{ec1}})$ , which is a function of the stellar mass of the embedded cluster,  $M_{\text{ec1}}$ , and (iii) massive embedded clusters are underrepresented in interarm regions (eqn. 44). This explains why  $\alpha_{3,\text{field}} > \alpha_{3,\text{can}}$  (Sec. 2). A lack of massive embedded star clusters may be an explanation for this difference because the Sun is in a region between spiral arms lacking star-forming activity (Vallée, 2018). The influence of the variation of the SFR on the deduced shape of the local composite (i.e. field) IMF is studied by Elmegreen and Scalo (2006).

Concerning pressure-supported (i.e. elliptical) galaxies their formation through the monolithic collapse of a pre-galactic primordial gas cloud needs to be modelled (Eappen et al., 2022). Every radially infalling volume element would be forming stars at a rate given by the gas density. A prescription related to the one used for axisymmetric disk galaxies above would be appropriate in terms of the locally most massive embedded cluster,  $M_{\text{ec1,max}}$ , in an infalling radial shell for some assumed radial gas density law. Qualitatively this leads to the result that the time-integrated local IGIMF will be more bottom-heavy and more top-heavy in the innermost regions of the galaxy, and will be bottom light and top-light in the outermost regions where the metallicity will remain low. No explicit modelling exists on this however, and will require analytical models of collapsing gas clouds that form stars throughout to be developed. Alternatively, the IGIMF theory needs to be incorporated into galaxy formation codes (e.g. as suggested by Ploekinger et al. (2014), Sec. 7.2).

#### Galactic building blocks

In conclusion, all three cases A, B and C link star-formation in molecular cloud clumps to the galaxy scale. Case A is the most elementary according to which star-formation in molecular cloud clumps is irrelevant. In Case B the stellar IMF is also a probability density distribution function but subject to the condition that star-formation occurs in embedded clusters of given masses. Cases A and B lead to two galaxies with the same SFH having different intrinsic properties. In Case C the stellar populations on the galaxy scale are calculated from the properties of the molecular cloud clumps assuming the stellar IMF to be an optimal distribution function, treating the embedded clusters as the fundamental building blocks of galaxies. Case C leads to two galaxies with the same SFH being identical.

## 7 Observational evidence

Observations of stellar populations in galaxies provide important constraints on galaxy evolution models. These depend on cosmological theory and also on assumptions concerning the gwIMF. The stellar IMF forms on the molecular clump scale (Sec. 5), but observations relate to galaxy-wide scales.

An important constraint is provided by the stellar population in the Milky Way and is discussed in Sec. 6.3. An independent test of the Galaxy's gwIMF comes from microlensing events towards the inner Galaxy. This test relies on the phase-space distribution of all components of free-floating planets, brown dwarfs, stars, stellar remnants (and if existing, of dark matter) and on knowledge of the Galactic potential which is directly linked to this distribution. Available constraints on the brown dwarf and stellar gwIMFs are broadly consistent with the canonical form (eqn. 5–8, e.g. Koshimoto et al. 2021). These constraints are subject to uncertainties from the varying stellar IMF which has not been accommodated in the data analysis, the formation history which remains largely unknown, the presence of stellar streams, and the Galactic potential in the inner Galaxy which depends on the mixture of unseen mass in various forms.

Considering these factors, the available extragalactic information that may connect the molecular cloud clump and the galaxy-wide scales is explored next.

### 7.1 Late type / star-forming galaxies

Massive stars die after a few Myr and because many are evident in galaxies these need to replenish their gas content to continue forming stars. In order to quantify the rate with which stars are being born from the gas various tracers of the star formation activity are employed (for a complete overview see Zezas and Buat 2021). Massive stars ionise the gas in their wider vicinity which recombines with emission of  $\text{H}\alpha$  photons. By relating the  $\text{H}\alpha$  flux to the number of ionising massive stars and with an assumed shape of the gwIMF it is possible to calculate the total mass of stars formed per unit time within the life time of the massive stars. This is the basis of an often employed method to measure the SFRs of nearby galaxies.

Following Pflamm-Altenburg et al. (2007), the number of ionising photons a stellar population of a galaxy emits in the time interval  $\delta t$  can be calculated from

$$N_{\text{ion},\delta t} = \int_{m_{\text{H}}}^{m_{\text{max,g}}} \xi_x(m) N_{\text{ion},\delta t}(m) dm, \quad (45)$$

where  $\xi_x(m)$  can be, for example, the invariant canonical stellar IMF (eqn. 5–8) or the IGIMF (eqn. 34).  $N_{\text{ion},\delta t}(m)$  is the number of ionising photons a star of mass  $m$  emits in a time interval  $\delta t$ . The energy of one  $\text{H}\alpha$  photon is  $L_{\text{H}\alpha} = 3.0207 \times 10^{-12}$  erg and  $\mu_r$  is the fraction of these that lead to recombination ( $\text{H}\alpha$ ) emission in the surrounding gas (typically  $\mu_r = 1$  is adopted). It follows that

$$L_{\text{H},\alpha} = \mu_r 3.0207 \times 10^{-12} \text{ erg } N_{\text{ion},\delta t} / \delta t. \quad (46)$$

The  $\psi = \psi(L_{H\alpha})$  relation follows by calculating  $L_{H\alpha}$  via eqn. 45 and 46 which links the IMF with the SFR via eqn. 39.

By assuming the gwIMF to be an invariant probability distribution function (see Sec. 5) and of Miller and Scalo (1979) form (which is comparable to the canonical stellar IMF, see Kroupa et al. 2013) such that it always retains the same fraction of ionising stars relative to all stars formed, Kennicutt (1983) applied the linear relation

$$\psi = L_{H\alpha} / (1.12 \times 10^{41} \text{ erg/s}) M_{\odot}/\text{yr} \quad (47)$$

to quantify the SFRs of 170 nearby galaxies therewith quantifying, among other properties, gas consumption time scales and establishing this as the method of choice for subsequent research.

An often practiced approach is thus to assume Case A in Sec. 6.1 such that star-formation is a stochastic process in disk and dwarf galaxies and the gwIMF is an invariant probability distribution function (e.g. da Silva et al. 2014). According to this approach, all galaxies will be alike statistically in terms of their properties except for an increasingly large dispersion of these towards smaller galaxy masses. However, more recent surveys of hundreds of nearby galaxies have shown that star-forming dwarf galaxies lack the emission of ionising radiation relative to that expected for an invariant canonical stellar IMF (Lee et al., 2009). Similarly, massive disk galaxies have been found to have an overabundance of ionising stars (Gunawardhana et al., 2011). The authors of these observational studies discuss possible effects that may mimic such a variation with the underlying gwIMF being of Case A. Dust obscuration and reddening is unlikely to be the culprit of an apparently increasing lack of massive stars with decreasing SFR because galaxies with small SFRs are dwarfs that are of lower-metallicity than their Milky-Way-type counterparts. A loss of ionising radiation in the dwarf galaxies (i.e. a small value of  $\mu_r$  in eq. 46), and thus a decrease in the  $H\alpha$  recombination flux, appears unlikely because dwarf galaxies have significantly larger gas fractions than their more massive counterparts (fig. 4 in Lelli et al. 2016). It is also unlikely that the gwIMF is invariant with the expectation being that over a long-time-average dwarf galaxies have the same number of ionising stars relative to late type stars as their more massive counterparts. This would require the more than 100 galaxies with  $\psi < 10^{-2} M_{\odot}/\text{yr}$  in the sample of Lee et al. (2009) to currently have dropped their SFRs in-phase with each other despite not being in causal contact and being separated by a few Mpc. An invariant, stochastically sampled gwIMF is favoured by Kennicutt and Evans (2012).

In contrast, the evidence based on isotopologue data suggest galaxies with high SFRs at different redshifts to have top-heavy gwIMFs (Zhang et al., 2018). Further evidence for a top-heavy gwIMF through very early metal enrichment at high redshifts ( $9.4 < z < 10.6$ ) is being studied based on JWST data (e.g. Curti et al. 2024; Kobayashi and Ferrara 2024).

Thus, if the gwIMF varies according to the IGIMF theory (eqn. 34) then the proportionality between  $L_{H\alpha}$  and  $\psi$  (eqn 47) does not hold because dwarf galaxies with small SFRs lack ionising stars, i.e., for every  $H\alpha$  photon they emit, many more low-mass stars are forming in them than in major disk galaxies that have gwIMFs that are comparable to the canonical form or are even top-heavy (e.g. Fig. 11). This leads to the SFRs deduced using eqn 47 to be significantly too small for late-type dwarf galaxies and too large for late-type massive galaxies. In combination with the data by Lee et al. (2009) and Gunawardhana et al. (2011), this suggests that the gwIMF is increasingly top-light with decreasing SFR (for  $\psi < 1 M_{\odot}/\text{yr}$ ), while it becomes increasingly top-heavy with increasing SFR (for  $\psi > 1 M_{\odot}/\text{yr}$ ).

Indeed, the calculation of the SFR-dependent gwIMF using the IGIMF theory (Case C in Sec. 6.3) predicts a dependency of the gwIMF on the SFR with dwarf galaxies having a gwIMF with a deficit of ionising stars and disk galaxies with  $\psi > 1 M_{\odot}/\text{yr}$  having a top-heavy gwIMF consistent with the observational constraints (e.g. Haslbauer et al. 2024). The radial cutoff in  $H\alpha$  emission despite star-forming galaxies having extended UV disks also follows from the IGIMF theory (Sec. 6.3.2). Therewith the IGIMF theory passes an important observational test demonstrating the power of bridging the formation of stellar populations on the molecular clump scale to extragalactic data. A number of important theoretical implications arise from this if the true gwIMF is correctly represented by the IGIMF theory:

- Dwarf galaxies with  $\psi < 10^{-3} M_{\odot}/\text{yr}$  have a significant deficit of ionising stars relative to their UV fluxes that are a measure of the number of intermediate-mass stars (Fig. 13, Pflamm-Altenburg et al. 2009). Given observed  $H\alpha$  recombination fluxes, the true SFRs of late-type dwarf galaxies are significantly larger such that their gas-consumption time scales become comparable to those of major disk galaxies being near 3 Gyr. This result implies that star-forming galaxies of all masses need to be accreting gas at a rate comparable to their SFRs to sustain their near-constant SFHs with implications for cosmological theory (Haslbauer et al., 2023, 2024).
- The systematically evolving gwIMF leads to a theoretical stellar-mass–metallicity relation of galaxies over the galaxy-mass range  $10^4 M_{\odot}$  to  $10^{13} M_{\odot}$  matching the observed one of galaxies very well without the need of outflows of enriched gas from galaxies (Haslbauer et al., 2024).
- Traditionally, models with an invariant gwIMF have estimated, by eqn. 47, small SFRs for dwarf galaxies, suggesting it would take longer than the age of the universe (a Hubble time) for these galaxies to build up their observed stellar masses, as indicated by their B-band magnitudes. This has been a known long-standing problem. The application of the IGIMF theory, however, suggests that dwarf galaxies have higher true SFRs. This results in shorter timescales for these galaxies to accumulate their observed stellar masses, resolving the known problem (Pflamm-Altenburg and Kroupa, 2009; Haslbauer et al., 2024).
- The significantly larger true SFRs of dwarf galaxies (assuming the gwIMF is given by the IGIMF theory) implies that dwarf and major disk galaxies have had approximately constant SFRs with implications for the interpretation of the Lilly-Madau plot of the redshift-dependent star-formation rate density in a comoving cosmological volume in terms of Gpc-scale cosmological structure (Haslbauer et al., 2023).
- With the implied significantly larger true SFRs of dwarf galaxies, and the implied smaller true SFRs of massive disk galaxies (the IGIMF theory predicting them to have top-heavy gwIMFs), the main sequence of galaxies flattens significantly (Haslbauer et al., 2024).
- Gas-rich dwarf galaxies can have  $H\alpha$ -invisible, i.e. dark, star formation appearing as intergalactic gas clouds with little traces of star formation (Pflamm-Altenburg et al., 2007).

**Cosmological implications of the IGIMF theory**

These implications demonstrate how an understanding of the gwIMF and its variation connects stellar populations to the cosmological arena.

**7.2 Early type galaxies (ETGs), high-redshift galaxies and ultra-faint dwarfs (UFDs)**

ETGs, or more specifically elliptical galaxies, are often associated with cooling flows that appear to deposit a large amount of gas in their inner regions the fate of which remains unknown (Fabian et al. 2024 and references therein). One way to assess if it turns into faint low-mass stars is to use spectroscopic features that are sensitive to the gravitational field strength in the photospheres of stars to assess the dwarf to giant star ratio (Kroupa and Gilmore, 1994). Matteucci (1994) developed a chemical enrichment code to calculate models of elliptical galaxies and deduced, given observational constraints on the alpha-element over iron,  $[\text{Mg}/\text{Fe}]$ , ratio that these formed within a time of about  $3 \times 10^8 M_\odot$  and with a top-heavy gwIMF. Less-massive elliptical galaxies formed over a longer time scale than more massive ones. Vazdekis et al. (1996) also developed an elaborate model for calculating the chemical enrichment and spectro-photometry and applied it to three well observed ETGs. The result of this work is that these ETGs formed in a short phase lasting less than a Gyr with a top-heavy gwIMF with some star formation continuing over a longer time with a bottom-heavy gwIMF. Modern observational surveys using stellar surface-gravity-sensitive spectroscopic indices confirm the result that elliptical galaxies typically have significantly bottom-heavy gwIMFs (e.g. Ferreras et al. 2013 based on data for 40000 ETGs). This can be combined with lensing and dynamical constraints (see Smith 2020 for a review). These constraints however suffer from the degeneracy that faint late-type stars and stellar remnants appear as dark matter that is thought to dominate galaxy masses. It needs to be kept in mind that the inner regions of elliptical galaxies constitute high-density environments such that the long-lived late-type stars may have formed from and accreted over time heavily enriched gas such that the templates and stellar model libraries used in the above modelling that relies on surface-gravity-sensitive spectral indices may not represent the true stellar population. In the Solar neighbourhood the stars have been existing in a very different low density gas environment with significantly less-intense chemical enrichment.

The high alpha-element abundances of elliptical galaxies imply these to have formed within typically a Gyr, with the more massive ones forming more rapidly (referred to as *downsizing*) and with star formation over the past few Gyr adding negligible stellar mass (Thomas et al., 2005; Salvador-Rusiñol et al., 2020). Their solar and super-solar metallicity implies the gwIMFs to have been top-heavy (Matteucci, 1994; Vazdekis et al., 1996). The constraints on the stellar and stellar-remnant content of elliptical galaxies, paired with the small mass-to-light ratios of high-redshift galaxies needed for consistency with cosmological structure formation theory (see Haslbauer et al. 2022) suggest elliptical galaxies to have formed with bottom-heavy and top-heavy gwIMFs (van Dokkum and Conroy, 2024), thus confirming the findings by Matteucci (1994) and Vazdekis et al. (1996).

Interestingly, the application of the IGIMF theory (Sec. 6.3) to the problem of forming and evolving elliptical galaxies leads to consistency with these constraints including those from ultra-faint dwarf galaxies (UFDs, Yan et al. 2021, 2024). Elliptical galaxies thus appear to have formed monolithically on a gravitational collapse time which leads to the downsizing relation of formation time vs mass (Eappen et al., 2022). The observed increase of the dynamical mass-to-light ratios of elliptical galaxies with increasing mass follows from the top-heavy gwIMFs having not only produced the large metallicity and thus a bottom-heavy gwIMF but also a very significant mass in remnants (Dabringhausen and Kroupa, 2023). Massive elliptical galaxies may in reality be a few to ten times more massive than implied when using an invariant canonical gwIMF. Given the downsizing times over which ETGs formed a correlation emerges naturally within the IGIMF theory: ETGs with a larger stellar velocity dispersion have a more top-heavy and a more bottom-heavy gwIMF than ETGs with a smaller velocity dispersion as these have a smaller mass formed over a longer time and thus with a smaller SFR.

The survey by La Barbera et al. (2019) of seven elliptical galaxies used stellar surface-gravity sensitive absorption lines in the empirical EMILES spectral library to model the radial dependency of the stellar population. The results show a pronounced radial gradient with the innermost regions of the galaxies by characterised by very bottom-heavy local gwIMFs while the outermost parts have a canonical IMF of late-type stars. This is qualitatively consistent with the expectations of the IGIMF theory (Sec. 6.3.2).

According to the IGIMF theory the gwIMF is very bottom-heavy at  $[Z] > 0$  such that even high SFRs remain dark (Fig. 12). This may suggest a solution to the above mentioned cooling flow problem.

Empirical evidence for the gwIMF having been top-light and thus lacking massive stars in galaxies that had very low SFRs as calculated using the IGIMF theory is evident from detailed chemical evolution studies of the very old dwarf-spheroidal satellite galaxies (e.g. Mucciarelli et al. 2021; Tang et al. 2023).

Concerning the UFDs, these are resolved into individual stars such that the problem with using the correct stellar luminosity-mass relation is critically important. The published stellar mass functions for these need to be revisited in view of theoretical stellar luminosity-mass relations being incorrect (see Fig. 2). The prediction from the IGIMF theory is that the gwIMF in UFDs is bottom-light due to the low metallicity and that is was top light due to the small SFR. (Yan et al. 2024 and references therein).

**7.3 Ultra compact dwarf galaxies (UCDs) and globular star clusters (GCs)**

UCDs are typically many Gyr old and ten to a hundred times as massive as GCs and show a large range of dynamical mass-to-light ratios. These and their photometric properties can be readily understood (Mahani et al., 2021):

- UCDs with large dynamical mass-to-light ratios formed through a monolithic collapse as embedded clusters. These had very top-heavy IMFs (eqn. 28) leaving a population of stellar remnants in the object that have a mass that is up to ten times larger than the mass in main sequence stars. When less than about 50 Myr old, the monolithically-formed UCDs attained luminosities comparable to high-redshift

quasars (Jeřábková et al., 2017).

- Those UCDs that have GC-like dynamical mass-to-light ratios can be understood to have formed from the amalgamation of many star clusters in star-cluster complexes as are observed to be forming in massively interacting galaxies. These latter UCDs have stellar populations as obtained though applying the IGIMF theory (Sec. 6.3).

GCs are many Gyr old and have been thought to be simple stellar populations thus having formed monolithically in very massive molecular cloud clumps as massive embedded clusters ( $M_{\text{ecl}} > 10^5 M_{\odot}$ ). The observational finding that many GCs have sub-populations of stars that have different chemical abundances and also a small degree of spread in Fe suggests this understanding of their formation to be challenged with currently no consensus existing on their formation and the emergence of these multiple populations. The significant, and sometimes dominant, fraction of the enriched population poses a problem for nearly all chemical enrichment scenarios. This problem may however disappear if GCs do form monolithically with only one simple stellar population which, however, is binary-rich and with a top-heavy stellar IMF (eqn. 28). The stellar-dynamical encounters during the formation process of the stars lead to mergers between massive binary-star components and the winds from the massive stars expell synthesised elements into the interstellar medium in the young GC. Stars forming in the vicinity will thus be enriched to different degrees with light elements before core-collapse supernovae quench further star formation (Wang et al. 2020 and references therein). The quenching is not sudden and the first core-collapse supernovae enrich the gas from which stars are still forming with Fe accounting for the observed Fe spreads (Wirth et al., 2022). The top-heavy stellar IMF accounts for the large fraction of enriched stars through the many enrichment events, and the large embedded cluster mass ensures that massive-star feedback alone cannot remove the gas with gas removal needing mutple core-collapse supernova events (fig. 3 in Baumgardt et al. 2008).

## 7.4 Supermassive black holes

The formation and early appearance of supermassive black holes (SMBHs) remains a major area of research. The IMF of population III stars appears to be relevant for this problem (Klessen and Glover, 2023). A possible solution follows from elliptical galaxies and bulges forming on a free-fall time from primordial pre-galactic gas clouds (Eappen et al., 2022). The central region of such a collapse undergoes a star burst as a UCD-type nuclear cluster. Since elliptical galaxies and bulges more massive than a few  $10^9 M_{\odot}$  formed with  $\psi \gtrsim \text{few } M_{\odot}/\text{yr}$  this most massive cluster (eq. 37) has a mass  $M_{\text{ecl,max}} \gtrsim \text{few } 10^5 M_{\odot}$ . It has a quasar-like luminosity (Sec. 7.3) due to the top-heavy stellar IMF because of the low initial metallicity and very high density (eqn. 28). When the intense radiation field of this cluster collapses after the massive stars die the cluster contains more than  $10^5$  stellar-mass black holes (BHs) and neutron stars. Gas falling into this cluster compresses it until the BHs orbit at relativistic speeds such that they radiate gravitational waves and the BH cluster collapses. SMBHs weighing more than  $10^5 M_{\odot}$  can thus form within a few hundred Myr at the centres of forming elliptical galaxies and bulges and their masses correlate with the masses of the hosting galaxies by the IGIMF theory (Kroupa et al., 2020).

## 7.5 The combined extragalactic evidence

The various studies of star-forming dwarf and major (disk) galaxies, faint satellite galaxies and of massive elliptical galaxies suggest that the gwIMF changes as follows: with increasing SFR the gwIMF becomes increasingly top-heavy. At very low metallicity the gwIMF becomes bottom light which is evident in faint dwarf satellite galaxies. This is shown graphically in Fig. 14. The IGIMF theory accounts for this naturally without having been developed to do so as it primarily rests on the observations of nearby and resolved star forming regions and stellar populations. Other interpretations of the observational data insisting the gwIMF remains invariant (e.g. through a systematic current lull in the SFRs across all gas rich dwarf galaxies, a fine-tuned loss of ionising photons, particularly designed dust obscuration) have been suggested (Sec. 7.1) but do not naturally lead to the observed trend shown in Fig. 14.

### Extragalactic evidence for the variation of the gwIMF

From Fig. 14 it is clear that the extragalactic data and the IGIMF theory inform us that the gwIMF is top-light for  $\psi \lesssim 1 M_{\odot}/\text{yr}$  and top-heavy for  $\psi \gtrsim 1 M_{\odot}/\text{yr}$ .

## 8 Existence statement

For modelling the evolution of star clusters and galaxies initial distribution functions are required for the initialisation of the stellar population. These are the stellar IMF,  $\xi(m)$ , and the birth distribution functions defining the binary population in terms of the primary-star-mass ( $m_{\text{prim}}$ ) dependent fraction of stars born as binaries or multiple systems,  $f_{\text{bin/mult}} \approx 1$ , their distribution of periods,  $f_P(P : m_{\text{prim}})$ , their distribution of mass ratios,  $f_q(q : m_{\text{prim}})$  and eccentricities,  $f_e(e : m_{\text{prim}})$  as well as the birth half-mass radius,  $r_{0.5}(M_{\text{ecl}})$ , of the embedded cluster this population with a stellar mass of  $M_{\text{ecl}}$  is born in.

It is useful to keep in mind that these functions do not exist in reality because stars form over a few free-fall times,  $t_{\text{ff}}$ , of their proto-embedded cluster, they experience stellar-dynamical encounters within it and are ejected from it within a fraction of  $t_{\text{ff}}$  such that an embedded cluster neither ever contains all the stars born in it nor is there ever a time when an observer can, by direct star-counts, construct the above distribution functions.

By being mathematical descriptions of in reality non-existing functions, they are mathematical *hilfskonstrukts*, i.e., auxiliary functions needed for the mathematical description of idealised initial conditions (for example, models usually assume all stars to be born instantly

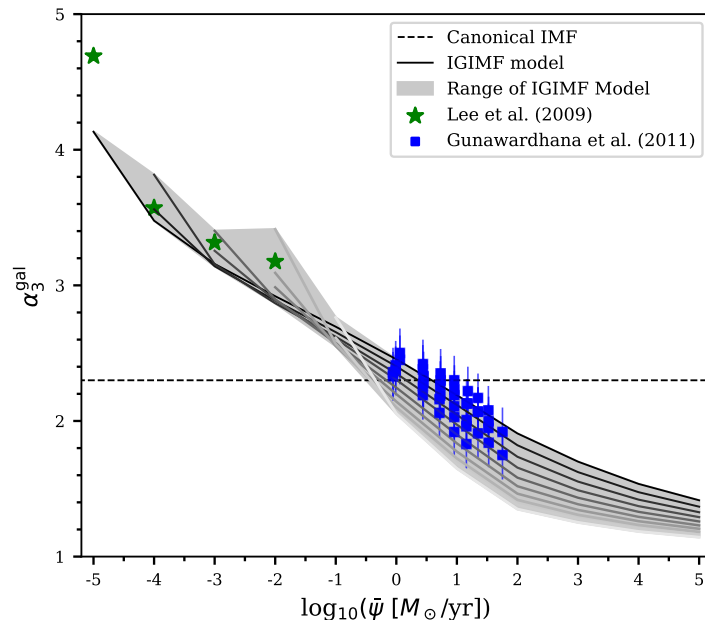


**Fig. 14** The variation of the shape of the IMF of stars forming in a galaxy with a SFR  $\bar{\psi}$  (the average SFR in a time interval of  $\delta t = 10 \text{ Myr}$ ). The green stars are from the observational survey of Lee et al. (2009) of nearby dwarf galaxies, the blue squares are from the survey of major disk galaxies by Gunawardhana et al. (2011). The shaded/grey region gives the gwIMFs calculated with the IGIMF theory for different stellar mass ranges and metallicities. It shows the shape of the gwIMF in terms of its stellar-mass-dependent power-law index,  $\alpha_3^{\text{gal}}$ , that represents the gwIMF for stars more massive than  $1 M_\odot$  as a function of the galaxy-wide SFR,  $\bar{\psi}$ . For a given SFR and at each  $m$  value, there exists a different  $\alpha_3^{\text{gal}} - \bar{\psi}$  relation because the gwIMF cannot be represented by a small set of power laws (see Fig. 11) but can be approximated by power-law sections with indices that change with the stellar mass,  $m$ . The solid lines are for mass ranges centred on  $m/M_\odot = 1.58, 2.51, \dots, 100$  from dark to light. Elliptical galaxies formed with  $\bar{\psi} > 1000 M_\odot/\text{yr}$  with top-heavy gwIMFs that are needed to account for their Solar and super-Solar metallicities and high  $[\alpha/\text{Fe}]$  ratios (Yan et al., 2021). The horizontal dashed line is the invariant canonical gwIMF (eq. 8) which would be valid if the stellar IMF were an invariant probability density distribution function. The survey data reproduce the IGIMF-theory quantitatively and do not support an invariant probability density distribution nature of the IMF. Adapted from fig. 6 in Yan et al. (2017). A depiction of the variation of the gwIMF for low-mass stars in observational extragalactic data in comparison to the IGIMF-theoretical calculation is available in fig. 4 in Yan et al. (2024).

for their initialisation in the computer). These hilfskonstrukts are needed because the construction of a realistic stellar population in an embedded cluster, let alone a whole galaxy, is not possible using magneto-hydrodynamical radiation-transfer computer simulations of sufficient resolution for star formation. Although these functions cannot be constructed through direct observation, they and their possible dependency on the physical parameters,  $\{P_i\}_P^N$ , of the star-forming molecular cloud clump, can be inferred from the observed properties of stars.

## 9 Computer codes

As the shape of the IMF is essential information, estimators for the exponent and upper limit with goodness-of-fit tests for truncated power law distributions have been compared and published by Maschberger and Kroupa (2009). The estimators covered include binning, the cumulative distribution, Beg's estimator and the maximum likelihood estimator. The package `STARPL` is downloadable from the Astrophysics Source Code Library<sup>2</sup>

Nearly all galaxy and cosmological structure formation simulation codes assume Case A (Sec. 6) such that fractions of supernovae can occur at small SFRs (e.g. one tenth of a supernova producing one tenth of the enrichment and one tenth of the explosion energy can occur if the IMF is undersampled such that it includes fractions of stars). An implementation into the adaptive mesh-refinement `FLASH` code of the IGIMF theory (Case C) by Ploekinger et al. (2014) and Steyrlleithner and Hensler (2023) such that only full stars are allowed demonstrated that dwarf galaxies form significantly more stellar mass over time than when an invariant canonical gwIMF is assumed which produces more feedback through fractions of stellar winds and fractions of core-collapse supernovae than the top-light gwIMF computed with the

<sup>2</sup><https://ascl.net/1206.006>

IGIMF theory. These ideas are likely to have important implications for galaxies forming in a cosmological context (see Sec. 7.1).

Various publicly-available computer programs have been written to model stellar populations under different assumptions Case A, B and C (Sec. 6). A few such codes are mentioned here:

For Case A, the LIBIMF C-library is available to set up a stellar population according to a pre-chosen stellar IMF (Pflamm-Altenburg and Kroupa, 2006) downloadable from the Astrophysics Source Code Library<sup>3</sup>. the STARBURST99 code has been much used to model starbursts for pre-chosen stellar IMFs (Leitherer et al., 1999)<sup>4</sup>. The PEGASE3 code is available for a similar purpose (Fioc and Rocca-Volmerange, 2019)<sup>5</sup>.

For Cases A and B, the binary population and spectral synthesis (BPASS) programme<sup>6</sup> has been developed to calculate the properties and spectral energy distributions of synthetic stellar populations. The impact of binary star interactions and evolution processes are explicitly modelled. BPASS assumes stochastic sampling of the stellar IMF subject to the  $M_{\text{ecl}}$  mass constraint to model a simple stellar population's properties and astrophysical (not star-cluster-dynamical) evolution. The stochastically lighting up galaxies (SLUG) software has been developed to model the photometric properties of star clusters and galaxies assuming the stellar IMF is invariant (e.g. Krumholz et al. 2015<sup>7</sup>). To set up a realistic stellar plus binary star population for modelling star clusters the MCLUSTER code has been developed (e.g. Wang et al. 2019<sup>8</sup>). Garling et al. (2024) published the open-source Julia package STARFORMATIONHISTORIES.JL<sup>9</sup> for measuring resolved SFHs. It includes modelling unresolved photometric binaries and supports arbitrary IMFs.

For cases A and C, the initialisation and efficient dynamical processing of a binary-star population in an embedded cluster and a galactic field is coded in BiPos<sup>10</sup> (Dabringhausen et al., 2022).

For Case C, the PHOTGALIMF<sup>11</sup> code is available as an extension of GALIMF<sup>12</sup>. It allows the calculation of the photometric evolution in various pass bands of a one-zone chemical enrichment model of a galaxy by applying the IGIMF theory to track the changing gwIMF through an evolving SFR and due to the self-enrichment by metals (e.g. Haslbauer et al. 2024). PHOTGALIMF is currently the only chemical enrichment code to self-consistently account for the evolution of the gwIMF and the luminosity of a forming galaxy. The GWIMF FORTRAN code<sup>13</sup>, allowing the calculation of the gwIMF using the IGIMF theory following Jeřábková et al. (2018), has been written by A. H. Zonoozi, who has also developed the SPS-VARIMF FORTRAN program to allow the calculation of spectral energy distributions of galaxies evolved via the IGIMF theory (to be published by Zonoozi and collaborators). The efficient GALCEM code allows one-zone chemical evolution models of galaxies to be calculated based on 86 elements and 451 isotopes for a pre-chosen invariant gwIMF (Gjergo et al., 2023)<sup>14</sup>. It is being extended as the PYIGIMF module to include the IGIMF theoretical formalism<sup>15</sup>.

## 10 Conclusions and outlook

The understanding of the stellar IMF has advanced considerably over the past two decades such that a good understanding of stellar populations in the cosmological context is available (Fig. 14). But key issues remain: Relying only on theoretical stellar luminosity–mass relations is prone to lead to failure in the construction of a stellar IMF. Corrections for missed components of multiple stellar systems critically depend on the degree of dynamical processing of the stellar population under scrutiny – there is no universal correction for unresolved multiple stellar systems that can be applied to star counts. An important advance has been the realisation that the stellar IMF of a simple stellar population born in one molecular cloud clump as an embedded cluster is unlikely to be the same as the stellar IMF of all freshly formed stars in a galaxy, the gwIMF.

Observational data are, however, often interpreted with the use of a stellar IMF that is assumed to be an invariant probability density distribution function and to be the same in star-forming molecular cloud clumps and on the galaxy scale. This provides a useful benchmark model.

As the observations probe ever more extreme star-forming regions their interpretation increasingly points to the stellar IMF not being equal to the gwIMF. The observations of high redshift ( $z > 10$ ) star-formation activity also increasingly indicate the stellar IMF to depend on the physical properties of the star-forming gas,  $\text{IMF} = \text{IMF}(\{P_i\}^{N_p})$ , where  $\{P_i\}^{N_p}$  is a set of  $N_p$  physical parameters such as the density of the molecular cloud core, its metallicity, its temperature, specific angular momentum, magnetic field, the shear of the galaxy's rotational velocity field. This variation is expected to carry through to the corrections needed for calculating the stellar IMF from star-counts with unresolved multiple systems because the properties of their birth distribution functions as well as the properties of their birth embedded clusters are likely to also depend on the physical properties ( $f_p = f_p(P, \{P_i\}^{N_p} : m_{\text{prim}})$ ,  $f_q = f_q(q, \{P_i\}^{N_p} : m_{\text{prim}})$ ,  $f_e = f_e(e, \{P_i\}^{N_p} : m_{\text{prim}})$ ,  $r_{0.5} = r_{0.5}(M_{\text{ecl}} : \{P_i\}^{N_p})$ ). Currently available data are limited and do not indicate strong dependencies of these (Sec. 3.1, Sec. 3.4).

<sup>3</sup><https://ascl.net/1206.009>

<sup>4</sup><http://ascl.net/1104.003>

<sup>5</sup><https://cdsarc.u-strasbg.fr/viz-bin/qcat?J/A+A/623/A143#/browse>

<sup>6</sup><https://bpass.auckland.ac.nz>

<sup>7</sup><https://bitbucket.org/krumholz/slug2/src/master/>

<sup>8</sup><https://github.com/lwang-astro/mcluster>

<sup>9</sup><https://github.com/cgarling/StarFormationHistories.jl>

<sup>10</sup><https://github.com/JDabringhausen/BiPos1>

<sup>11</sup><https://github.com/juzikong/photGalIMF>, <https://ascl.net/code/v/4066>

<sup>12</sup><https://github.com/Azeret/galIMF>

<sup>13</sup><https://github.com/ahzonoozi/GWIMF>

<sup>14</sup><https://github.com/egjergo/GalCEM>

<sup>15</sup><https://github.com/egjergo/pyIGIMF>

One approach is to condense the variation only to a background temperature dependency related to the cosmological model and to treat the gwIMF as being the same as the stellar IMF. This approach does not capture that the physical conditions vary within a galaxy and that information on the temperature under which a stellar population formed is lost with the gas such that a gauging of the stellar IMF/gwIMF dependence on temperature using star-counts is not easily possible. An alternative approach is to gauge the variation of the stellar IMF by the masses of the born simple stellar populations, the radii of the embedded clusters in which the populations were born, and the metallicities of the populations. The so-gauged IMF = IMF(molecular cloud clump density, metallicity) can then be used to construct the forming stellar population of a galaxy by integration over all new embedded clusters. Although previous studies had assumed it to be a probability density distribution function, inherent to the current IGIMF-theoretical approach is the interpretation that the stellar IMF emerging within a molecular cloud clump is an optimally sampled distribution function. This may be a result of significant feedback-self-regulation of the star-formation process on the molecular clump scale as is indicated to be the case by the small star-formation efficiency of  $\epsilon < 0.4$  per clump. The existence of a tight  $m_{\max} = m_{\max}(M_{\text{ecl}})$  relation for embedded clusters supports significant feedback-self-regulation in the star-formation process. The correlation between the mass of the most massive young cluster,  $M_{\text{ecl,max}} = M_{\text{ecl,max}}(\psi)$ , and the SFR,  $\psi$ , of its hosting galaxy suggests a self-regulation process on the galaxy scale, probably through the galaxy-wide potential determining the dynamics of the star-forming gas.

According to the IGIMF theory, late-type dwarf galaxies would have a top-light gwIMF while massive disk galaxies would have a top-heavy gwIMF. Elliptical galaxies end up to have a bottom-heavy and had a top-heavy gwIMF. Ultra faint dwarf galaxies would have a bottom-light and had a top-light gwIMF. A correlation of the overall shape of the gwIMF with the velocity dispersion of an ETG arises naturally due to the radius-mass relation of ETGs and the mass-SFR relation via the downsizing time. The properties of elliptical galaxies and the rapid formation of supermassive black holes, the stellar content of late type dwarf galaxies and the radial H $\alpha$  cutoff in UV-extended galactic disks would be explained naturally. Massive elliptical galaxies would be up to ten times as massive due to their content in faint red dwarf stars, neutron stars and black holes. According to the IGIMF theory, at super-Solar metallicity large SFRs remain dark because the gwIMF is bottom-heavy and top-light, suggesting a possible solution of the cooling flow problem. Late-type dwarf disk galaxies would have similar gas-consumption time-scales as major disk galaxies and the galaxy main sequence would include late-type dwarf galaxies and would be flatter. The stellar IMF on the molecular cloud clump scale becomes connected to the cosmological scale.

*It is important to keep in mind* that any proposed model of the variation of the stellar IMF and of the gwIMF must account for their connection and the locally observed canonical shape of the stellar IMF and of the Milky Way's gwIMF. Given the available observational constraints spanning the local to the high redshift Universe, the galaxy-wide stellar populations appear to require a varying stellar IMF on the molecular clump scale that needs to be essentially similar to the formulation provided by eqn. 28.

The future will inform us about the true nature and the variation of the stellar IMF, the role of additional parameters,  $P_i$  beyond  $M_{\text{ecl}}$  and  $Z$ , and the role of feedback self-regulation in the star-formation process.

## Acknowledgments

We thank Jiadong Li at Heidelberg University for providing the data for Fig. 2. P.K. acknowledges support through the DAAD Bonn-Prague Eastern-Europe Exchange programme. E.G. acknowledges the support of the National Natural Science Foundation of China (NSFC) under grants NOs. 12173016, 12041305. E.G. acknowledges the science research grants from the China Manned Space Project with NOs. CMS-CSST-2021-A08, CMS-CSST-2021-A07. E.G. acknowledges the Program for Innovative Talents, Entrepreneur in Jiangsu.

## References

- Adams FC and Fatuzzo M (1996), Jun. A Theory of the Initial Mass Function for Star Formation in Molecular Clouds. *ApJ* 464: 256. doi: 10.1086/177318. astro-ph/9601139.
- André P, Men'shchikov A, Bontemps S, Könyves V, Motte F, Schneider N, Didelon P, Minier V, Saraceno P, Ward-Thompson D, di Francesco J, White G, Molinari S, Testi L, Abergel A, Griffin M, Henning T, Royer P, Merin B, Vavrek R, Attard M, Arzoumanian D, Wilson CD, Ade P, Aussel H, Baluteau JP, Benedettini M, Bernard JP, Blommaert JADL, Cambrésy L, Cox P, di Giorgio A, Hargrave P, Hennemann M, Huang M, Kirk J, Krause O, Launhardt R, Leeks S, Le Penec J, Li JZ, Martin PG, Maury A, Olofsson G, Omont A, Peretto N, Pezzuto S, Prusti T, Rousset H, Russeil D, Sauvage M, Sibthorpe B, Sicilia-Aguilar A, Spinoglio L, Waelkens C, Woodcraft A and Zavagno A (2010), Jul. From filamentary clouds to prestellar cores to the stellar IMF: Initial highlights from the Herschel Gould Belt Survey. *A&A* 518, L102. doi:10.1051/0004-6361/201014666. 1005.2618.
- André P, Di Francesco J, Ward-Thompson D, Inutsuka SI, Pudritz RE and Pineda JE (2014), Jan., From Filamentary Networks to Dense Cores in Molecular Clouds: Toward a New Paradigm for Star Formation, Beuther H, Klessen RS, Dullemond CP and Henning T, (Eds.), *Protostars and Planets VI*, 27–51, 1312.6232.
- André P, Arzoumanian D, Könyves V, Shimajiri Y and Palmeirim P (2019), Sep. The role of molecular filaments in the origin of the prestellar core mass function and stellar initial mass function. *A&A* 629, L4. doi:10.1051/0004-6361/201935915. 1907.13448.
- Banerjee S and Kroupa P (2012), Nov. On the true shape of the upper end of the stellar initial mass function. The case of R136. *A&A* 547, A23. doi:10.1051/0004-6361/201218972. 1209.4079.
- Banerjee S, Kroupa P and Oh S (2012), Oct. The emergence of super-canonical stars in R136-type starburst clusters. *MNRAS* 426 (2): 1416–1426. doi:10.1111/j.1365-2966.2012.21672.x. 1208.0826.
- Bartko H, Martins F, Trippe S, Fritz TK, Genzel R, Ott T, Eisenhauer F, Gillessen S, Paumard T, Alexander T, Dodds-Eden K, Gerhard O, Levin Y, Mascetti L, Nayakshin S, Perets HB, Perrin G, Pfuhl O, Reid MJ, Rouan D, Zilka M and Sternberg A (2010), Jan. An Extremely Top-Heavy

- Initial Mass Function in the Galactic Center Stellar Disks. *ApJ* 708 (1): 834–840. doi:10.1088/0004-637X/708/1/834. 0908.2177.
- Bate MR (2012), Feb. Stellar, brown dwarf and multiple star properties from a radiation hydrodynamical simulation of star cluster formation. *MNRAS* 419 (4): 3115–3146. doi:10.1111/j.1365-2966.2011.19955.x. 1110.1092.
- Bate MR (2019), Apr. The statistical properties of stars and their dependence on metallicity. *MNRAS* 484 (2): 2341–2361. doi:10.1093/mnras/stz103. 1901.03713.
- Bate MR (2023), Feb. The statistical properties of stars at redshift,  $z = 5$ , compared with the present epoch. *MNRAS* 519 (1): 688–708. doi:10.1093/mnras/stac3481. 2211.15727.
- Battisti AJ and Heyer MH (2014), Jan. The Dense Gas Mass Fraction of Molecular Clouds in the Milky Way. *ApJ* 780 (2), 173. doi:10.1088/0004-637X/780/2/173. 1312.0643.
- Baumgardt H, Kroupa P and Parmentier G (2008), Mar. The influence of residual gas expulsion on the evolution of the Galactic globular cluster system and the origin of the Population II halo. *MNRAS* 384 (3): 1231–1241. doi:10.1111/j.1365-2966.2007.12811.x. 0712.1591.
- Baumgardt H, Hénault-Brunet V, Dickson N and Sollima A (2023), May. Evidence for a bottom-light initial mass function in massive star clusters. *MNRAS* 521 (3): 3991–4008. doi:10.1093/mnras/stad631. 2303.01636.
- Belloni D, Askar A, Giersz M, Kroupa P and Rocha-Pinto HJ (2017), Nov. On the initial binary population for star cluster simulations. *MNRAS* 471 (3): 2812–2828. doi:10.1093/mnras/stx1763. 1707.04271.
- Bertelli Motta C, Clark PC, Glover SCO, Klessen RS and Pasquali A (2016), Nov. The IMF as a function of supersonic turbulence. *MNRAS* 462 (4): 4171–4182. doi:10.1093/mnras/stw1921. 1608.01306.
- Burrows A, Heng K and Nampaisarn T (2011), Jul. The Dependence of Brown Dwarf Radii on Atmospheric Metallicity and Clouds: Theory and Comparison with Observations. *ApJ* 736 (1), 47. doi:10.1088/0004-637X/736/1/47. 1102.3922.
- Carney BW, Aguilar LA, Latham DW and Laird JB (2005), Apr. A Survey of Proper-Motion Stars. XVII. A Deficiency of Binary Stars on Retrograde Galactic Orbits and the Possibility that  $\omega$  Centauri is Related to the Effect. *AJ* 129 (4): 1886–1905. doi:10.1086/427542. astro-ph/0412111.
- Chabrier G (2003), Jul. Galactic Stellar and Substellar Initial Mass Function. *PASP* 115 (809): 763–795. doi:10.1086/376392. astro-ph/0304382.
- Chen Y, Girardi L, Fu X, Bressan A, Aringer B, Dal Tio P, Pastorelli G, Marigo P, Costa G and Zhang X (2019), Dec. YBC: a stellar bolometric corrections database with variable extinction coefficients. Application to PARSEC isochrones. *A&A* 632, A105. doi:10.1051/0004-6361/201936612. 1910.09037.
- Corbelli E, Verley S, Elmegreen BG and Giovanardi C (2009), Feb. The cluster birthline in M 33. *A&A* 495 (2): 479–490. doi:10.1051/0004-6361/200811086. 0901.1530.
- Curti M, Witstok J, Jakobsen P, Kobayashi C, Curtis-Lake E, Hainline K, Ji X, D'Eugenio F, Chevillard J, Maiolino R, Scholtz J, Carniani S, Aribas S, Baker WM, Bhatawdekar R, Boyett K, Bunker AJ, Cameron A, Cargile PA, Charlot S, Eisenstein DJ, Ji Z, Johnson BD, Kumari N, Maseda MV, Robertson B, Silcock MS, Tacchella S, Ubler H, Venturi G, Williams CC, Willmer CNA and Willott C (2024), Jul. JADES: The star-formation and chemical enrichment history of a luminous galaxy at  $z=9.43$  probed by ultra-deep JWST/NIRSpec spectroscopy. *arXiv e-prints*, arXiv:2407.02575doi:10.48550/arXiv.2407.02575. 2407.02575.
- da Silva RL, Fumagalli M and Krumholz MR (2014), Nov. SLUG - Stochastically Lighting Up Galaxies - II. Quantifying the effects of stochasticity on star formation rate indicators. *MNRAS* 444 (4): 3275–3287. doi:10.1093/mnras/stu1688. 1403.4605.
- Dabringhausen J and Kroupa P (2023), Dec. The integrated galaxy-wide stellar initial mass function over the radial acceleration range of early-type galaxies. *MNRAS* 526 (2): 2301–2322. doi:10.1093/mnras/stad2825. 2309.06466.
- Dabringhausen J, Marks M and Kroupa P (2022), Feb. BIPOS1 - a computer programme for the dynamical processing of the initial binary star population. *MNRAS* 510 (1): 413–432. doi:10.1093/mnras/stab3288. 2111.05942.
- De Marchi G, Paresce F and Pulone L (2007), Feb. Why Haven't Loose Globular Clusters Collapsed Yet? *ApJL* 656 (2): L65–L68. doi:10.1086/512856. astro-ph/0701613.
- De Marchi G, Paresce F and Portegies Zwart S (2010), Jul. On the Temporal Evolution of the Stellar Mass Function in Galactic Clusters. *ApJ* 718 (1): 105–111. doi:10.1088/0004-637X/718/1/105. 1005.4593.
- Dib S (2022), Oct. The galaxy-wide stellar initial mass function in the presence of cluster-to-cluster IMF variations. *A&A* 666, A113. doi:10.1051/0004-6361/202243793. 2204.09064.
- Dib S (2023), Dec. Variation of the High-mass Slope of the Stellar Initial Mass Function: Theory Meets Observations. *ApJ* 959 (2), 88. doi:10.3847/1538-4357/ad09bc. 2309.10842.
- Dib S, Kim J and Shadmehri M (2007), Oct. The origin of the Arches stellar cluster mass function. *MNRAS* 381 (1): L40–L44. doi:10.1111/j.1745-3933.2007.00362.x. 0706.0950.
- Dib S, Piau L, Mohanty S and Braine J (2011), Aug. Star formation efficiency as a function of metallicity: from star clusters to galaxies. *MNRAS* 415 (4): 3439–3454. doi:10.1111/j.1365-2966.2011.18966.x. 1102.3839.
- Dib S, Schmeja S and Hony S (2017), Jan. Massive stars reveal variations of the stellar initial mass function in the Milky Way stellar clusters. *MNRAS* 464 (2): 1738–1752. doi:10.1093/mnras/stw2465. 1605.08438.
- Dickson N, Hénault-Brunet V, Baumgardt H, Gieles M and Smith PJ (2023), Jul. Multimass modelling of Milky Way globular clusters - I. Implications on their stellar initial mass function above  $1 M_{\odot}$ . *MNRAS* 522 (4): 5320–5339. doi:10.1093/mnras/stad1254. 2303.01637.
- Dinnbier F, Kroupa P and Anderson RI (2022), Apr. Do the majority of stars form as gravitationally unbound? *A&A* 660, A61. doi:10.1051/0004-6361/202142082. 2201.06582.
- Duarte-Cabral A, Bontemps S, Motte F, Hennemann M, Schneider N and André P (2013), Oct. CO outflows from high-mass Class 0 protostars in Cygnus-X. *A&A* 558, A125. doi:10.1051/0004-6361/201321393. 1308.6490.
- Eappen R, Kroupa P, Wittenburg N, Haslbauer M and Famaey B (2022), Oct. The formation of early-type galaxies through monolithic collapse of gas clouds in Milgromian gravity. *MNRAS* 516 (1): 1081–1093. doi:10.1093/mnras/stac2229. 2209.00024.
- Elmegreen BG (2011), Apr. On the Initial Conditions for Star Formation and the Initial Mass Function. *ApJ* 731 (1), 61. doi:10.1088/0004-637X/731/1/61. 1102.5232.
- Elmegreen BG and Scalo J (2006), Jan. The Effect of Star Formation History on the Inferred Stellar Initial Mass Function. *ApJ* 636 (1): 149–157. doi:10.1086/497889. astro-ph/0509282.
- Fabian AC, Sanders JS, Ferland GJ, McNamara BR, Pinto C and Walker SA (2024), Jun. Consequences of a low-mass high-pressure star formation mode in early galaxies. *MNRAS* 531 (1): 267–270. doi:10.1093/mnras/stae1206. 2405.01865.
- Ferreras I, La Barbera F, de La Rosa IG, Vazdekis A, de Carvalho RR, Falcon-Barroso J and Ricciardelli E (2013), Feb. Systematic variation of the stellar initial mass function with velocity dispersion in early-type galaxies. *MNRAS* 429: L15–L19. doi:10.1093/mnras/ls014. 1206.1594.
- Fioc M and Rocca-Volmerange B (2019), Mar. PÉGASE.3: A code for modeling the UV-to-IR/submm spectral and chemical evolution of galaxies with dust. *A&A* 623, A143. doi:10.1051/0004-6361/201833556. 1902.07929.
- Fumagalli M, da Silva RL and Krumholz MR (2011), Nov. Stochastic Star Formation and a (Nearly) Uniform Stellar Initial Mass Function. *ApJL* 741 (2), L26. doi:10.1088/2041-8205/741/2/L26. 1105.6101.
- Garling CT, Kallivayalil N, McQuinn KBW, Warfield JT, Gennaro M and Cohen RE (2024), Jul. Measuring Resolved Star Formation Histories from



- High-Precision Color-Magnitude Diagrams with StarFormationHistories.jl. *arXiv:2407.19534*, *arXiv:2407.195342407.19534*.
- Gerasimov R, Bedin LR, Burgasser AJ, Apai D, Nardiello D, Alvarado E and Anderson J (2024), Aug. JWST Imaging of the Closest Globular Clusters. II. Discovery of Brown Dwarfs in NGC 6397 and Measurement of Age from the Brown Dwarf Cooling Sequence, Using SANDee—A New Grid of Model Isochrones across the Hydrogen-burning Limit. *ApJ* 971 (1), 65. doi:10.3847/1538-4357/ad5551. 2405.01634.
- Gjergo E, Sorokin AG, Ruth A, Spitoni E, Matteucci F, Fan X, Liang J, Limongi M, Yamazaki Y, Kusakabe M and Kajino T (2023), Feb. GaLCEM. I. An Open-source Detailed Isotopic Chemical Evolution Code. *ApJS* 264 (2), 44. doi:10.3847/1538-4365/aca7c7. 2301.02257.
- González-Samaniego A and Vazquez-Semadeni E (2020), Nov. The effect of photoionizing feedback on the shaping of hierarchically-forming stellar clusters. *MNRAS* 499 (1): 668–680. doi:10.1093/mnras/staa2921. 2003.12711.
- Goodwin SP, Kroupa P, Goodman A and Burkert A (2007), Jan., The Fragmentation of Cores and the Initial Binary Population, Reipurth B, Jewitt D and Keil K, (Eds.), *Protostars and Planets V*, pp. 133. astro-ph/0603233.
- Groenewegen MAT (2006), Mar. The mid- and far-infrared colours of AGB and post-AGB stars. *A&A* 448 (1): 181–187. doi:10.1051/0004-6361:20054163. astro-ph/0511475.
- Grudić MY, Guszejnov D, Offner SSR, Rosen AL, Raju AN, Faucher-Giguère CA and Hopkins PF (2022), May. The dynamics and outcome of star formation with jets, radiation, winds, and supernovae in concert. *MNRAS* 512 (1): 216–232. doi:10.1093/mnras/stac526. 2201.00882.
- Grudić MY, Offner SSR, Guszejnov D, Faucher-Giguère CA and Hopkins PF (2023), Dec. Does God play dice with star clusters? *The Open Journal of Astrophysics* 6, 48. doi:10.21105/astro.2307.00052. 2307.00052.
- Guilherme-Garcia P, Krone-Martins A and Moitinho A (2023), May. Detection of open cluster rotation fields from Gaia EDR3 proper motions. *A&A* 673, A128. doi:10.1051/0004-6361/202142826. 2309.03396.
- Gunawardhana MLP, Hopkins AM, Sharp RG, Brough S, Taylor E, Bland-Hawthorn J, Maraston C, Tuffs RJ, Popescu CC, Wijesinghe D, Jones DH, Croom S, Sadler E, Wilkins S, Driver SP, Liske J, Norberg P, Baldry IK, Bamford SP, Loveday J, Peacock JA, Robotham ASG, Zucker DB, Parker QA, Conselice CJ, Cameron E, Frenk CS, Hill DT, Kelvin LS, Kuijken K, Madore BF, Nichol B, Parkinson HR, Pimbblet KA, Prescott M, Sutherland WJ, Thomas D and van Kampen E (2011), Aug. Galaxy and Mass Assembly (GAMA): the star formation rate dependence of the stellar initial mass function. *MNRAS* 415 (2): 1647–1662. doi:10.1111/j.1365-2966.2011.18800.x. 1104.2379.
- Guszejnov D, Hopkins PF and Graus AS (2019), Jun. Is it possible to reconcile extragalactic IMF variations with a universal Milky Way IMF? *MNRAS* 485 (4): 4852–4862. doi:10.1093/mnras/stz736. 1903.01533.
- Hacar A, Tafalla M and Alves J (2017), Oct. Fibers in the NGC 1333 proto-cluster. *A&A* 606, A123. doi:10.1051/0004-6361/201630348. 1703.07029.
- Haghi H, Khalaj P, Hasani Zonoozi A and Kroupa P (2017), Apr. A Possible Solution for the ML-[Fe/H] Relation of Globular Clusters in M31. II. The Age-Metallicity Relation. *ApJ* 839 (1), 60. doi:10.3847/1538-4357/aa6719. 1703.04635.
- Haslbauer M, Kroupa P, Zonoozi AH and Haghi H (2022), Nov. Has JWST Already Falsified Dark-matter-driven Galaxy Formation? *ApJL* 939 (2), L31. doi:10.3847/2041-8213/ac9a50. 2210.14915.
- Haslbauer M, Kroupa P and Jerabkova T (2023), Sep. The cosmological star formation history from the Local Cosmological Volume of galaxies and constraints on the matter homogeneity. *MNRAS* 524 (3): 3252–3262. doi:10.1093/mnras/stad1986. 2306.16436.
- Haslbauer M, Yan Z, Jerabkova T, Gjergo E, Kroupa P and Hasani Zonoozi A (2024), May. The effect of the environment-dependent stellar initial mass function on the photometric properties of star-forming galaxies. *arXiv e-prints*, arXiv:2405.05313doi:10.48550/arXiv.2405.05313. 2405.05313.
- Hennebelle P and Grudić MY (2024), Apr. The Physical Origin of the Stellar Initial Mass Function. *ARAA, in press*, arXiv:2404.07301doi:10.48550/arXiv.2404.07301. 2404.07301.
- Hopkins AM (2018), Nov. The Dawes Review 8: Measuring the Stellar Initial Mass Function. *PASA* 35, e039. doi:10.1017/pasa.2018.29. 1807.09949.
- Hopkins PF, Grudić MY, Kremer K, Offner SSR, Guszejnov D and Rosen AL (2024), Apr. FORGE'd in FIRE III: The IMF in Quasar Accretion Disks from STARFORGE. *arXiv e-prints*, arXiv:2404.08046doi:10.48550/arXiv.2404.08046. 2404.08046.
- Hsu WH, Hartmann L, Allen L, Hernández J, Megeath ST, Mosby G, Tobin JJ and Espaillat C (2012), Jun. The Low-mass Stellar Population in L1641: Evidence for Environmental Dependence of the Stellar Initial Mass Function. *ApJ* 752 (1), 59. doi:10.1088/0004-637X/752/1/59. 1204.3704.
- Jadhav VV, Kroupa P, Wu W, Pflamm-Altenburg J and Thies I (2024), Jul. The spin, expansion, and contraction of open star clusters. *A&A* 687, A89. doi:10.1051/0004-6361/202349115. 2404.05327.
- Jerabkova T, Beccari G, Boffin HMJ, Petr-Gotzens MG, Manara CF, Prada Moroni PG, Tognelli E and Degl'Innocenti S (2019), Jul. When the tale comes true: multiple populations and wide binaries in the Orion Nebula Cluster. *A&A* 627, A57. doi:10.1051/0004-6361/201935016. 1905.06974.
- Jermyn AS, Steinhardt CL and Tout CA (2018), Nov. The cosmic microwave background and the stellar initial mass function. *MNRAS* 480 (3): 4265–4272. doi:10.1093/mnras/sty2123. 1809.03502.
- Jeřábková T, Kroupa P, Dabringhausen J, Hilker M and Bekki K (2017), Dec. The formation of ultra compact dwarf galaxies and massive globular clusters. Quasar-like objects to test for a variable stellar initial mass function. *A&A* 608, A53. doi:10.1051/0004-6361/201713240. 1708.07127.
- Jeřábková T, Hasani Zonoozi A, Kroupa P, Beccari G, Yan Z, Vazdekis A and Zhang ZY (2018), Nov. Impact of metallicity and star formation rate on the time-dependent, galaxy-wide stellar initial mass function. *A&A* 620, A39. doi:10.1051/0004-6361/201833055. 1809.04603.
- Joncour I, Duchêne G, Moraux E and Motte F (2018), Nov. Multiplicity and clustering in Taurus star forming region. II. From ultra-wide pairs to dense NESTs. *A&A* 620, A27. doi:10.1051/0004-6361/201833042. 1809.02380.
- Kennicutt R. C. J (1983), Sep. The rate of star formation in normal disk galaxies. *ApJ* 272: 54–67. doi:10.1086/161261.
- Kennicutt RC and Evans NJ (2012), Sep. Star Formation in the Milky Way and Nearby Galaxies. *ARAA* 50: 531–608. doi:10.1146/annurev-astro-081811-125610. 1204.3552.
- Kirk H and Myers PC (2011), Feb. Young Stellar Groups and Their Most Massive Stars. *ApJ* 727 (2), 64. doi:10.1088/0004-637X/727/2/64. 1011.1416.
- Kirk H, Myers PC, Bourke TL, Gutermuth RA, Hedden A and Wilson GW (2013), Apr. Filamentary Accretion Flows in the Embedded Serpens South Protocluster. *ApJ* 766 (2), 115. doi:10.1088/0004-637X/766/2/115. 1301.6792.
- Kirkpatrick JD, Marocco F, Gelino CR and et al. (2023), Dec. The Initial Mass Function Based on the Full-sky 20-pc Census of ~3,600 Stars and Brown Dwarfs. *ApJ, in press*, arXiv:2312.03639, arXiv:2312.03639doi:10.48550/arXiv.2312.03639. 2312.03639.
- Klessen RS and Glover SCO (2023), Aug. The First Stars: Formation, Properties, and Impact. *ARAA* 61: 65–130. doi:10.1146/annurev-astro-071221-053453. 2303.12500.
- Kobayashi C and Ferrara A (2024), Feb. Rapid Chemical Enrichment by Intermittent Star Formation in GN-z11. *ApJL* 962 (1), L6. doi:10.3847/2041-8213/ad1de1. 2308.15583.
- Koshimoto N, Baba J and Bennett DP (2021), Aug. A Parametric Galactic Model toward the Galactic Bulge Based on Gaia and Microlensing Data. *ApJ* 917 (2), 78. doi:10.3847/1538-4357/ac07a8. 2104.03306.
- Kroupa P (1995a), Dec. Inverse dynamical population synthesis and star formation. *MNRAS* 277: 1491. doi:10.1093/mnras/277.4.1491. astro-ph/9508117.

- Kroupa P (1995b), Dec. The dynamical properties of stellar systems in the Galactic disc. *MNRAS* 277: 1507. doi:10.1093/mnras/277.4.1507. astro-ph/9508084.
- Kroupa P (2001), Apr. On the variation of the initial mass function. *MNRAS* 322 (2): 231–246. doi:10.1046/j.1365-8711.2001.04022.x. astro-ph/0009005.
- Kroupa P (2002), Jan. The Initial Mass Function of Stars: Evidence for Uniformity in Variable Systems. *Science* 295 (5552): 82–91. doi:10.1126/science.1067524. astro-ph/0201098.
- Kroupa P (2005), Jan., The Fundamental Building Blocks of Galaxies, Turon C, O’Flaherty KS and Perryman MAC, (Eds.), The Three-Dimensional Universe with Gaia, ESA Special Publication, 576, pp. 629. astro-ph/0412069.
- Kroupa P (2008), Initial Conditions for Star Clusters, Aarseth SJ, Tout CA and Mardling RA, (Eds.), The Cambridge N-Body Lectures, 760, pp. 181.
- Kroupa P and Bouvier J (2003), Dec. On the origin of brown dwarfs and free-floating planetary-mass objects. *MNRAS* 346 (2): 369–380. doi:10.1046/j.1365-2966.2003.07224.x. astro-ph/0309645.
- Kroupa P and Gilmore GF (1994), Aug. Low-mass stars in cooling-flow galaxies. *MNRAS* 269: 655–678. doi:10.1093/mnras/269.3.655.
- Kroupa P and Jerabkova T (2018), Jun. The Impact of Binaries on the Stellar Initial Mass Function. *arXiv e-prints*, arXiv:1806.10605doi:10.48550/arXiv.1806.10605. 1806.10605.
- Kroupa P and Jerabkova T (2019), Jun. The Salpeter IMF and its descendants. *Nature Astronomy* 3: 482–484. doi:10.1038/s41550-019-0793-0. 1910.01126.
- Kroupa P and Jerabkova T (2021), Dec. The initial mass function of stars and the star-formation rates of galaxies. *arXiv e-prints*, arXiv:2112.10788doi:10.48550/arXiv.2112.10788. 2112.10788.
- Kroupa P and Tout CA (1997), May. The theoretical mass-magnitude relation of low mass stars and its metallicity dependence. *MNRAS* 287: 402–414. doi:10.1093/mnras/287.2.402. astro-ph/9701213.
- Kroupa P and Weidner C (2003), Dec. Galactic-Field Initial Mass Functions of Massive Stars. *ApJ* 598 (2): 1076–1078. doi:10.1086/379105. astro-ph/0308356.
- Kroupa P, Tout CA and Gilmore G (1990), May. The low-luminosity stellar mass function. *MNRAS* 244: 76–85.
- Kroupa P, Tout CA and Gilmore G (1991), Jul. The effects of unresolved binary stars on the determination of the stellar mass function. *MNRAS* 251: 293–302. doi:10.1093/mnras/251.2.293.
- Kroupa P, Tout CA and Gilmore G (1993), Jun. The Distribution of Low-Mass Stars in the Galactic Disc. *MNRAS* 262: 545–587. doi:10.1093/mnras/262.3.545.
- Kroupa P, Weidner C, Pflamm-Altenburg J, Thies I, Dabringhausen J, Marks M and Maschberger T (2013), The Stellar and Sub-Stellar Initial Mass Function of Simple and Composite Populations, Oswalt TD and Gilmore G, (Eds.), Planets, Stars and Stellar Systems. Volume 5: Galactic Structure and Stellar Populations, 5, pp. 115.
- Kroupa P, Jeřábková T, Dinnbier F, Beccari G and Yan Z (2018), Apr. Evidence for feedback and stellar-dynamically regulated bursty star cluster formation: the case of the Orion Nebula Cluster. *A&A* 612, A74. doi:10.1051/0004-6361/201732151. 1801.03095.
- Kroupa P, Subr L, Jerabkova T and Wang L (2020), Nov. Very high redshift quasars and the rapid emergence of supermassive black holes. *MNRAS* 498 (4): 5652–5683. doi:10.1093/mnras/staa2276. 2007.14402.
- Krumholz MR and Federrath C (2019), Feb. The Role of Magnetic Fields in Setting the Star Formation Rate and the Initial Mass Function. *Frontiers in Astronomy and Space Sciences* 6, 7. doi:10.3389/fspas.2019.00007. 1902.02557.
- Krumholz MR, Fumagalli M, da Silva RL, Rendahl T and Parra J (2015), Sep. SLUG - stochastically lighting up galaxies - III. A suite of tools for simulated photometry, spectroscopy, and Bayesian inference with stochastic stellar populations. *MNRAS* 452 (2): 1447–1467. doi:10.1093/mnras/stv1374. 1502.05408.
- La Barbera F, Vazdekis A, Ferreras I, Pasquali A, Allende Prieto C, Martín-Navarro I, Aguado DS, de Carvalho RR, Rembold S, Falcón-Barroso J and van de Ven G (2019), Nov. IMF radial gradients in most massive early-type galaxies. *MNRAS* 489 (3): 4090–4110. doi:10.1093/mnras/stz2192. 1909.01382.
- Lada CJ and Lada EA (2003), Jan. Embedded Clusters in Molecular Clouds. *ARAA* 41: 57–115. doi:10.1146/annurev.astro.41.011802.094844. astro-ph/0301540.
- Larson RB (1992), Jun. Towards understanding the stellar initial mass function. *MNRAS* 256: 641–646. doi:10.1093/mnras/256.3.641.
- Lee JC, Gil de Paz A, Tremonti C, Kennicutt Robert C. J, Salim S, Bothwell M, Calzetti D, Dalcanton J, Dale D, Engelbracht C, Funes SJJG, Johnson B, Sakai S, Skillman E, van Zee L, Walter F and Weisz D (2009), Nov. Comparison of H $\alpha$  and UV Star Formation Rates in the Local Volume: Systematic Discrepancies for Dwarf Galaxies. *ApJ* 706 (1): 599–613. doi:10.1088/0004-637X/706/1/599. 0909.5205.
- Leitherer C, Schaerer D, Goldader JD, Delgado RMG, Robert C, Kune DF, de Mello DF, Devost D and Heckman TM (1999), Jul. Starburst99: Synthesis Models for Galaxies with Active Star Formation. *ApJS* 123 (1): 3–40. doi:10.1086/313233. astro-ph/9902334.
- Lelli F, McGaugh SS and Schombert JM (2016), Dec. SPARC: Mass Models for 175 Disk Galaxies with Spitzer Photometry and Accurate Rotation Curves. *AJ* 152 (6), 157. doi:10.3847/0004-6256/152/6/157. 1606.09251.
- Lewis SC, McMillan SLW, Mac Low MM, Cournoyer-Cloutier C, Polak B, Wilhelm MJC, Tran A, Sills A, Portegies Zwart S, Klessen RS and Wall JE (2023), Feb. Early-forming Massive Stars Suppress Star Formation and Hierarchical Cluster Assembly. *ApJ* 944 (2), 211. doi:10.3847/1538-4357/acb0c5. 2212.01465.
- Li P, Cunningham A, Gaches B, Klein R, Krumholz M, Lee A, McKee C, Offner S, Rosen A and Skinner A (2021), Dec. ORION2: A magnetohydrodynamics code for star formation. *The Journal of Open Source Software* 6 (68), 3771. doi:10.21105/joss.03771.
- Li J, Liu C, Zhang ZY, Tian H, Fu X, Li J and Yan ZQ (2023), Jan. Stellar initial mass function varies with metallicity and time. *Nature* 613 (7944): 460–462. doi:10.1038/s41586-022-05488-1. 2301.07029.
- Lieberz P and Kroupa P (2017), Mar. On the origin of the Schechter-like mass function of young star clusters in disc galaxies. *MNRAS* 465 (4): 3775–3783. doi:10.1093/mnras/stw2953.
- Luhman KL (2004), Dec. New Brown Dwarfs and an Updated Initial Mass Function in Taurus. *ApJ* 617 (2): 1216–1232. doi:10.1086/425647. astro-ph/0411447.
- Mahani H, Zonoozi AH, Haghi H, Jeřábková T, Kroupa P and Mieske S (2021), Apr. Do ultracompact dwarf galaxies form monolithically or as merged star cluster complexes? *MNRAS* 502 (4): 5185–5199. doi:10.1093/mnras/stab330. 2103.10439.
- Maíz Apellániz J (2006), Feb. A Recalibration of Optical Photometry: Tycho-2, Strömgren, and Johnson Systems. *AJ* 131 (2): 1184–1199. doi:10.1086/499158. astro-ph/0510785.
- Mansfield S and Kroupa P (2023), Nov. The convective kissing instability in low-mass M-dwarf models: convective overshooting, semi-convection, luminosity functions, surface abundances, and star cluster age dating. *MNRAS* 525 (4): 6005–6014. doi:10.1093/mnras/stad2587. 2309.07523.
- Marino AF, Milone AP, Legnardi MV, Renzini A, Dondoglio E, Cavecchi Y, Cordini G, Dotter A, Lagioia EP, Ziliotto T, Bernizzoni M, Bortolan E, Carlos MG, Jang S, Mohandasan A, Muratore F and Tailo M (2024), Apr. A JWST Project on 47 Tucanae. Overview, Photometry, and Early Spectroscopic Results of M Dwarfs and Observations of Brown Dwarfs. *ApJ* 965 (2), 189. doi:10.3847/1538-4357/ad293e. 2401.06681.

- Marks M and Kroupa P (2011), Nov. Dynamical population synthesis: constructing the stellar single and binary contents of galactic field populations. *MNRAS* 417 (3): 1702–1714. doi:10.1111/j.1365-2966.2011.19519.x. 1109.2896.
- Marks M and Kroupa P (2012), Jul. Inverse dynamical population synthesis. Constraining the initial conditions of young stellar clusters by studying their binary populations. *A&A* 543, A8. doi:10.1051/0004-6361/201118231. 1205.1508.
- Marks M, Kroupa P, Dabringhausen J and Pawlowski MS (2012), May. Evidence for top-heavy stellar initial mass functions with increasing density and decreasing metallicity. *MNRAS* 422 (3): 2246–2254. doi:10.1111/j.1365-2966.2012.20767.x. 1202.4755.
- Marks M, Kroupa P and Dabringhausen J (2022), Mar. A possible solution to the Milky Way's binary-deficient retrograde stellar population. Evidence that  $\omega$  Centauri has formed in an extreme starburst. *A&A* 659, A96. doi:10.1051/0004-6361/202141846. 2112.00753.
- Maschberger T and Clarke CJ (2008), Dec. Maximum stellar mass versus cluster membership number revisited. *MNRAS* 391 (2): 711–717. doi:10.1111/j.1365-2966.2008.13903.x. 0808.4089.
- Maschberger T and Kroupa P (2009), May. Estimators for the exponent and upper limit, and goodness-of-fit tests for (truncated) power-law distributions. *MNRAS* 395 (2): 931–942. doi:10.1111/j.1365-2966.2009.14577.x. 0905.0474.
- Massey P (2003), Jan. MASSIVE STARS IN THE LOCAL GROUP: Implications for Stellar Evolution and Star Formation. *ARAA* 41: 15–56. doi:10.1146/annurev.astro.41.071601.170033.
- Matteucci F (1994), Aug. Abundance ratios in ellipticals and galaxy formation. *A&A* 288: 57–64.
- Megeath ST, Gutermuth R, Muzerolle J, Kryukova E, Hora JL, Allen LE, Flaherty K, Hartmann L, Myers PC, Pipher JL, Stauffer J, Young ET and Fazio GG (2016), Jan. The Spitzer Space Telescope Survey of the Orion A and B Molecular Clouds. II. The Spatial Distribution and Demographics of Dusty Young Stellar Objects. *AJ* 151 (1), 5. doi:10.3847/0004-6256/151/1/5. 1511.01202.
- Miller GE and Scalo JM (1979), Nov. The Initial Mass Function and Stellar Birthrate in the Solar Neighborhood. *ApJS* 41: 513. doi:10.1086/190629.
- Moe M and Di Stefano R (2017), Jun. Mind Your Ps and Qs: The Interrelation between Period (P) and Mass-ratio (Q) Distributions of Binary Stars. *ApJS* 230 (2), 15. doi:10.3847/1538-4365/aa6fb6. 1606.05347.
- Mor R, Robin AC, Figueras F and Lemasle B (2017), Mar. Constraining the thin disc initial mass function using Galactic classical Cepheids. *Astronomy & Astrophysics* 599, A17. doi:10.1051/0004-6361/201629464. 1610.08520.
- Mor R, Robin AC, Figueras F and Antoja T (2018), Dec. BGM FAST: Besançon Galaxy Model for big data. Simultaneous inference of the IMF, SFH, and density in the solar neighbourhood. *Astronomy & Astrophysics* 620, A79. doi:10.1051/0004-6361/201833501. 1809.03511.
- Mucciarelli A, Massari D, Minelli A, Romano D, Bellazzini M, Ferraro FR, Matteucci F and Origlia L (2021), Dec. A relic from a past merger event in the Large Magellanic Cloud. *Nature Astronomy* 5: 1247–1254. doi:10.1038/s41550-021-01493-y. 2110.10561.
- Murray N (2011), Mar. Star Formation Efficiencies and Lifetimes of Giant Molecular Clouds in the Milky Way. *ApJ* 729 (2), 133. doi:10.1088/0004-637X/729/2/133. 1007.3270.
- Myers PC (2009), Aug. Filamentary Structure of Star-forming Complexes. *ApJ* 700 (2): 1609–1625. doi:10.1088/0004-637X/700/2/1609. 0906.2005.
- Nayakshin S and Sunyaev R (2005), Nov. The 'missing' young stellar objects in the central parsec of the Galaxy: evidence for star formation in a massive accretion disc and a top-heavy initial mass function. *MNRAS* 364 (1): L23–L27. doi:10.1111/j.1745-3933.2005.00097.x. astro-ph/0507687.
- Oh S and Kroupa P (2016), May. Dynamical ejections of massive stars from young star clusters under diverse initial conditions. *A&A* 590, A107. doi:10.1051/0004-6361/201628233. 1604.00006.
- Papadopoulos PP (2010), Sep. A Cosmic-ray-dominated Interstellar Medium in Ultra Luminous Infrared Galaxies: New Initial Conditions for Star Formation. *ApJ* 720 (1): 226–232. doi:10.1088/0004-637X/720/1/226. 1009.1134.
- Pavlik V, Kroupa P and Šubr L (2019), Jun. Do star clusters form in a completely mass-segregated way? *A&A* 626, A79. doi:10.1051/0004-6361/201834265. 1905.09289.
- Pflamm-Altenburg J and Kroupa P (2006), Nov. A highly abnormal massive star mass function in the Orion Nebula cluster and the dynamical decay of trapezium systems. *MNRAS* 373 (1): 295–304. doi:10.1111/j.1365-2966.2006.11028.x. astro-ph/0610230.
- Pflamm-Altenburg J and Kroupa P (2008), Oct. Clustered star formation as a natural explanation for the  $H\alpha$  cut-off in disk galaxies. *Natur* 455 (7213): 641–643. doi:10.1038/nature07266. 0905.0898.
- Pflamm-Altenburg J and Kroupa P (2009), Nov. The Fundamental Gas Depletion and Stellar-Mass Buildup Times of Star-Forming Galaxies. *ApJ* 706 (1): 516–524. doi:10.1088/0004-637X/706/1/516. 0910.1089.
- Pflamm-Altenburg J, Weidner C and Kroupa P (2007), Dec. Converting  $H\alpha$  Luminosities into Star Formation Rates. *ApJ* 671 (2): 1550–1558. doi:10.1086/523033. 0705.3177.
- Pflamm-Altenburg J, Weidner C and Kroupa P (2009), May. Diverging UV and  $H\alpha$  fluxes of star-forming galaxies predicted by the IGIMF theory. *MNRAS* 395 (1): 394–400. doi:10.1111/j.1365-2966.2009.14522.x. 0901.4335.
- Pflamm-Altenburg J, González-Lópezlira RA and Kroupa P (2013), Nov. The galactocentric radius dependent upper mass limit of young star clusters: stochastic star formation ruled out. *MNRAS* 435 (3): 2604–2609. doi:10.1093/mnras/stt1474. 1310.0012.
- Ploekinger S and Schaye J (2020), Oct. Radiative cooling rates, ion fractions, molecule abundances, and line emissivities including self-shielding and both local and metagalactic radiation fields. *MNRAS* 497 (4): 4857–4883. doi:10.1093/mnras/staa2172. 2006.14322.
- Ploekinger S, Hensler G, Recchi S, Mitchell N and Kroupa P (2014), Feb. Chemo-dynamical evolution of tidal dwarf galaxies. I. Method and IMF dependence. *MNRAS* 437 (4): 3980–3993. doi:10.1093/mnras/stt2211. 1311.2932.
- Randriamanakoto Z, Escala A, Väisänen P, Kankare E, Kotilainen J, Mattila S and Ryder S (2013), Oct. Near-infrared Adaptive Optics Imaging of Infrared Luminous Galaxies: The Brightest Cluster Magnitude-Star Formation Rate Relation. *ApJL* 775 (2), L38. doi:10.1088/2041-8205/775/2/L38. 1308.6293.
- Rybizki J and Just A (2015), Mar. Towards a fully consistent Milky Way disc model - III. Constraining the initial mass function. *MNRAS* 447 (4): 3880–3891. doi:10.1093/mnras/stu2734. 1501.02630.
- Salpeter EE (1955), Jan. The Luminosity Function and Stellar Evolution. *ApJ* 121: 161. doi:10.1086/145971.
- Salvador-Rusiñol N, Vazdekis A, La Barbera F, Beasley MA, Ferreras I, Negri A and Dalla Vecchia C (2020), Jan. Sub one per cent mass fractions of young stars in red massive galaxies. *Nature Astronomy* 4: 252–259. doi:10.1038/s41550-019-0955-0. 1912.06700.
- Scalo JM (1986), May. The Stellar Initial Mass Function. *Fundamentals of Cosmic Physics* 11: 1–278.
- Schaefer D, Guibert J, Marques-Chaves R and Martins F (2024), Jul. Observable and ionizing properties of star-forming galaxies with very massive stars and different IMFs. *arXiv:2407.12122*, arXiv:2407.12122doi:10.48550/arXiv.2407.12122. 2407.12122.
- Schneider FRN, Izzard RG, Langer N and de Mink SE (2015), May. Evolution of Mass Functions of Coeval Stars through Wind Mass Loss and Binary Interactions. *ApJ* 805 (1), 20. doi:10.1088/0004-637X/805/1/20. 1504.01735.
- Schneider FRN, Sana H, Evans CJ, Bestenlehner JM, Castro N, Fossati L, Gräfener G, Langer N, Ramírez-Agudelo OH, Sabin-Sanjulián C, Simón-Díaz S, Tramper F, Crowther PA, de Koter A, de Mink SE, Dufton PL, Garcia M, Gieles M, Hénault-Brunet V, Herrero A, Izzard RG, Kalari V, Lennon DJ, Maíz Apellániz J, Markova N, Najarro F, Podsiadlowski P, Puls J, Taylor WD, van Loon JT, Vink JS and Norman C (2018), Jan. An excess of massive stars in the local 30 Doradus starburst. *Science* 359 (6371): 69–71. doi:10.1126/science.aan0106. 1801.03107.

- Schulz C, Pflamm-Altenburg J and Kroupa P (2015), Oct. Mass distributions of star clusters for different star formation histories in a galaxy cluster environment. *A&A* 582, A93. doi:10.1051/0004-6361/201425296. 1507.00860.
- Shara MM and Hurley JR (2002), Jun. Star Clusters as Type Ia Supernova Factories. *ApJ* 571 (2): 830–842. doi:10.1086/340062. astro-ph/0202179.
- Smith RJ (2020), Aug. Evidence for Initial Mass Function Variation in Massive Early-Type Galaxies. *ARAA* 58: 577–615. doi:10.1146/annurev-astro-032620-020217.
- Stanway ER and Eldridge JJ (2023), Jul. Exploring the impact of IMF and binary parameter stochasticity with a binary population synthesis code. *MNRAS* 522 (3): 4430–4443. doi:10.1093/mnras/stad1185. 2304.09549.
- Steinhardt CL, Sneppen A, Hensley H, Jermyn AS, Mostafa B, Weaver JR, Brammer G, Clark TH, Davidzon I, Diaconu AC, Mobasher B, Rusakov V and Toft S (2022), Jul. Implications of a Temperature-dependent Initial Mass Function. III. Mass Growth and Quiescence. *ApJ* 934 (1), 22. doi:10.3847/1538-4357/ac7642. 2206.01750.
- Steyrleithner P and Hensler G (2023), Dec. Why should models of dwarf galaxy evolution care about the initial mass function at low star-formation rates? *MNRAS* 526 (2): 1713–1727. doi:10.1093/mnras/stad2787. 2309.04714.
- Tang B, Zhang J, Yan Z, Zhang Z, Carigi L and Fernández-Trincado JG (2023), Jan. Near-infrared chemical abundances of stars in the Sculptor dwarf galaxy. *A&A* 669, A125. doi:10.1051/0004-6361/202244052. 2210.06731.
- Thies I and Kroupa P (2007), Dec. A Discontinuity in the Low-Mass Initial Mass Function. *ApJ* 671 (1): 767–780. doi:10.1086/522512. 0708.1764.
- Thies I, Kroupa P, Goodwin SP, Stamatellos D and Whitworth AP (2010), Jul. Tidally Induced Brown Dwarf and Planet Formation in Circumstellar Disks. *ApJ* 717 (1): 577–585. doi:10.1088/0004-637X/717/1/577. 1005.3017.
- Thies I, Pflamm-Altenburg J, Kroupa P and Marks M (2015), Feb. Characterizing the Brown Dwarf Formation Channels from the Initial Mass Function and Binary-star Dynamics. *ApJ* 800 (1), 72. doi:10.1088/0004-637X/800/1/72. 1501.01640.
- Thomas D, Maraston C, Bender R and Mendes de Oliveira C (2005), Mar. The Epochs of Early-Type Galaxy Formation as a Function of Environment. *ApJ* 621 (2): 673–694. doi:10.1086/426932. astro-ph/0410209.
- Vallée JP (2018), Nov. Meta-analysis from different tracers of the small Local Arm around the Sun—extent, shape, pitch, origin. *Astrophysics and Space Science* 363 (11), 243. doi:10.1007/s10509-018-3463-2. 1810.12995.
- van Dokkum P and Conroy C (2024), Jul. Reconciling M/L Ratios Across Cosmic Time: a Concordance IMF for Massive Galaxies. *arXiv:2407.06281*, arXiv:2407.062812407.06281.
- Vazdekis A, Casuso E, Peletier RF and Beckman JE (1996), Oct. A New Chemo-evolutionary Population Synthesis Model for Early-Type Galaxies. I. Theoretical Basis. *ApJS* 106: 307. doi:10.1086/192340. astro-ph/9605112.
- Wang L, Kroupa P and Jerabkova T (2019), Apr. Complete ejection of OB stars from very young star clusters and the formation of multiple populations. *MNRAS* 484 (2): 1843–1851. doi:10.1093/mnras/sty2232. 1810.07697.
- Wang L, Kroupa P, Takahashi K and Jerabkova T (2020), Jan. The possible role of stellar mergers for the formation of multiple stellar populations in globular clusters. *MNRAS* 491 (1): 440–454. doi:10.1093/mnras/stz3033. 1910.14040.
- Watts AB, Meurer GR, Lagos CDP, Bruzese SM, Kroupa P and Jerabkova T (2018), Jul. Star formation in the outskirts of DDO 154: a top-light IMF in a nearly dormant disc. *MNRAS* 477 (4): 5554–5567. doi:10.1093/mnras/sty1006. 1804.07072.
- Weidner C and Kroupa P (2005), Jun. The Variation of Integrated Star Initial Mass Functions among Galaxies. *ApJ* 625 (2): 754–762. doi:10.1086/429867. astro-ph/0502525.
- Weidner C, Kroupa P and Larsen SS (2004), Jun. Implications for the formation of star clusters from extragalactic star formation rates. *MNRAS* 350 (4): 1503–1510. doi:10.1111/j.1365-2966.2004.07758.x. astro-ph/0402631.
- Weidner C, Kroupa P and Pflamm-Altenburg J (2013), Sep. The  $m_{\max}$ - $M_{\text{ecl}}$  relation, the IMF and IGIMF: probabilistically sampled functions. *MNRAS* 434 (1): 84–101. doi:10.1093/mnras/stt1002. 1306.1229.
- Weidner C, Kroupa P and Pflamm-Altenburg J (2014), Jul. Sampling methods for stellar masses and the  $m_{\max}$ - $M_{\text{ecl}}$  relation in the starburst dwarf galaxy NGC 4214. *MNRAS* 441 (4): 3348–3358. doi:10.1093/mnras/stu640. 1404.1075.
- Wirth H, Kroupa P, Haas J, Jerabkova T, Yan Z and Šubr L (2022), Nov. The giants that were born swiftly - implications of the top-heavy stellar initial mass function on the birth conditions of globular clusters. *MNRAS* 516 (3): 3342–3353. doi:10.1093/mnras/stac2424. 2209.00045.
- Wright NJ, Jeffries RD, Jackson RJ, Sacco GG, Arnold B, Franciosini E, Gilmore G, Gonneau A, Morbidelli L, Prisinzano L, Randich S and Worley CC (2024), Sep. The Gaia-ESO Survey: 3D dynamics of young groups and clusters from GES and Gaia EDR3. *MNRAS* 533 (1): 705–728. doi:10.1093/mnras/stae1806. 2311.08358.
- Wuchterl G and Tscharnuter WM (2003), Feb. From clouds to stars. Protostellar collapse and the evolution to the pre-main sequence I. Equations and evolution in the Hertzsprung-Russell diagram. *A&A* 398: 1081–1090. doi:10.1051/0004-6361:20021707.
- Yan Z, Jerabkova T and Kroupa P (2017), Nov. The optimally sampled galaxy-wide stellar initial mass function. Observational tests and the publicly available GalIMF code. *A&A* 607, A126. doi:10.1051/0004-6361/201730987. 1707.04260.
- Yan Z, Jerabková T and Kroupa P (2021), Nov. Downsizing revised: Star formation timescales for elliptical galaxies with an environment-dependent IMF and number of SNIa. *A&A* 655, A19. doi:10.1051/0004-6361/202140683. 2107.03388.
- Yan Z, Jerabkova T and Kroupa P (2023), Feb. The most massive stars in very young star clusters with a limited mass: Evidence favours significant self-regulation in the star formation processes. *A&A* 670, A151. doi:10.1051/0004-6361/202244919. 2211.13244.
- Yan Z, Li J, Kroupa P, Jerabkova T, Gjergo E and Zhang ZY (2024), Jul. The Variation in the Galaxy-wide Initial Mass Function for Low-mass Stars: Modeling and Observational Insights. *ApJ* 969 (2), 95. doi:10.3847/1538-4357/ad499d. 2405.05308.
- Zeas A and Buat V (2021). Star Formation Rates in Galaxies, 55, Cambridge University Press. doi:10.1017/9781316875445.
- Zhang ZY, Romano D, Ivison RJ, Papadopoulos PP and Matteucci F (2018), Jun. Stellar populations dominated by massive stars in dusty starburst galaxies across cosmic time. *Natur* 558 (7709): 260–263. doi:10.1038/s41586-018-0196-x. 1806.01280.
- Zhang GY, Andre P, Menshchikov A and Li JZ (2024), Jun. Probing the filamentary nature of star formation in the California giant molecular cloud. *arXiv:2406.08004*, arXiv:2406.08004doi:10.48550/arXiv.2406.08004. 2406.08004.
- Zhou JW, Liu T, Evans NJ, Garay G, Goldsmith PF, Gómez GC, Vázquez-Semadeni E, Liu HL, Stutz AM, Wang K, Juvela M, He J, Li D, Bronfman L, Liu X, Xu FW, Tej A, Dewangan LK, Li S, Zhang S, Zhang C, Ren Z, Tatematsu K, Shing Li P, Won Lee C, Baug T, Qin SL, Wu Y, Peng Y, Zhang Y, Liu R, Luo QY, Ge J, Saha A, Chakali E, Zhang Q, Kim KT, Ristorcelli I, Shen ZQ and Li JZ (2022), Aug. ATOMS: ALMA Three-millimeter Observations of Massive Star-forming regions - XI. From inflow to infall in hub-filament systems. *MNRAS* 514 (4): 6038–6052. doi:10.1093/mnras/stac1735. 2206.08505.
- Zhou JW, Kroupa P and Dib S (2024a), Aug. Physical properties of embedded clusters in ATLASGAL clumps with HII regions. *PASP, in press*, arXiv:2408.09867, arXiv:2408.09867doi:10.48550/arXiv.2408.09867. 2408.09867.
- Zhou JW, Kroupa P and Dib S (2024b), Jul. Self-similar cluster structures in massive star-forming regions: Isolated evolution from clumps to embedded clusters. *A & A, in press*, arXiv:2407.20150, arXiv:2407.201502407.20150.